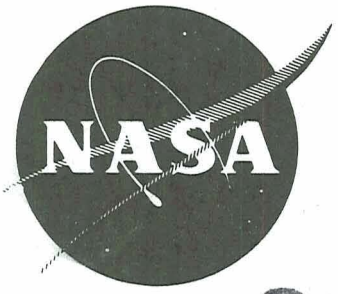

AN EVALUATION OF THE POST-IGNITION UNBLOCKING AND OSCILLATORY BEHAVIOR OF SOLID PROPELLANT AFT-END IGNITION SYSTEMS

by

J. D. Kilgroe, R. E. Fitch, and F. M. Placer

TECHNOLOGY INCORPORATED

prepared for

NATIONAL AERONAUTICS AND SPACE ADMINISTRATION

NASA Lewis Research Center
Contract NAS 3-12063
H. Bankaitis, Project Manager

Requests for copies of this report should be referred to

National Aeronautics and Space Administration
Office of Scientific and Technical Information
Attention: AFSS-A
Washington, D. C. 20546

ERRATA

NASA Contractor Report CR-72841

AN EVALUATION OF THE POST-IGNITION UNBLOCKING AND OSCILLATORY BEHAVIOR OF SOLID PROPELLANT AFT-END IGNITION SYSTEMS

by J. D. Kilgroe, R. E. Fitch, and F. M. Placer

Technology, Inc.

The number of the report should be CR-72831 instead of CR-72841.

Nov 3 - 12063

N-30020

Please put in the case file

Thank you so very much

HH

NASA CR 72 841
TECH. INC. 36920

FINAL REPORT

AN EVALUATION OF THE POST-IGNITION UNBLOCKING BEHAVIOR OF SOLID PROPELLANT AFT-END IGNITION SYSTEMS

by

J. D. Kilgroe, R. E. Fitch, and F. M. Placer

TECHNOLOGY INCORPORATED
7400 Colonel Glenn Highway
Dayton, Ohio 45431

prepared for

NATIONAL AERONAUTICS AND SPACE ADMINISTRATION

February 1971

Contract NAS 3-12063

NASA Lewis Research Center
Cleveland, Ohio
H. Bankaitis, Project Manager
Solid Rocket Technology Branch
Chemical Rocket Division

FOREWORD

The research described herein, which was conducted by CETEC Corporation, a subsidiary of Technology Incorporated, and later by Technology Incorporated as Successor in Interest, was performed under Contract NAS 3-12063. The work was done under the management of the NASA Project Manager, Mr. H. Bankaitis, Chemical Rocket Division, NASA - Lewis Research Center.

Major contributions to the test effort by Mr. Darrell Edzards, Test Crew Chief, and the assistance of members of the Department of Aeronautics and Astronautics, Leland Stanford Junior University, are gratefully acknowledged.

One of the authors, Mr. Fernando M. Placer, participated in the program as a Stanford graduate student, under the subcontract with Stanford University.

ABSTRACT

Aft-end ignition experiments with heated air simulation of solid propellant exhaust were conducted to determine the post-ignition interactions between igniter and main motor flow. The opposed, supersonic, confined flows exhibited bimodal behavior, each mode having distinctly different main motor unblocking characteristics. Previously reported severe oscillations resulted from unstable separation of the overexpanded igniter nozzle flow, principally due to alternation between the two separation flow field structures which characterized each mode. Use of a slotted igniter nozzle successfully modified the amplitude of the oscillations and the conditions under which the oscillations occurred. Flow field analyses were conducted to aid in experimental data evaluation and in development of design criteria.

TABLE OF CONTENTS

LIST OF ILLUSTRATIONS

LIST OF ILLUSTRATIONS (continued)

LIST OF ILLUSTRATIONS (continued)

LIST OF ILLUSTRATIONS (concluded)

LIST OF TABLES

1.0 SUMMARY

During a previous study of the aft-end ignition of solid-propellant motors (NASA CR-72447), severe oscillations in the interaction between the motor flow and the overexpanded igniter flow were discovered to exist during the post-ignition period. Nine aft-end ignition tests of a subscale (5.0 inch, 0.127 m, dia throat) model of the 260 inch (6.6 m) diameter solid booster all exhibited such behavior, which resulted in large-amplitude fluctuations in the motor nozzle wall pressure distribution. Furthermore, the oscillations appeared to provoke erratic and random unblocking and reblocking of the motor throat, thus leading to intermittent overpressures in the motor chamber. The oscillations were believed to be directly produced by unstable separation of the overexpanded igniter nozzle flow.

The purpose of this program was to experimentally examine the oscillations, develop techniques to reduce or eliminate the oscillations, and modify existing analytical models to incorporate the results of the study. Design criteria were to be developed to provide for selection of critical design parameters which would result in post-ignition operation without oscillations or overpressures, while preserving those conditions which produce satisfactory ignition.

To achieve these objectives, approximately 120 tests were conducted of the aft-end post-ignition behavior, using heated air to simulate a solid-propellant exhaust. The closed connected-pipe test section was constructed to duplicate, in subscale, the critical features of the rocket motor and igniter used in the previous program, and was incorporated into the Stanford University Hypersonic Wind Tunnel. This facility includes a high-pressure air-storage vessel, gas-fired pebble-bed heater, and sound-suppression exhaust tower. The test motor nozzle (3.0 inch, 0.0763 m. throat diameter) and igniter nozzle were fitted with numerous static-pressure taps.

Five basic igniter nozzle models were tested at various axial locations within the motor nozzle, over a wide span of igniter to motor chamber pressure ratios. Tests were conducted with igniter both aligned and misaligned axially, and with the igniter at far-aft conditions to simulate booster lift-off. Additionally, several techniques were tested to stabilize the igniter nozzle overexpanded flow separation.

Analytical models of the flow fields were developed to aid in data evaluation and to support the generation of design criteria. The existing blockage model was slightly modified.

The results of the testing and data evaluation clearly showed the existence of two distinctly different types of igniter-nozzle flow-field structures. The first, Mode A, occurred at relatively high igniter to motor chamber pressure ratios (PR), when the igniter flow was underexpanded or moderately overexpanded. Mode B existed at lower chamber pressure ratios when the

degree of igniter flow overexpansion was more severe. Mode A was a stable flow structure, and although Mode B tended to be unstable, each exhibited regular and well-ordered motor throat-unblocking characteristics.

The severe flow-field oscillations were observed to result from abrupt shifting of the flow field between Modes A and B when the igniter nozzle separation reached a critical position during the decay of the chamber pressure ratio. Depending upon igniter location, the onset of oscillations produced intermittent reblocking of the motor throat. One technique, an igniter nozzle which was deeply slotted in the region of the unstable separation, was successful in reducing and, in some cases, eliminating the oscillatory behavior.

Within the entire range of igniter to motor chamber pressure ratio, PR, and igniter placement, there were several regions of stable or unstable, blocked or unblocked flow. One well-defined region exists, however, of stable, unblocked flow. Post-ignition operation of the system in this region can be achieved by proper selection of the chamber pressure ratio and igniter placement. Thus, oscillations and motor overpressure can be avoided, without compromising satisfactory ignition of the motor. An example problem is used to illustrate the recommended approach in the application of the aft-end igniter design criteria which were developed.

2.0 INTRODUCTION

Under Contract NAS 3-10297, CETEC Corporation conducted an experimental and analytical program to study and characterize several specific features of the aft-end ignition of solid-propellant motors[1]. Unexpected severe flow-field and static-pressure oscillations were discovered. This led to the efforts reported herein, to more fully characterize and to control these oscillations while preserving the gasdynamical and geometric conditions which result in satisfactory ignition with no motor overpressure.

Head-end ignition systems, both pyrotechnic and pyrogen, have been favored in the past over aft-end systems[2] and have performed satisfactorily in most cases. However, in many instances aft-end pyrogen igniters are superior in several respects, owing to their separation from the main motor: increased reliability through redundancy and design conservatism; motor case and grain head-end design flexibility; reduction in stage weight. However, two potential problems have long been known to exist: long ignition intervals and possible overpressure of the motor through aerodynamic blockage of the motor throat. Earlier work[3, 4, 5, 6, 7] has shown that these problems can be severe, but that they can be avoided by proper design of the ignition system.

The difficulties of ejecting an igniter system to prevent overpressures of a pad-launched booster system such as the 260 inch (6.6 m) solid booster are considerable. Consequently the previous program[1] was undertaken, largely in support of the Large Solid Booster Program, to develop design criteria for aft-end pyrogen ignition systems which would provide satisfactory ignition without overpressures. In that program nine hot-firing tests were conducted of a subscale model of the 260 inch (6.6 m) motor and grain (5.0 inch, 0.127 m, dia throat, 56 inch, 1.42 m, grain length including 8-point head-end star), and an analytical model was developed to predict conditons under which the motor throat is blocked. In each of the nine tests, severe oscillations existed in the interactions in the motor nozzle between the opposed igniter and main flows. These resulted in major fluctuations in the pressure loads on the nozzle and usually produced intermittent blocking and unblocking of the motor throat. These oscillations were believed to be produced by inherent instability in the separation of the highly overexpanded igniter flow. During the post-contract period, additional study revealed the existence of at least two distinctly different flow-field structures, one of which was generally unstable, while the other appeared to be stable over a wide range of conditions. The evidence indicated that the most severe fluctuations occurred when the flow alternated between the two flow fields.

This program was undertaken to identify the origins, to characterize, and to develop methods of control of the oscillations, through a combined experimental and analytical effort. In the interest of flexibility and economy, the tests were conducted using heated air in an especially constructed apparatus in the Stanford University Hypersonic Wind Tunnel Facility. Approximately 120 record tests were conducted with different igniter models, both aligned

and misaligned. Based upon the test results, the original blockage model was modified, a new blockage model was developed for the alternate flow field, and development of a model to predict the onset of oscillation was attempted.

3.0 TECHNICAL ACTIVITIES

The purpose of the program reported herein was to develop aft-end igniter design criteria suitable for 260-inch-diameter type of solid-rocket motors, through a combined experimental/analytical approach satisfying the following objectives:

(1) Characterization of the motor-nozzle exit-cone oscillations and their causes.

(2) Development of techniques to control or eliminate the oscillations.

(3) Evaluation of the effects of igniter misalignment and withdrawal (simulation of motor lift-off during igniter operation).

(4) Modification of analytical models to predict unblocking and onset of oscillations.

These objectives were to be achieved by experimental study of the gas-dynamical interactions between the igniter and main motor flows in a heated-air simulation of the significant events (called cold flow in contrast to the hot firings using live propellants). The facility used was the high-pressure air-storage system, pebble-bed heater, and sound-suppression exhaust tower of the Hypersonic Wind Tunnel Facility of the Department of Aeronautics and Astronautics of Leland Stanford Junior University.

The program was comprised of the following technical work tasks:

(1) Design and fabrication of the test apparatus featuring a high degree of flexibility to provide for a wide range of test and instrumentation conditions and configurations.

(2) Cold-flow testing of approximately 120 record tests, including tests at varying positions and flow conditions of five basic igniter nozzle configurations; several modifications to one of these models to control the oscillations; misalignment (lateral, angular, and combined) and lift-off simulation.

(3) Evaluation of the test data and development of analytical model modifications to predict the ratios between igniter and motor total pressure for which unblocking of the motor throat and onset of oscillations occur for given igniter configurations and positions. The aim of this task was to develop models having sufficient generality to accommodate systems with variable gas properties, and both conical and contoured igniter and motor nozzles.

All of the above tasks were performed by CETEC personnel, with the exception of fabrication of most of the test hardware, which was performed by local machine shops and the machine shop of the Stanford Department of Aeronautics and Astronautics.

A detailed description of the technical activities appears in the following subsections and in the Appendix.

3.1 TECHNICAL BACKGROUND

The successful ignition of a solid-propellant motor with an aft-end igniter system can be considered to have culminated when the igniter is withdrawn or ejected from the motor nozzle (or vice versa). This can occur either before or after the igniter has terminated its action. The following sequence of events leading to that successful culmination is generally typical:

(1) Initiation of igniter firing when entire system is at ambient pressure.

(2) Ignition, flame spread, and build-up of the igniter flow and chamber pressure.

(3) Penetration of the igniter flow into the main motor cavity where it reverses and flows out the motor nozzle.

(4) Radiative and convective heat transfer to the motor propellant grain.

(5) Ignition of the propellant at some point on its surface.

(6) Spread of the flame over the entire propellant surface.

(7) Filling of the motor chamber and increase of chamber pressure until the design pressure is reached. This event will generally occur over several steps beginning with event (3).

(8) Forcing of the igniter flow back out of the motor throat and establishment of full sonic flow in the throat (called unblocking) at or before attainment of design chamber pressure.

(9) Interaction between the opposed igniter and motor flows within the confinement of the motor-nozzle exit cone.

(10) Termination and/or withdrawal of the igniter.

The activities described in this report were devoted entirely to study of the post-ignition events (8), (9), and (10). These problems are wholly gas-dynamical in nature and were treated as such. For a review of the ignition events and performance of igniters under a variety of conditions, the reader is referred to the results of the previous program[1].

The results of the previous program with respect to blockage and oscillations, and the later interpretation of those results will be briefly described in order to lay a foundation for the approach taken in this program. Figure 1 is a schematic of the geometric arrangement of the system. The igniter is placed within the motor-nozzle exit cone, axially aligned with the motor. Two nondimensional parameters have been shown to be especially significant in describing the behavior of this system during the post-ignition period. They are the ratio, PR, of the igniter and motor chamber pressures, and the ratio, ϵ^*, shown in Figure 2, of the conical annular area between the motor nozzle and igniter exit base to the motor throat area.

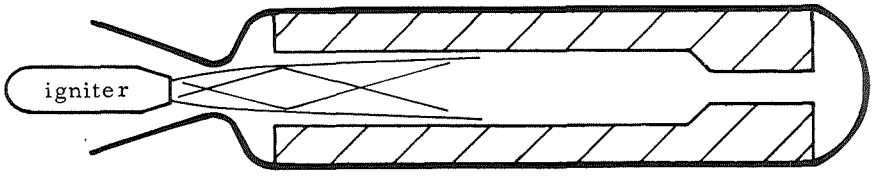

Figure 1. General Arrangement of Aft-End Ignition System

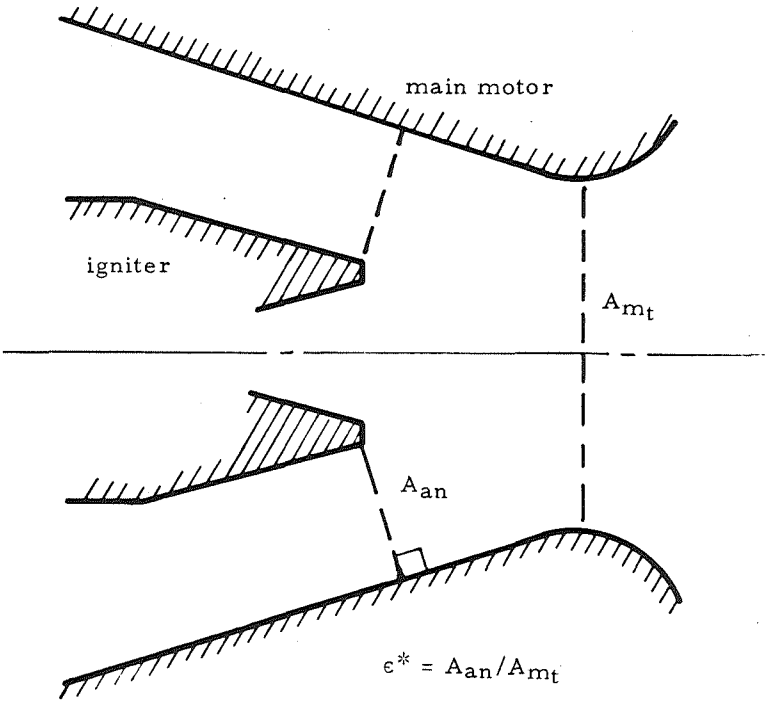

Figure 2. Epsilon Star—Igniter Placement Parameter

General Behavior

The behavior of the combined systems during the post-ignition period appeared to be many-faceted and usually random. The discovery of the existence of first unblocking, reblocking, oscillations, and final unblocking, coupled with the fact that the order of appearance of these different events varied from run to run, provided a good deal of speculation and confusion.

The basic instability of the overexpanded igniter-nozzle flow separation was recognized to be significant during the previous program. The operating conditions of the system under which unstable separation occurred, and its effect on the system, were not clearly identified at that time, however. During preparation for this program additional data evaluation was performed, which led to the conclusion that the behavior of the overall system was generally well-ordered and rational. It was found that the regions of blocking and unblocking and the oscillations could be separately and clearly mapped and that they were largely independent of each other.

Operating Maps

The blocking/unblocking and oscillation behavior of the hot motor test system is shown in Figure 3 as a function of PR and ϵ^*. These plots have been referred to as operating maps and define the regions in which specific behavior was observed and the boundaries at which specific events occurred.

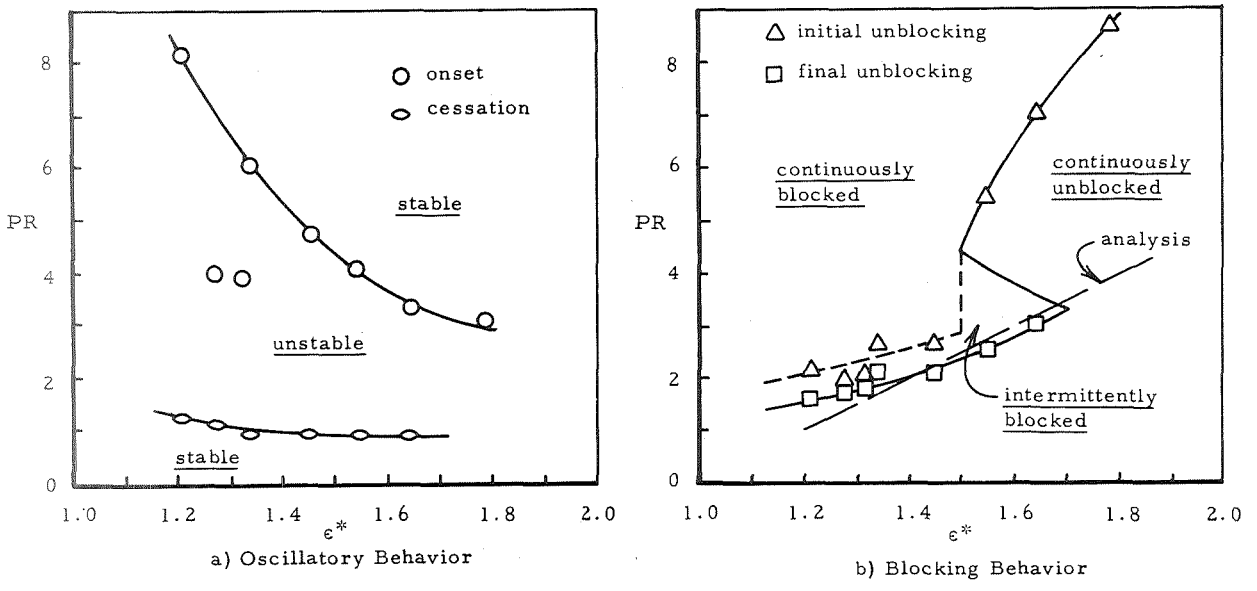

Figure 3. Hot-Firing Operating Maps

There are two regions of stable operation separated by one large unstable region, as shown. The upper boundary of the unstable region is most significant, the lower boundary being reached only when igniter action is

terminated. It will be customary, in this report, to identify events and conditions in terms of their appearance in the usual schedule of ignition of a motor. The upper boundary will be referred to as the "onset of oscillations," in the sense that the flow is first stable and then begins to oscillate at the boundary as the pressure ratio, PR, is decreasing.

The blocking map of Figure 3b shows three clearly separate regions of blocking conditions. First, there is a region at generally higher pressure ratios and low ε^* in which the main motor flow is continuously blocked. Second, there is a region at higher ε^* and lower pressure ratios, for which the flow is continuously unblocked. It is apparent that there are at least two specific flow structures or conditions which may exist, depending upon PR and ε^*, during a time of unblocking. The upper line, which is called initial unblocking, has its characteristic igniter/motor flow structure, while the lower line is called final unblocking, again in terms of a decreasing pressure ratio being the normal operating condition. There is a third peculiarly shaped region in which the motor throat intermittently reblocks and unblocks. In the third region it appears that the system is oscillating between the flow-field structures which are characteristic of the initial and final unblocking. The location of the unblocking predicted by the analytical model developed during the previous program (slightly modified to incorporate measured nozzle wall pressure distribution) is also shown in Figure 3b. The agreement between the analysis and the measured final unblocking strongly suggests that final unblocking occurs when the highly overexpanded igniter flow separates within its nozzle through a normal shock. This was the major assumption upon which the analytical model was based.

On the basis of a review of the literature[8, 9, 10] on severely overexpanded supersonic nozzles, it was concluded that the instabilities of the overall system were either triggered or more likely directly produced by inherent instabilities of the igniter-nozzle flow separation. Evaluation of the experimental data did not reveal evidence of motor instability or other flow interaction instability originating outside of the igniter nozzle.

Method of Approach

The program reported herein was undertaken with the objective of confirming, modifying, or rejecting the above evaluation of the behavior of the system. Because there was evidence that several flow-field structures might exist, the test apparatus was designed to provide for modeling the hot-firing system in accordance with several independent similiarity or scale factors, e.g., Mach numbers, pressure ratios, area ratios, Reynolds number effects. The flow system was designed to provide great latitude in establishing schedules for both increasing and decreasing pressure ratios between igniter and motor, and for varying absolute pressure. The test system was extensively instrumented with static pressure taps, affording a wide selection

of tap location and response rate to thoroughly map the steady-state and transient pressure distributions in both igniter and nozzle. It was anticipated that study and evaluation of the pressure distributions and comparison with analytical models would reveal the nature of the most significant flow fields.

3.2 EXPERIMENTAL ACTIVITIES

3.2.1 Description of Experiment

The experimental apparatus was designed to model the aft-end igniter and motor configurations tested during the program under Contract NAS-3-10297[1].

In the current program more extensive instrumentation was provided to characterize the igniter and motor nozzle flow interaction. The effects of variations in the igniter nozzle design parameters were studied. Motor and igniter sizes were designed to be as large as possible within the limits of the test facility airflow capacity.

Flow System

Design of the flow system was based upon results of trade-off studies which considered facility constraints, modeling requirements, and costs. A schematic of the flow system which resulted from these studies is shown in Figure 4. The system was designed within the constraints of the facility gas storage capacity (104 cu. ft., 2.94 m^3, at 2800 psia, 19.3 MN/m^2) and the maximum heater flow capacity (approximately 5 lb., 2.27 kg, of air/sec at 2000 psia, 13.79 MN/m^2, and 3400° R, 1889° K). It was calculated that a total gas flow of 18 lb/sec at 1000° R (8.172 kg/sec at 556° K) would provide acceptable model size and flow conditions within facility constraints. To achieve these conditions, facility equipment was replumbed to accommodate approximately a 3.4 lb/sec (1.544 kg/sec) heater flow and a 14.5 lb/sec (6.583 kg/sec) by-pass flow of cold air. The hot and cold air were mixed downstream of the heater in a mixing chamber. Maximum temperature and pressure conditions at the mixing chamber outlet were 1000° R (556° K) and 850 psia (5.86 MN/m^2), respectively. Downstream of the mixing chamber the flow was divided into supplies for the main motor and igniter. The main motor flow was passed through a multiple-hole round-edge orifice plate. By plugging varying numbers of holes in the orifice plate, the flow could be adjusted to provide motor chamber pressures between 75 and 100 psia (0.517 and 0.690 MN/m^2).

The igniter flow was passed through four parallel throttling valves, each in series with a solenoid-operated flow-shutoff valve. By presetting the igniter throttling valves and by proper sequencing of the solenoid valves during the test cycle, a maximum of ten different total pressure ratio steps (flow rates) could be achieved for any single test run.

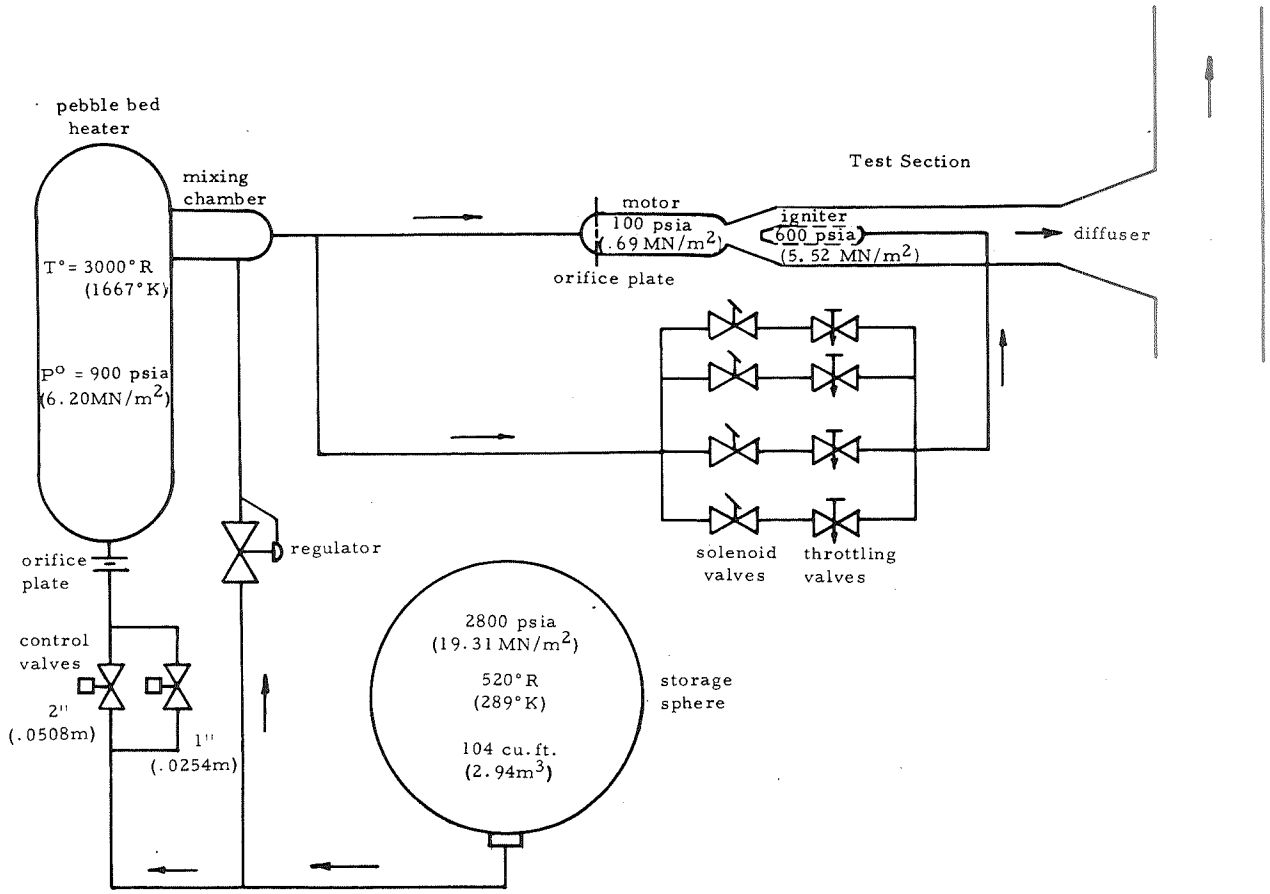

Figure 4. Flow System Schematic

A round-edge throttling nozzle was used in the pebble-bed heater supply line to limit the heater flow. Mixing chamber pressure and temperature were controlled through regulation of the cold airflow by a manually loaded pressure regulator in the cold air leg to the mixing chamber.

A diverging diffuser section was installed downstream of the test section flow ducting. This permitted testing at the sub-atmospheric flow duct pressures necessary for unseparated flow in the model motor nozzle. The diffuser section dumped into a vertical sound-suppression exhaust tower.

Thermal expansion stresses in the flow piping and ducting were minimized by two high-temperature ball-joint flexures. Fore and aft movement of the igniter within the igniter flow duct was permitted through use of a high-pressure stainless-steel flux hose.

Figure 5 shows a picture of the mixing chamber, flow system, and test sections downstream of the pebble-bed heater outlet.

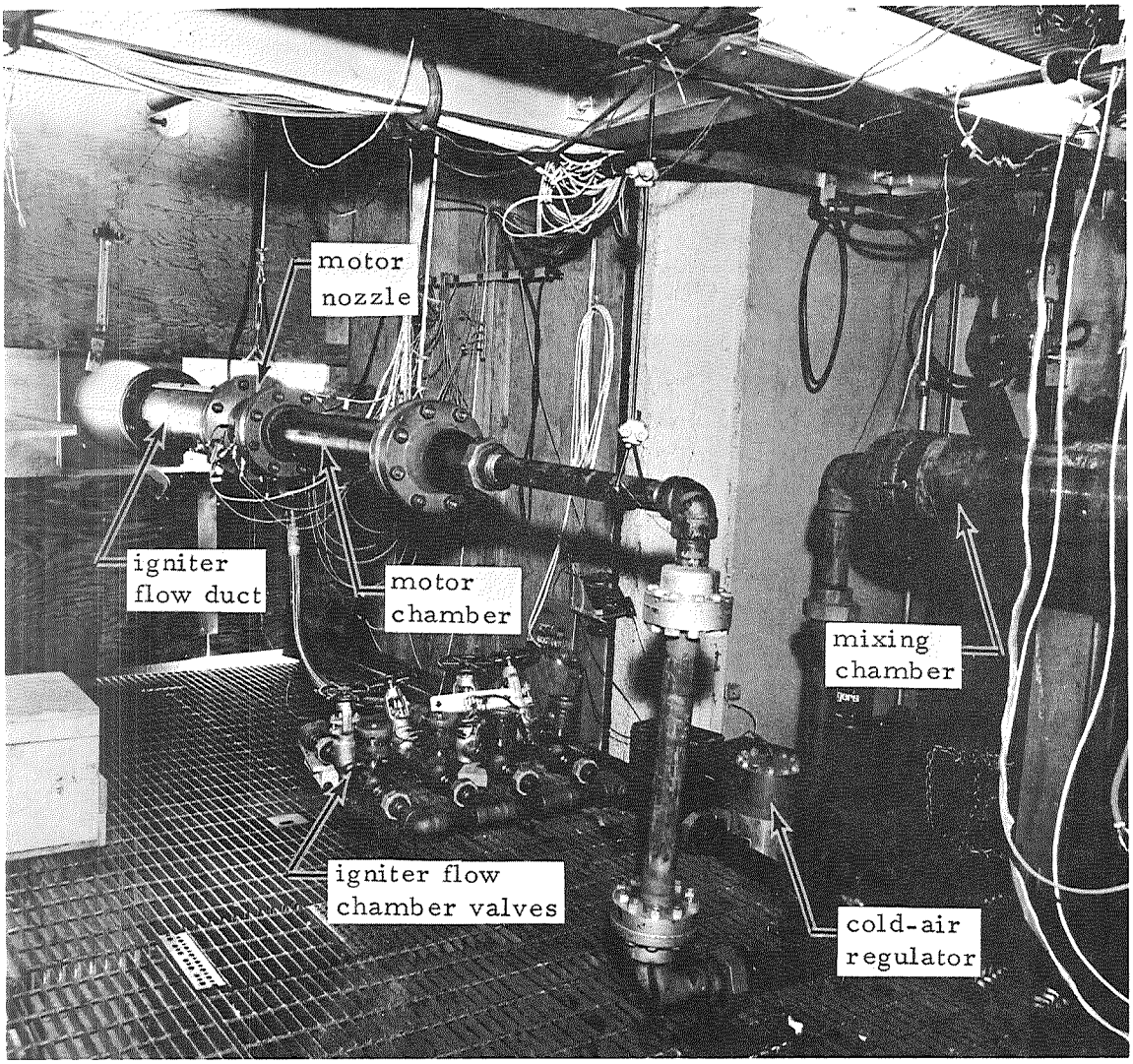

Figure 5. Experimental Apparatus

Mixing Chamber

A critical feature of the experiment design was the hot and cold air mixing chamber. The purpose of the mixing chamber was to completely mix the hot pebble-bed heater air with the cold by-pass air without excessive total pressure and temperature losses. Fabrication cost constraints dictated a fairly simple design without complex internal water-cooling passages.

The mixing chamber configuration, shown schematically in Figure 6, consisted of four fabricated components: the main body, inlet section, mixing tube, and large-volume mixing chamber. A picture of the mixer chamber components is shown in Figure 7. Critical elements of the design were the inlet section lip (subjected to the high-velocity heater air-gas stream) and the mixing tube.

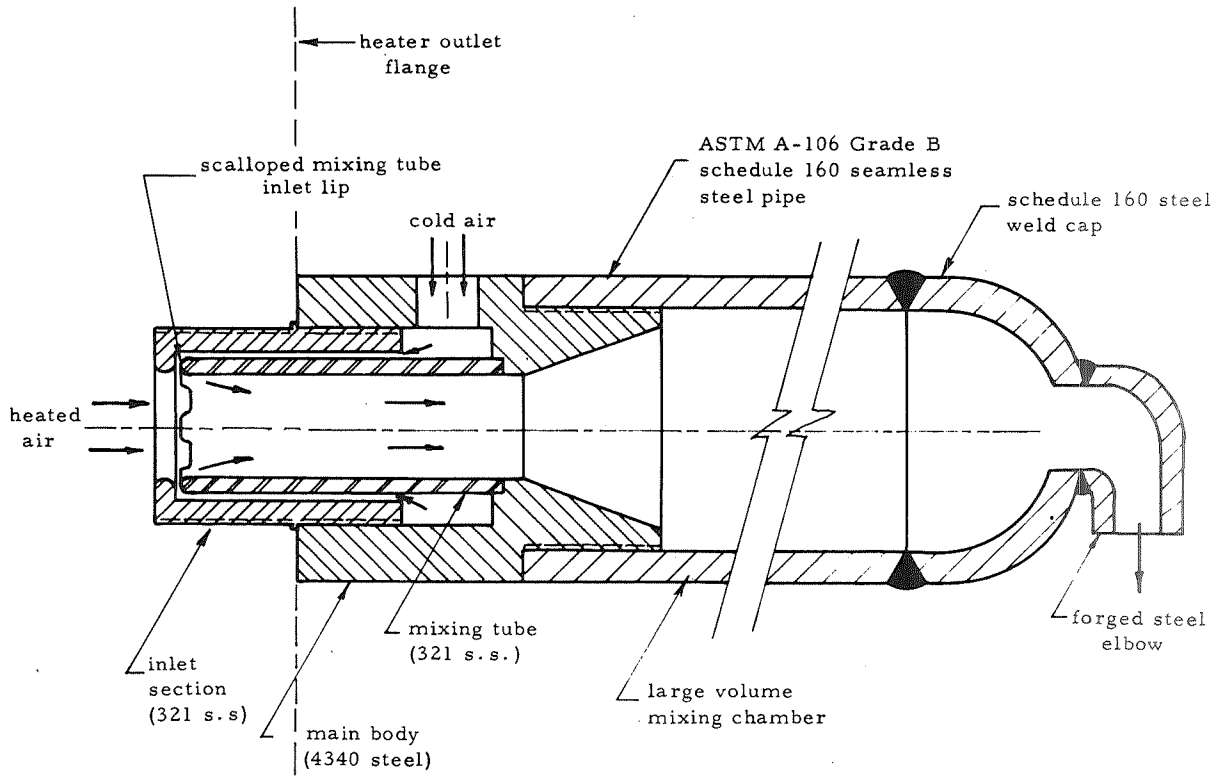

Figure 6. Mixing-Chamber Design Schematic

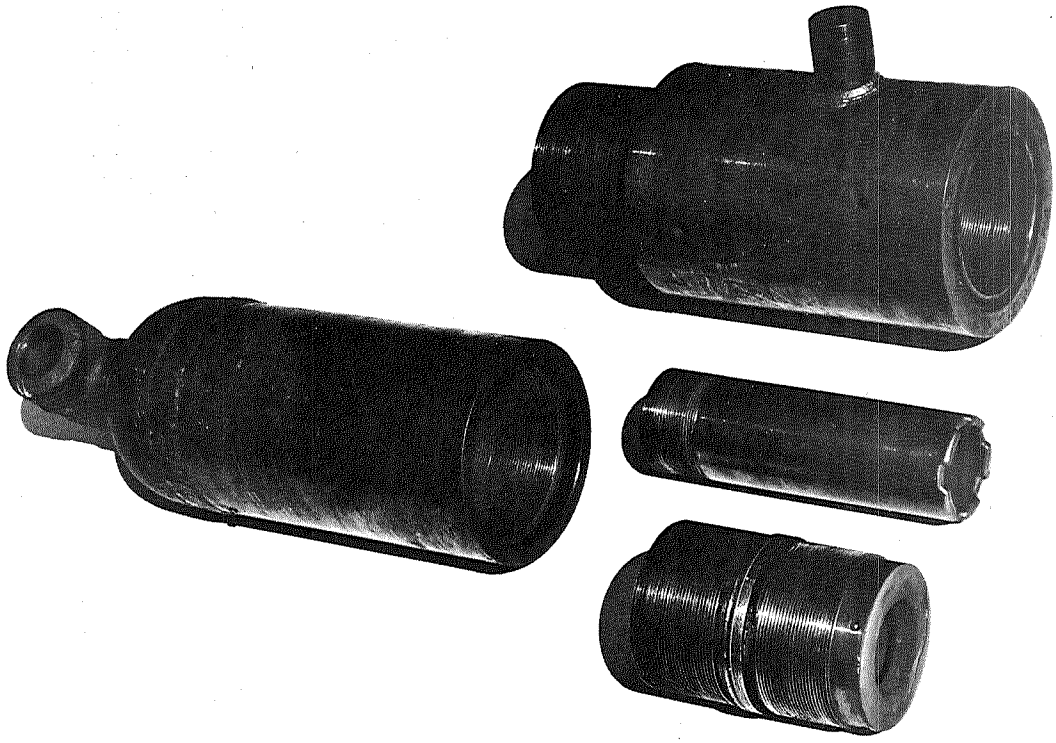

Figure 7. Mixing-Chamber Components

Heat transfer studies of the inlet lip configuration indicated that the lip should remain cool enough to retain sufficient structural strength for its intended use. However, the indicated safety factor was small because the assumed heat transfer coefficients were believed to be conservative. To guard against the possibility of error, the front face and lip of the inlet section were covered with an insulating Zi 0_2 coating. This covering consisted of an undercoating for better bonding, a coat of low-density thermospray Zi 0_2 for thermal protection, and a surface coat of plasma spray Zi 0_2 for erosion resistance. A coating of Zi 0_2 thermospray was sprayed on the interior surfaces of the large mixing chamber weld-end cap and outlet elbow for thermal protection.

The mixing tube was configured to mix the high-momentum hot and cold gas streams before they expanded into the large mixing chamber. To enhance mixing, the leading edge of the mixing tube was machined to have a scalloped or slotted configuration, as shown in Figure 8. Each slot was 0.25 inch (0.00635 m) deep and approximately 0.8 inch (0.0203 m) long. The clearance from the back face of the inlet section to the forwardmost part of the mixing tube was 0.0625 inch (0.00159 m).

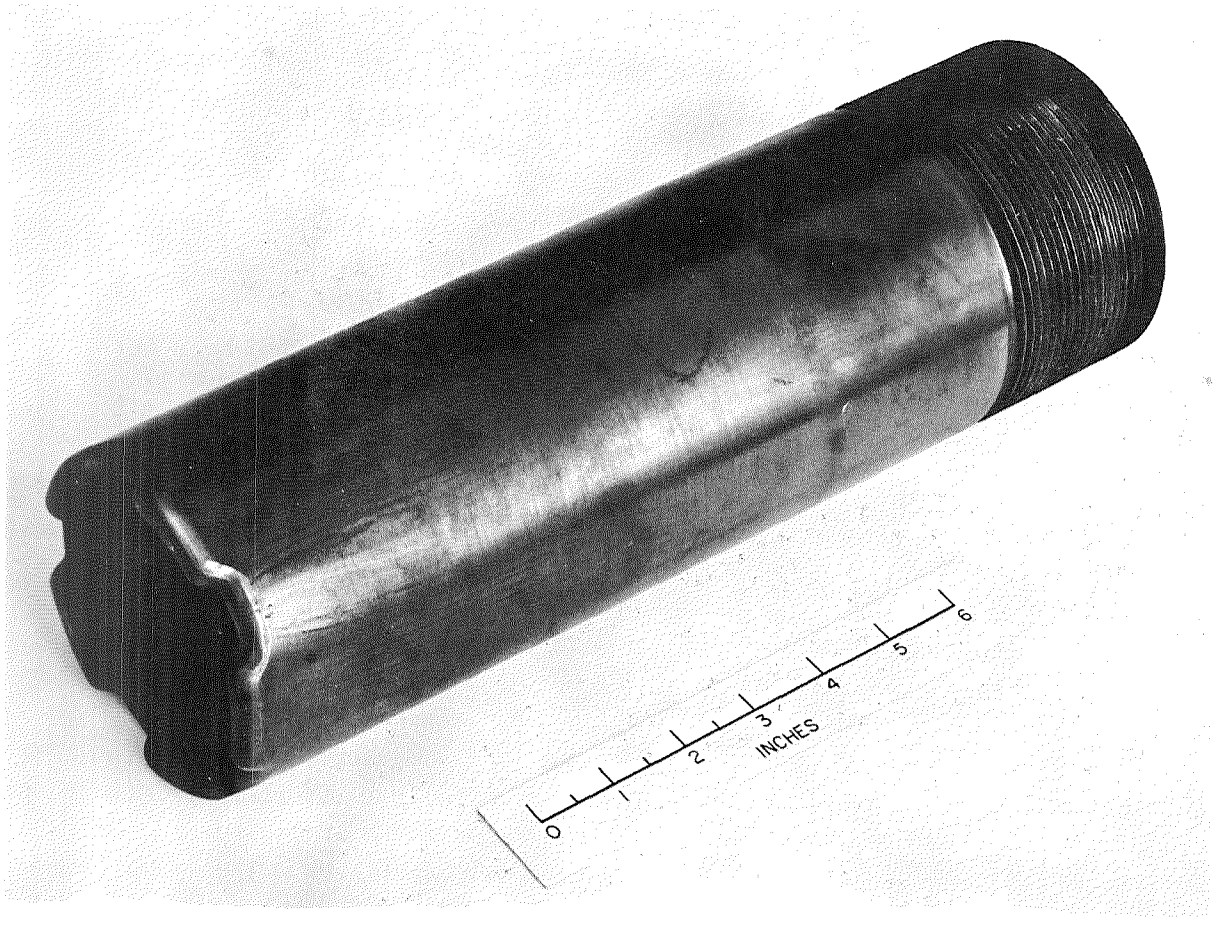

Figure 8. Mixing Tubes

The mixing-chamber assembly satisfactorily performed its intended function throughout the test program of over 130 hot airflow test cycles. Temperature-sensitive paint applied to the exterior surfaces of the mixer indicated that exterior temperatures did not exceed 500° F (533° K) even at the outlet elbow on the large mixing chamber. The mixed gas temperature at the mixer outlet did not exceed 600° F (589° K) for normal test conditions. Inspection of the mixer assembly after completion of the test program did not reveal any mixer component degradation, except for sand and pebble fragment erosion of the Zi 0_2 from the inlet section face and lip (see Figure 9).

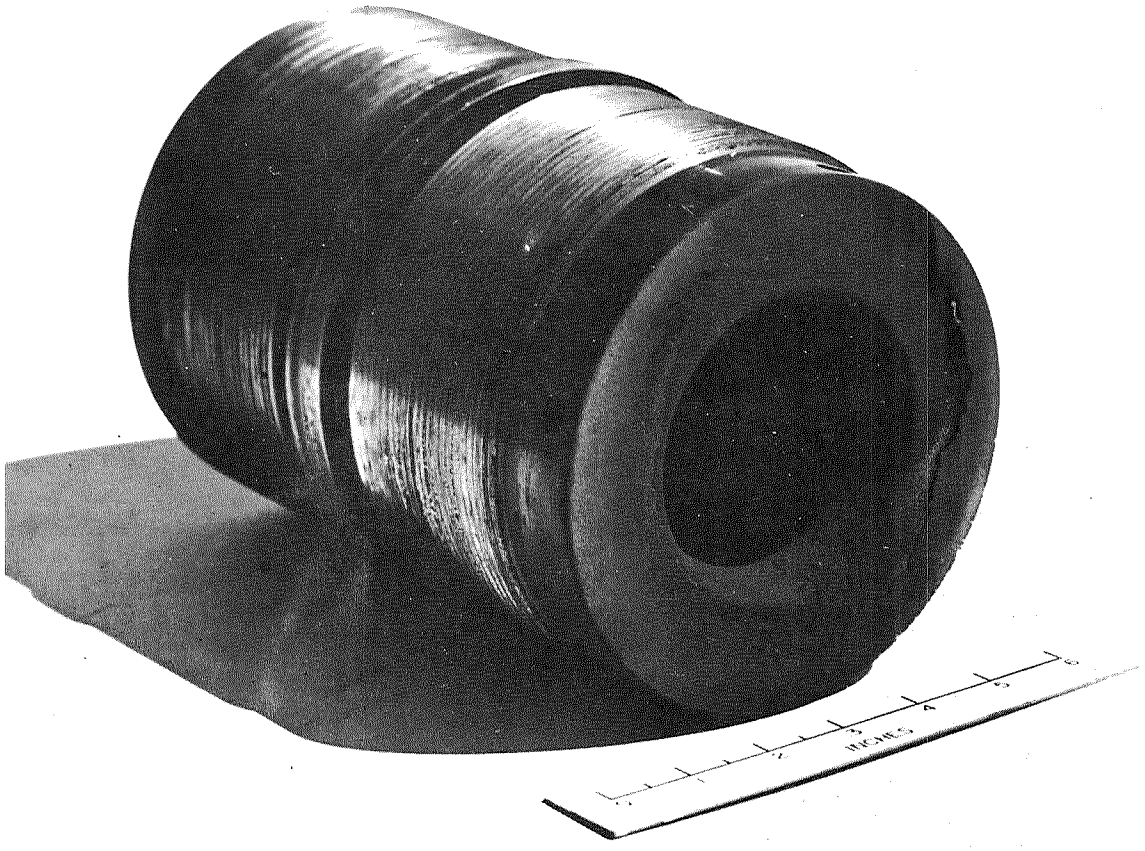

Figure 9. Mixing-Chamber Inlet Face

Models

Exact modeling requires geometric and dynamic similarity between prototype and model. For the aft-end experiments it was impossible to maintain dynamic similarity between the solid-propellant prototype and hot-air model because of differences in gas properties which define the isentropic flow relationships for geometrically similar locations. Specifically, the over-expanded igniter nozzle flow and shock relationships which are dependent

upon Mach number, static to total pressure ratio, and normal shock recovery pressure could not be exactly modeled because of differences in the gas specific heat ratios (γ). Therefore, the model igniter nozzle designs and expansion ratios deviated from geometric similarity with the prototype igniters, in order to obtain nozzle-exit flow conditions more closely approximating dynamic similarity. Geometric similarity on the other igniter and motor parameters was maintained.

A maximum model motor throat diameter of 3.0 inch (0.0762 m) was established by facility temperature, mass flow, and mass capacity constraints. A comparison of basic prototype and model dimensions is presented in Table I.

TABLE I

Model Design Parameter Comparison

Parameter	Prototype	Model
Motor		
Throat Diameter - D_m^*, in. (m)	5.0 (0.127)	3.00 (0.0762)
Expansion Ratio - A_e/A_m^*	10.0:1	7.0:1
Nozzle Half Angle, deg (rad)	17.5 (0.305)	17.5 (0.305)
Design Chamber Pressure, psia (MN/m^2)	500.0 (3.448)	100.0 (0.69)
Igniter		
Throat Diameter - D_i^*, in. (m)	0.885 (0.0225)	0.531 (0.0135)
Expansion Ratio - A_e/A_i^*	10.0:1	6.98:1
Nozzle Half Angle, deg (rad)	17.5 (0.305)	17.5 (0.305)
Design Chamber Pressure (max), psia (MN/m^2)	2750.0 (18.96)	650.0 (4.48)

The test section assembly (Figure 10) included a motor chamber, a motor nozzle, and an igniter assembly. The igniter assembly was enclosed within an igniter flow duct which contained the igniter and motor gases and positioned the igniter with respect to the motor nozzle. An access port was provided in the duct to permit positioning and aligning the igniter.

The model motor was fabricated from steel pipe, pipe flanges, and a flow-expander section. The 35 inch (0.889 m) long by 5.0 inch (0.127 m) diameter port was similar to the initial cylindrical port area of the solid-propellant motor. An orifice plate with nineteen 0.3125 inch (0.00794 m) diameter round-edged orifices for choking the main motor flow was located in between the two flanges at the model head-end.

The motor nozzle, which was fabricated from a single steel billet, is shown in Figure 11. It was designed to be geometrically similar to the prototype solid-propellant motor nozzle.

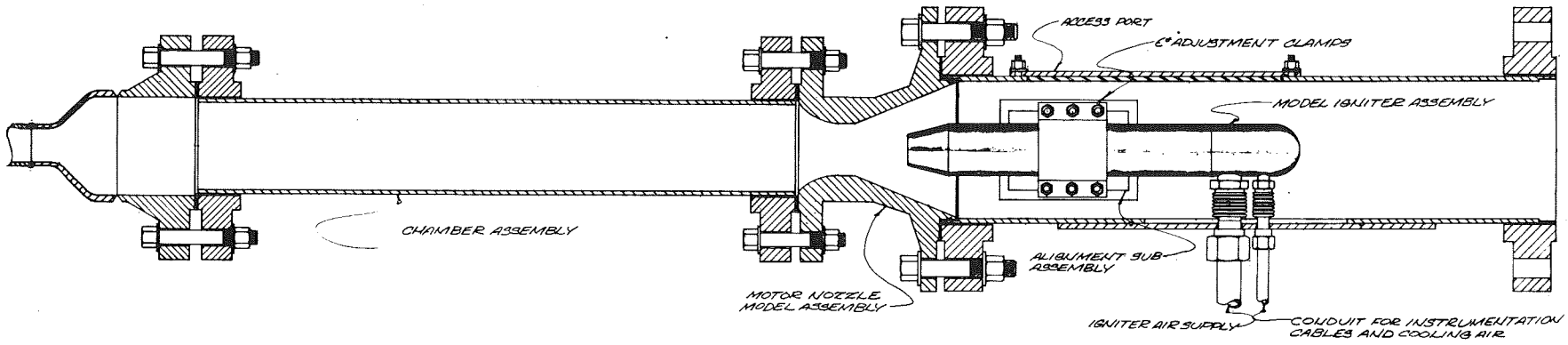

Figure 10. Test Section Assembly

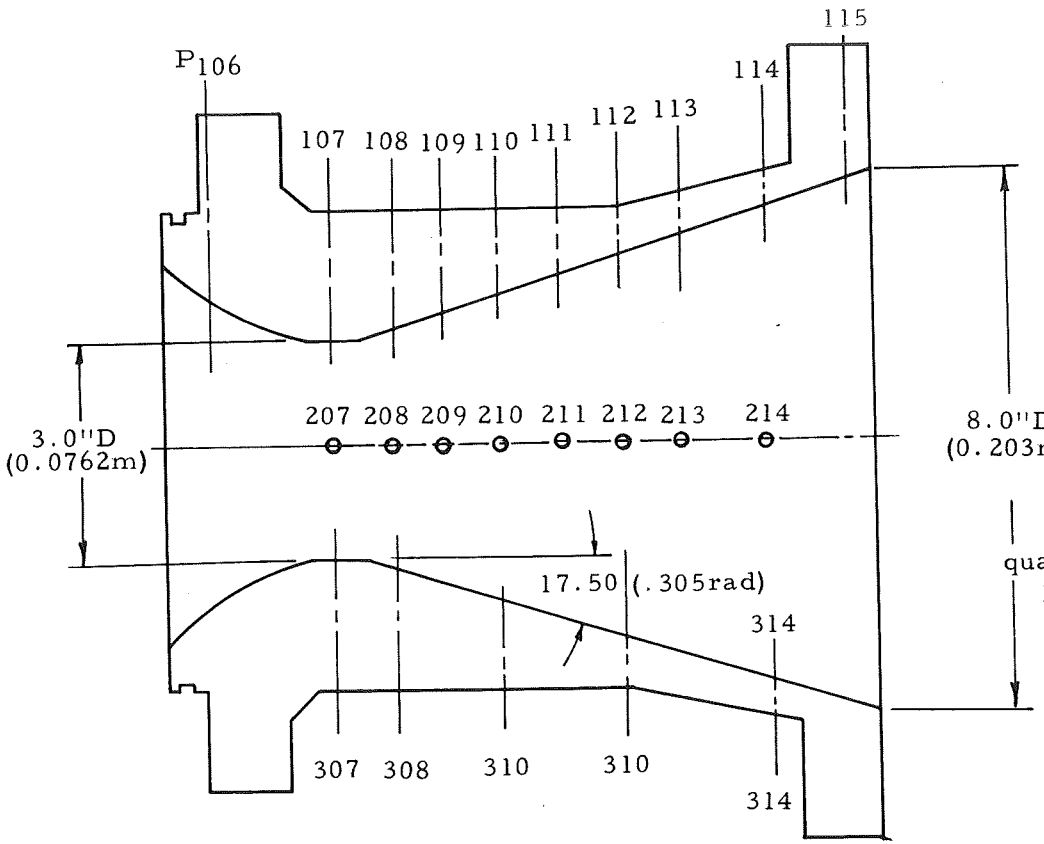

P_{xxx}	A/A^*
X06	1.59
X07	1.00
X08	1.16
X09	1.49
X10	1.86
X11	2.38
X12	2.97
X13	3.63
X14	4.60
X15	5.69

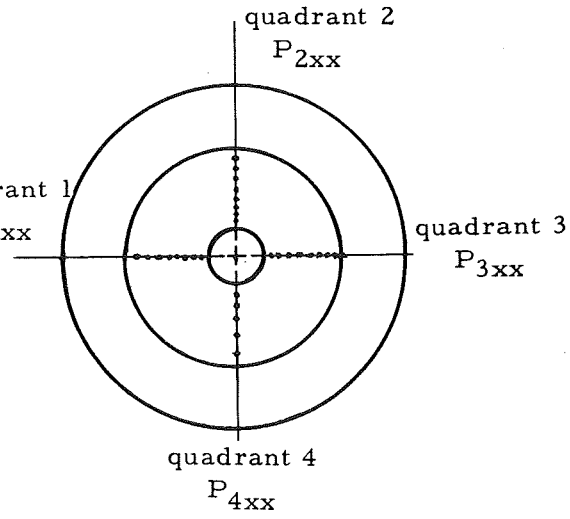

Quadrant Arrangement

Figure 11. Motor Nozzle

Major features of the igniter assembly were the high-pressure feed line with flexible hose, the igniter chamber, and interchangeable igniter nozzle and exterior sleeves (Figure 12). The assembly design provided space for installation of miniature pressure transducers and pressure lines between the igniter nozzle and exterior sleeve and permitted the use of different igniter nozzle configurations. Five basic configurations designated as Models A, B, C, D, and E were used. Table II presents the significant design parameters of each of these models. The Model A configuration was also modified to test methods of nozzle oscillation control. The first method incorporated bleed or boundary layer pressurization in the nozzle exit cone. The two configurations used to test this method, designated as AB1 and AB2, are shown in Figure 13. The other method used various step configurations designated as AS1, AS2, and AS3. These nozzles are schematically shown in Figure 14.

TABLE II

Igniter Design Parameters

	Hot Firing Prototype	Model A	B	C	D	E**
Throat Dia., in.	0.885	0.531	.0.463	0.531	0.463	0.531
(m)	(0.0225)	(0.0135)	(0.0118)	(0.0135)	(0.0118)	(0.0135)
Exit Dia., in.	2.80	1.405	1.405	1.1875	1.256	1.405
(m)	(0.0711)	(0.0357)	(0.0357)	(0.0302)	(0.0319)	(0.0357)
Expansion Ratio	10.0:1	7.0:1	9.2:1	5.0:1	7.0:1	7.0:1
Half Angle, deg	17.5	17.5	17.5	17.5	17.5	17.5
(rad)	(0.305)	(0.305)	(0.305)	(0.305)	(0.305)	(0.305)
Lip Dia., in.	3.375	1.693	1.693	1.431	1.513	2.000
(m)	(0.0857)	(0.043)	(0.043)	(0.0363)	(0.0384)	(0.0508)
Lip to Exit Diameter Ratio	1.205	1.205	1.205	1.205	1.205	1.423
P_e/P^o	0.0125	0.0125	0.00828	0.02114	0.0125	0.0125
P_2^o/P_1^{o*}	0.1603	0.2075	0.1603	0.02835	0.2075	0.2075

* Total pressure ratio across normal shock

** Same as Model "A" but with exterior sleeve

The igniter nozzle assembly was positioned within the igniter flow duct by a clamp and T-plate arrangement which rested in a well in the bottom of the flow duct. Curved slots were cut into the bottom of the T-plate so that it could be rotated with respect to the motor nozzle for angular misalignment. The base plate in the flow duct well could be moved in a lateral direction to provide lateral misalignment. Extreme care was taken in the fabrication of the nozzle, igniter, and flow duct components to insure proper alignment of the igniter and motor nozzle. Four milled reference flats and tap holes placed 90° (1.57 rad) apart were provided on both the flow duct and motor nozzle to permit the use of depth gages in setting the igniter ϵ^* location or in misaligning the igniter.

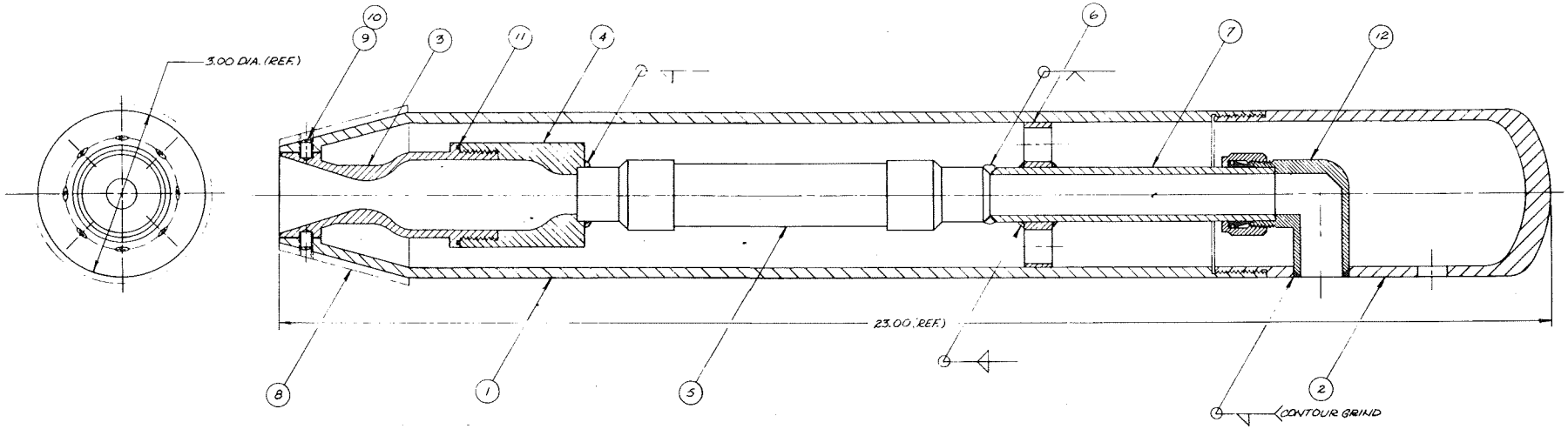

NO	QTY.	DESCRIPTION	MATL.
12	1	BUTT WELD ELBOW (SWAGELOK) #6W0-2-12M	BRASS
11	1	O-RING (PARKER) #E-031-E	RUBBER
10	8	1/4-28 UNF-3A x .438 LG. FL. PT. SET SCR.	STL.
9	8	1/4-28 UNF-3A x .312 LG. FL. PT. SET SCR.	STL.
8	1	DWG. 01900-17, EXTERIOR SLEEVE	N/A
7	1	DWG. 01900-18, EXTENSION	N/A
6	1	DWG. 01900-12, SPACER	N/A
5	1	DWG. 01900-11, FLEX HOSE	N/A
4	1	DWG. 01900-13, CHAMBER	N/A
3	4	DWG. 01900-16, NOZZLE	N/A
2	1	DWG. 01900-15, AFT-BODY	N/A
1	3	DWG. 01900-14, FORE-BODY	N/A

PARTS LIST

DWN. BY: [illegible] | APP'D. ENG: JDK | DATE: 10-1-65

CETEC IGNITER ASSEMBLY

HYPERSONIC WIND TUNNEL

UNLESS OTHERWISE SPECIFIED .X ± — .XX ± — .XXX ± — ANGLE ± — FINISH ± — | SCALE: FULL | MAT'L.: | D | 01900-6

Figure 12. Igniter Assembly

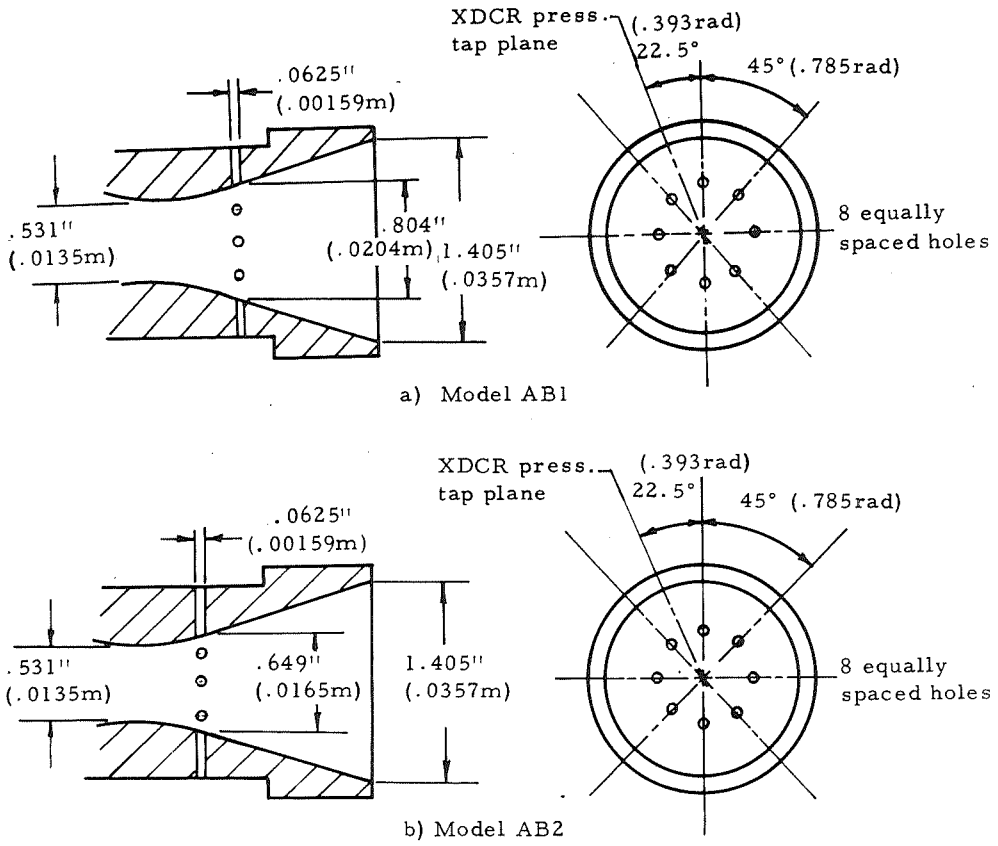

Figure 13. Igniter Perforated-Nozzle Configurations

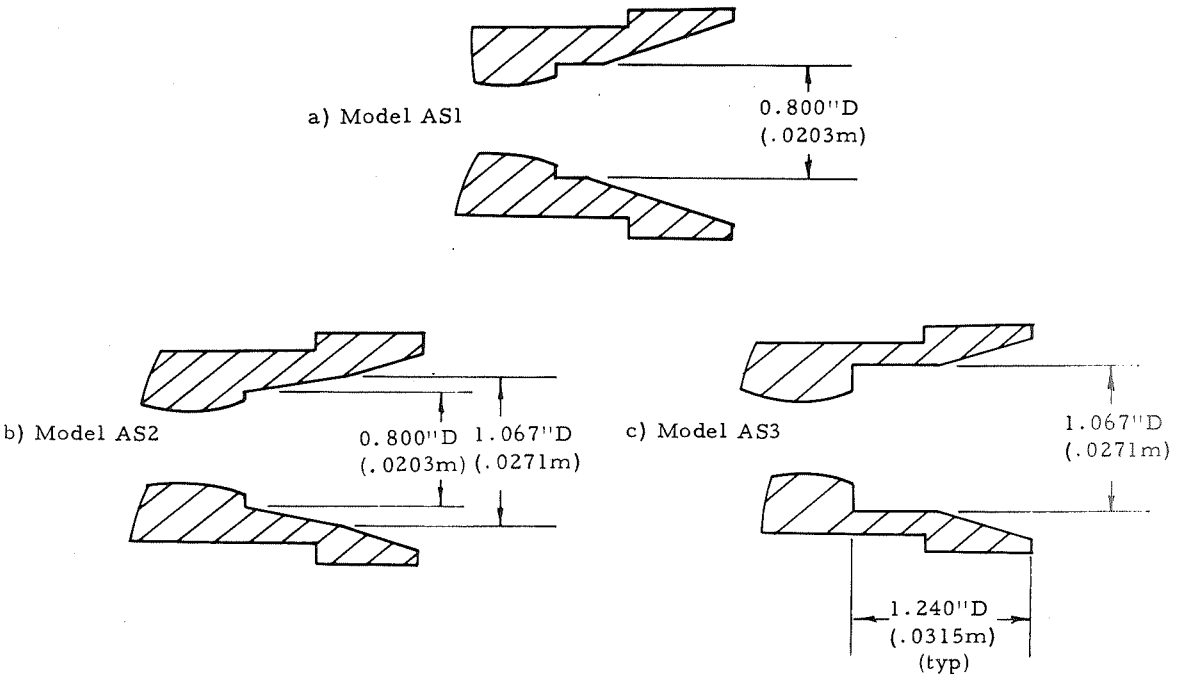

Figure 14. Stepped Igniter-Nozzle Configurations

Instrumentation

Motor and igniter pressure taps (0.055 inch, 0.0014 m, dia.) were located as shown in Figures 11 and 15. Motor-nozzle pressure-tap line lengths were approximately 3 inches (0.0762 m). The igniter pressure-tap lines were approximately 30 inches (0.762 m) in length in order to locate the transducers outside of the high-temperature environment of the igniter assembly. The length of the igniter sense lines resulted in some attenuation of high-frequency pressure oscillations, but did not appreciably affect the major oscillatory characteristics or phase relationships between the pressure taps.

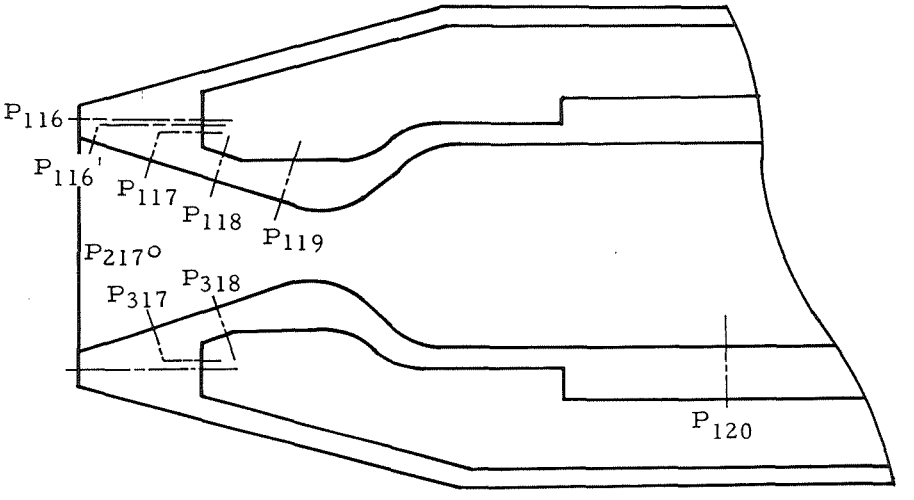

Model	A&E	B	C	D
$P_{117, 217, 317}$	3.90	5.07	3.54	3.84
$P_{118, 318}$	2.74	3.02	2.50	2.74
$P_{119, 319}$	1.82	1.51	1.64	1.81
$P_{116'}$	6.27			

Figure 15. Igniter-Nozzle Pressure-Tap Locations

A maximum of 24 pressure measurements was available for use on any test. Actual tap locations used during each test were varied according to test objective. Typical measurements of each test included: motor and igniter chamber pressure, three to five igniter nozzle pressure measurements, from nine to twelve motor nozzle pressure measurements, and motor total temperature. Igniter total temperature was measured on selected runs to compare igniter and motor total temperatures.

Temperature measurements were made with fast-response thermocouples, and pressures were measured with strain gage and semi-conductor pressure transducers.

Transducer test data were recorded on an oscillograph equipped with a direct-read recording magazine. Galvanometers which exceeded the minimum desirable frequency response for each measurement were used. Power amplification for six high-frequency-response galvanometers was provided by six D. C. differential amplifiers. Transducer excitation was provided with heavy-duty batteries.

Additional flow system measurements including mixing chamber pressure and temperature, motor chamber pressure and temperature, and pebble-bed pressure were recorded on a slow-speed strip chart. These measurements were used for real-time surveillance and control of the test airflow system.

3.2.2 Testing

Test Procedure

Test procedures were established to produce accurate and reliable data with minimum test recycle time. Data accuracy was provided by running pre-test and post-test calibrations on all pressure transducers and thermocouples. The strain gage pressure transducers were electrically calibrated to full transducer scale by use of a calibration resistor in the balancing bridge circuits. The miniature solid-state transducers were placed on a pressure manifold and calibrated against a standardized pressure gage. The thermocouples were calibrated by introducing a known millivolt electrical source into the thermocouple fitting at the measurement location. The zero and 100 percent calibration steps obtained by these methods were recorded on the oscillograph paper with its respective test run. The electrical calibration of the strain gages was periodically checked by placing the transducers on a pressure manifold which was pressurized to 25, 50, 75, and 100 percent of full transducer scale as determined by a standardized (tested with a dead-weight tester) pressure gage. The electrical and pressure calibrations were then compared and appropriate correction factors were assigned to each transducer electrical calibration for the purpose of data reduction.

Test recycle time was primarily a function of the time required to regain sufficient temperature (heat) in the pebble-bed heater and to recharge the high-pressure storage sphere. Initial heat-up time, i.e., the time to reach a stabilized temperature throughout the pebble bed with an indicated top bed temperature of 3000°F (1922°K), was from three to four days. For this reason the pebble-bed heater system was run continuously for the six- month test duration except when shut down for emergency repairs or for testing. During each test the temperature at the top of the pebble bed dropped approximately 400° to 500°F (478° to 533°K). Heating recovery time to regain a satisfactory pre-test temperature of 2800° to 3000°F (1811° to 1922°K) was approximately one hour.

Compressor run time to repressurize the high-pressure air-storage sphere was two hours and forty minutes with one compressor and one hour and twenty minutes with two compressors. One of the two facility compressors was inoperative with mechanical problems during a significant portion of the test program.

All tests were conducted after 5:00 p.m. because of the extreme noise generated by the experiment.

The igniter ε^* position and alignment or misalignment were set prior to each test. This task was accomplished by adjusting the igniter position within the clamping and aligning devices and by verifying proper placement with depth measurements at four locations on the motor nozzle and four locations on the igniter flow duct.

Each test was started by simultaneously opening the air-supply regulator valves on both the hot and the cold flow legs to the pebble bed and mixing chamber (see Figure 4). Approximately 20 seconds were required to reach a steady-state operating pressure of 800 psi (5.516 MN/m^2) in the pebble-bed heater and mixing chamber. Another 10 seconds under full-flow conditions were required before the mixing-chamber temperature reached 400° - 500° F (478° - 533° K). At that time, the total temperature of the main-motor gases was approximately 300° - 400° F (422° - 478° K). During this start-up period the hot gases from the mixing chamber were allowed to flow through the igniter sequencing valves as well as the main-motor valve, heating up the hardware to temperatures approaching the gas temperature. The automatic test sequencer was activated when the desired steady-state operating conditions were reached in the mixing chamber. The test sequencer automatically turned the oscillograph recorder to high speed and sequentially closed and reopened the igniter throttling valves. The automatic sequence during which test data was recorded lasted about 7 seconds with approximately 0.7 second between successive valve opening or closing signals. During this period the motor chamber pressure was essentially constant except for blockage perturbations while the igniter pressure changed plateau levels. Typical pressure and test events during a test cycle are shown schematically in Figure 16.

Test shut-down was accomplished by closing the hydraulic-controlled air-supply valve to the pebble-bed heater. Overheating of the test equipment was prevented by bleeding cold air into the mixing chamber with the manually operated pressure regulator during the hot-gas blowdown of the pebble bed. Post-test calibrations were completed and preparations for the next test were made.

Special Problems

Twenty tests were required to check out and calibrate the facility airflow system, pebble-bed heater, and instrumentation and to establish final test procedures.

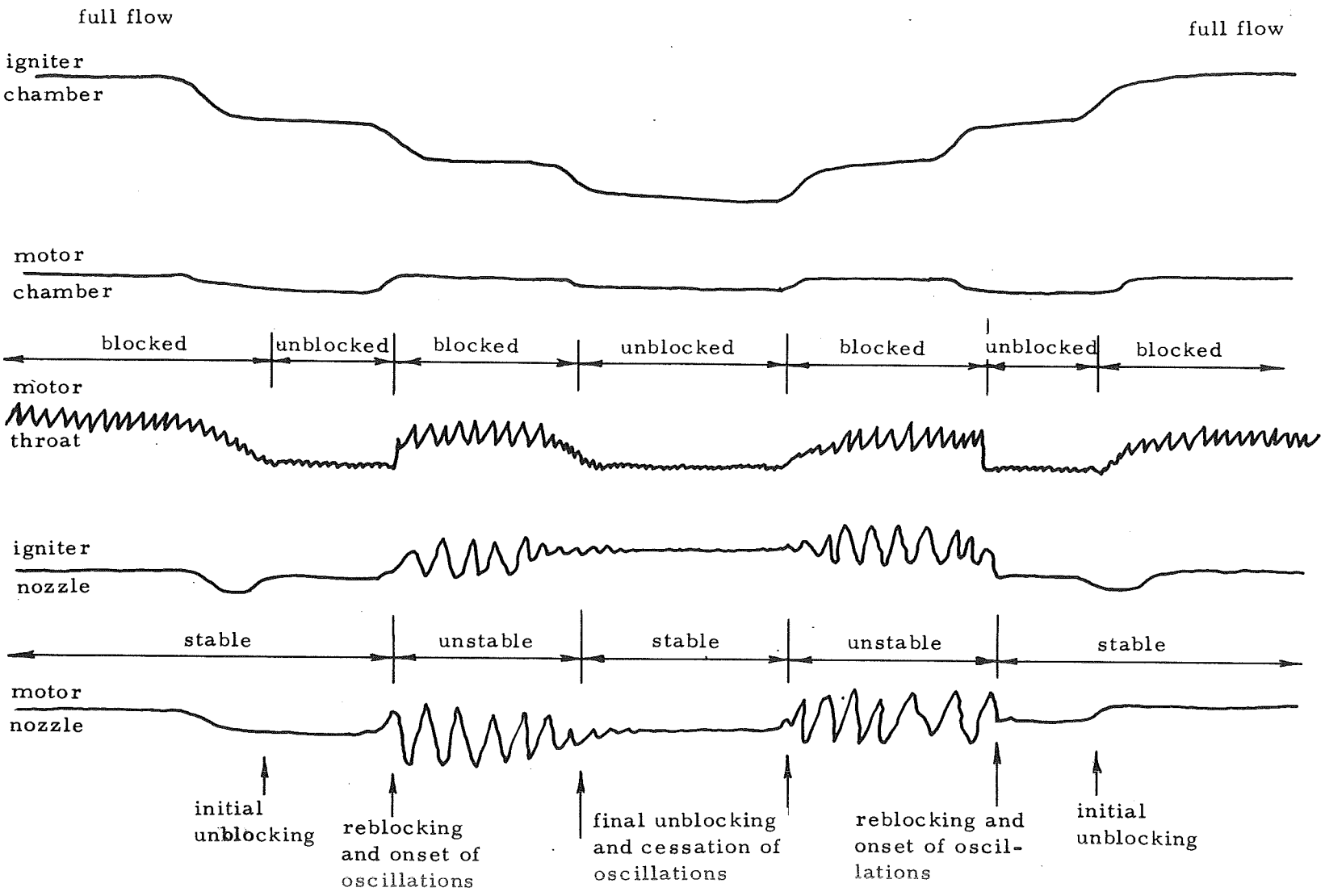

Figure 16. Schematic of Pressures and Events During Test Cycle

A large throttling valve was initially used to throttle the main motor flow. This resulted in an excessive pressure drop and the valve was replaced by a multiple-hole orifice plate at the model motor head-end. Cold airflow to the mixing chamber was also lower than desired because of excessive pipe flow-pressure losses. The cold-air pressure regulator was subsequently moved from its location adjacent to the storage sphere and placed just upstream of the mixing chamber.

Considerable trouble was experienced with the solenoid-actuated igniter throttling valves. Sand and dust from the pebble-bed heater frequently lodged between the valve piston and body, restricting opening or closing during the test. This problem was somewhat alleviated by cleaning and lubricating the valves just prior to each test and by replacing the stainless-steel valve rings with teflon rings.

Original plans called for installation of miniature solid-state pressure transducers in the igniter assembly cavity between the igniter nozzle and the exterior sleeve. However, problems were encountered in obtaining the proper calibration resistor for calibrating the transducers electrically. The hot environment inside the cavity and the requirement for adequate cavity cooling to prevent transducer damage were also of concern. These problems were resolved by mounting the transducers outside the igniter flow duct.

Test Conditions

Test conditions were varied to accomplish test objectives defined under the general categories of (1) flow characterization, (2) oscillation-control techniques, (3) misalignment effects, and (4) lift-off effects.

Five basic igniter nozzle configurations were used to characterize the flow interactions in the motor and igniter nozzles. Each configuration was tested by conducting a range of pressure ratios for selected ϵ^* locations between 1.20 and 1.80. For most tests the pressure ratios ranged from a value sufficient to cause main-motor throat blockage to an igniter-off condition (PR = 0). For high ϵ^* values it was necessary to reduce the main-motor chamber pressure to approximately 75 psia (0.517 MN/m^2). A number of tests were duplicated with identical test conditions, but with changes in instrumentation to provide more complete data than could be acquired from a single test. Tests were also run for identical ϵ^* locations, but at different absolute motor chamber pressures to verify that the observed phenomena were dependent only upon relative igniter to motor pressures and mass flows.

Igniter Model A configuration was modified and tested to evaluate techniques for igniter- and motor-nozzle-oscillation suppression or control. The first two techniques, using igniter Models AB1 and AB2, attempted to retard igniter-nozzle boundary-layer separation and hence unstable nozzle flow by boundary layer suction and blowing. A third technique used steps of varying

sizes (Models AS1, AS2, and AS3) to modify the igniter-nozzle flow-separation characteristics.

Several tests were conducted at selected igniter ϵ^* locations and PR values with sudden igniter termination to demonstrate satisfactory igniter operation without motor-nozzle blockage or oscillations.

Misalignment tests were conducted to define the effects of igniter-nozzle misalignment on motor-nozzle pressure distribution and characteristic operating conditions. Model A tests were conducted for the lateral, angular, lateral plus angular, and lateral minus angular geometries shown in Figure 17. Lateral misalignments were always 3 percent of the motor throat diameter (0.09 inch, 0.00229 m) and angular misalignments were restricted to angles of 1.5 degrees (0.0262 rad). Model B was tested for lateral misalignments only. Both models were tested over a wide ϵ^* and PR range.

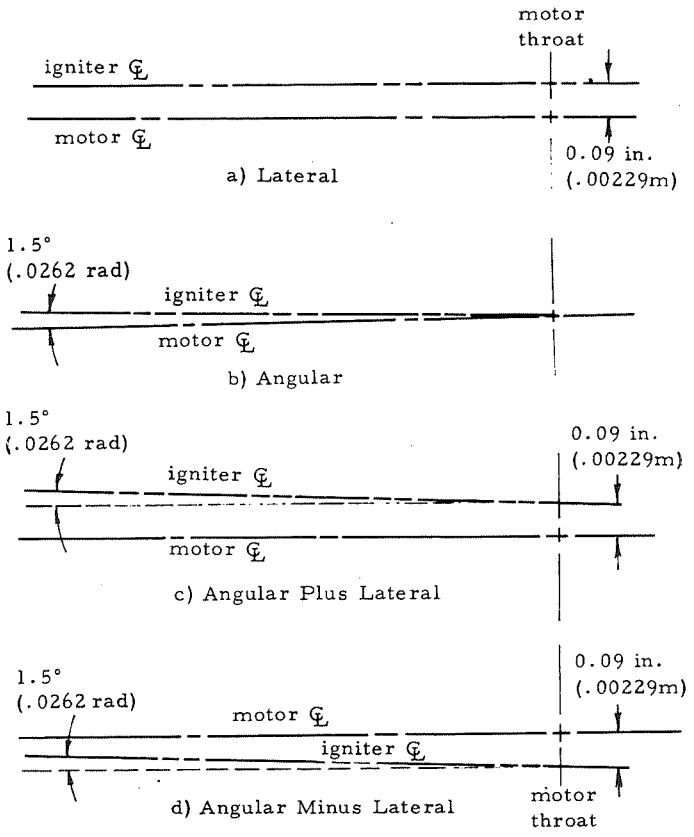

Figure 17. Misalignment Geometries

Lift-off tests were run at ϵ^* values from 2.0 to 3.0 (higher than those which would generally be used for ignition) to investigate the characteristic nozzle interactions which would occur during motor lift-off or igniter ejection.

A summary of all tests conducted, listing significant test conditions or objectives, is given in Table III.

TABLE III

Test Summary

Date	Test No.	Model	ϵ^*	Comments
2/20 - 3/18	1-19	A	1.2 -	checkout
3/25	20	B	1.82	characterization
3/26	21	B	1.65	"
3/26	22	B	1.49	"
3/27	23	B	1.32	"
3/27	24	B	1.19	"
3/27	25	B	1.24	"
4/1	26	C	1.24	"
4/1	27	C	1.36	"
4/2	28	C	1.51	"
4/3	29	C	1.67	"
4/3	30	C	1.79	"
4/7	31	E	1.21	"
4/7	32	E	1.34	"
4/8	33	E	1.48	characterization, high motor P^o
4/8	34	E	1.48	" low " "
4/8	35	E	1.64	"
4/9	36	E	1.79	characterization
4/10	37	E	1.40	"
4/10	38	E	1.40	"
4/13	39	E	1.28	"
4/14	40	A	1.31	"
4/14	41	A	1.53	"
4/15	42	A	1.61	"
4/17	43	D	1.82	"
4/17	44	D	1.66	"
4/22	45	D	1.50	characterization, low motor P^o
4/22	46	D	1.50	" high " "
4/22	47	D	1.36	characterization
4/23	48	D	1.20	"
4/23	49	D	1.42	"
4/24	50	D	1.55	"
4/24	51	D	1.28	"
4/27	52	AB1	1.50	osc. control, ign. cavity press 25 psia (0.172 MN/m^2)
4/28	53	AB1	1.50	" " " " " 50 " (0.345 MN/m^2)
4/28	54	AB1	1.50	" " " " " 75 " (0.517 MN/m^2)
4/29	55	AB1	1.50	" " low cavity vacuum
5/6	56	AB1	1.50	" " medium " "
5/6	57	AB1	1.65	" " " " "
5/7	58	AB1	1.78	" " " " "
5/8	59	AB1	1.34	" " " " "
5/8	60	AB1	1.18	" " " " "
5/11	61	AB1	1.79	" " " " "
5/11	62	AB1	1.66	" " " " "
5/12	63	A	1.80	characterization
5/13	64	A	1.64	"
5/13	65	A	1.48	"
5/14	66	A	2.00	lift-off
5/14	67	A	2.38	" "
5/15	68	A	3.00	" "
5/18	69	A	3.00	" "
5/19	70	AB2	1.51	osc. control, medium cavity vacuum
5/20	71	AB2	1.51	" " " " "
5/20	72	AB2	1.65	" " " " "
5/22	73	C	1.82	lift-off
5/26	74	C	2.01	" "
5/26	75	C	2.49	" "
5/26	76	C	1.67	characterization
5/27	77	B	1.42	"
5/27	78	B	1.59	"
6/2	79	B	1.72	"

TABLE III

Test Summary (concluded)

Date	Test No.	Model	ϵ^*	Comments
6/2	80	B	1.28	characterization
6/3	81	B	1.29	misalignment, lateral
6/3	82	B	1.45	" "
6/4	83	B	1.65	" "
6/5	84	B	1.82	" "
6/5	85	B	2.01	" "
6/8	86	A	1.20	" "
6/9	87	A	1.51	" "
6/9	88	A	1.81	" "
6/10	89	A	1.98	" "
6/10	90	A	1.64	" "
6/10	91	A	1.66	" angular
6/12	92	A	1.81	" "
6/15	93	A	1.50	" "
6/16	94	A	1.34	" "
6/17	95	A	1.50	" angular plus lateral
6/17	96	A	1.65	" " " "
6/18	97	A	1.79	" " " "
6/18	98	A	1.97	" " " "
6/19	99	A	1.97	" angular minus lateral
6/22	100	A	1.80	" " " "
6/23	101	A	1.65	" " " "
6/24	102	A	1.51	" " " "
6/24	103	A	1.35	" " " "
6/26	104	C	1.43	characterization
6/29	105	C	1.58	"
6/29	106	C	1.74	"
6/30	107	C	1.90	"
7/1	108	C	1.30	"
7/1	109	C	1.59	"
7/2	110	A	1.35	characterization, instrumentation changes
7/6	111	A	1.35	" " "
7/6	112	A	1.50	" " "
7/7	113	A	1.50	" " "
7/7	114	A	1.74	" " "
7/9	115	A	1.74	" " "
7/9	116	A	1.20	" " "
7/10	117	AS1	1.50	osc. control
7/15	118	AS1	1.64	" "
7/15	119	AS1	1.79	" "
7/16	120	AS1	1.99	" "
7/16	121	AS1	1.99	" "
7/17	122	AS1	1.34	" "
7/17	123	AS1	1.34	" "
7/21	124	A	1.35	characterization, instrumentation changes
7/22	125	A	1.20	" " "
7/23	126	A	1.80	" " "
7/23	127	A	1.34	" " "
7/24	128	A	1.35	" " "
7/24	129	A	1.80	" " "
7/27	130	AS2	1.49	osc. control
7/27	131	AS2	1.80	" "
7/28	132	AS2	1.60	" "
7/28	133	AS2	1.34	" "
7/29	134	AS3	1.50	" "
7/29	135	AS3	1.35	" "
7/30	136	AS3	1.41	" "
7/30	137	AS3	1.65	" "
7/31	138	A	1.34	characterization, high freq. ign. press.
7/31	139	A	1.50	" " " " "

3.2.3 Test Results

General

Test data indicated that motor-igniter nozzle-pressure behavior could be described, as expected, by the parameters PR and ϵ^*. The nozzle pressures were either stable or unstable with either choked (unblocked) or unchoked (blocked) motor-nozzle throat flow depending upon the igniter ϵ^* location and the instantaneous value of PR. Data for Model A showing representative aligned test results at low, intermediate, and high ϵ^* values are shown in Figures 18 through 21. Other unmodified model geometries displayed similar behavior with the exception that, for dissimilar igniter nozzle geometries, the transition from one characteristic operating mode to another occurred at different ϵ^* and PR values.

At low ϵ^* values the flow behavior can be characterized in order of decreasing pressure ratios as (1) initially blocked and stable, followed by (2) blocked unstable flow, with (3) unblocking and final cessation of oscillations just prior to termination of igniter flow. Figures 18 and 19 present data from test 116 conducted at $\epsilon^* = 1.20$ over a range of chamber pressure ratios from 5.29 to less than 1. At the highest igniter pressure (PR = 5.29), the motor throat was blocked and the pressure in both nozzles was stable. Following closure of an igniter flow-throttling valve, the igniter chamber pressure decayed gradually to a new steady-state level. The igniter nozzle pressures in turn decreased to some minimum level at which the flow at each pressure tap began to separate in response to the relative increase in back pressure. Motor nozzle blockage continued as indicated by the oscillatory character of the motor throat tap (p_{107}) and the subcritical throat pressure ratio. Although blocked, the motor-nozzle wall pressures were relatively stable until PR = 3.09 at which point high-amplitude pressure oscillations were recorded in both igniter and motor nozzles. Two successive periods of unstable and stable flow were observed at PR = 3.09, indicating marginally unstable flow conditions for that pressure ratio and ϵ^* value. During these periods of instability, increase in the motor throat (p_{107}) and chamber (p_{101}) pressures indicated more relative blockage of the motor nozzle throat through increased penetration of the igniter jet. Motor-nozzle unblocking and final cessation of oscillations occurred after the final igniter flow-throttling valve had been closed.

For tests of intermediate ϵ^* values the motor- and igniter-nozzle flow behavior was similar to that at low ϵ^* values except that the motor-nozzle throat flow choked (unblocked) prior to the onset of oscillations. Typically the motor throat again reblocked with oscillation onset and did not finally unblock until a lower pressure ratio. Igniter- and motor-nozzle pressure behavior for $\epsilon^* = 1.5$ is illustrated in Figure 20.

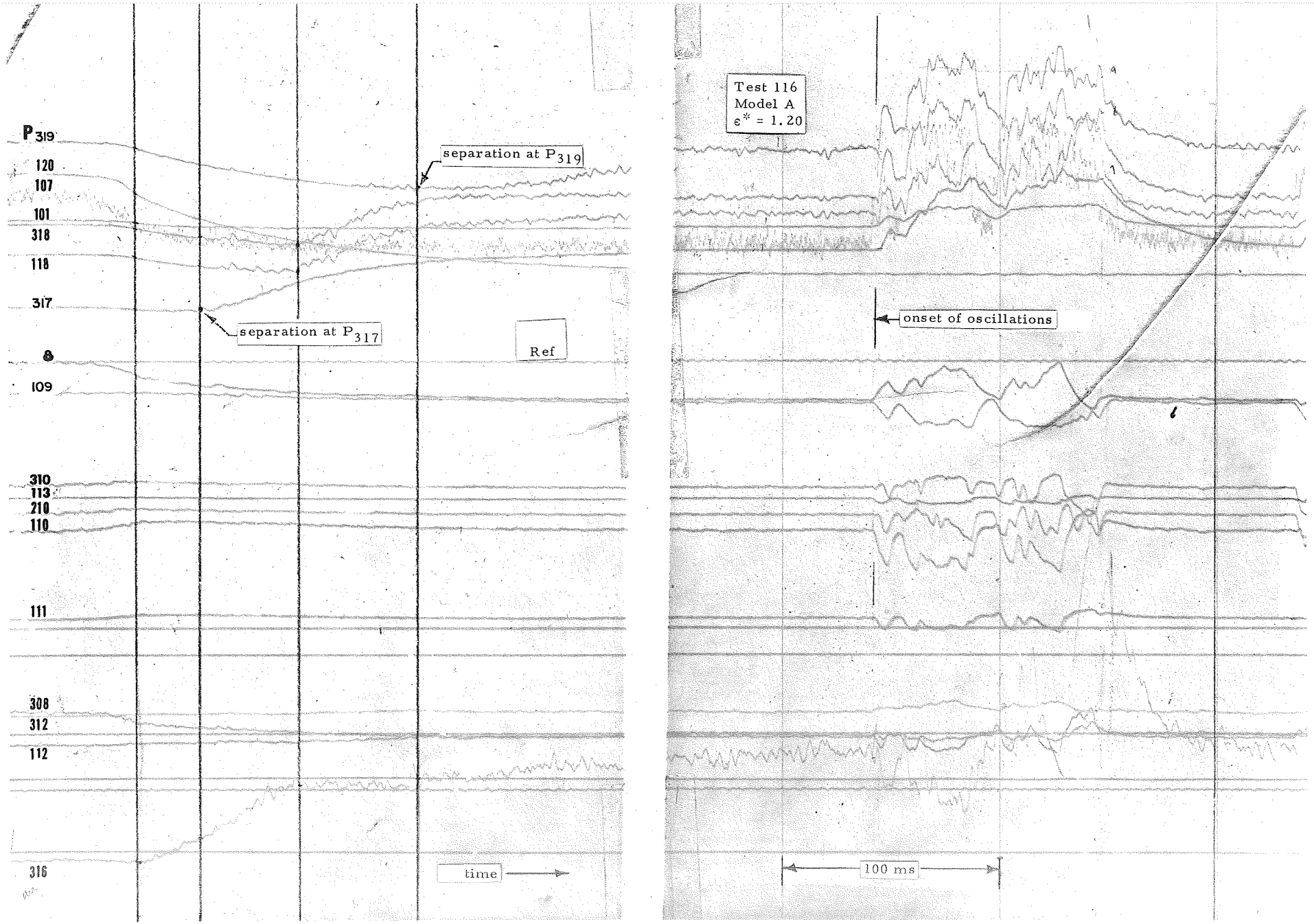

Figure 18. Aligned Model A Test Data $\epsilon^* = 1.20$

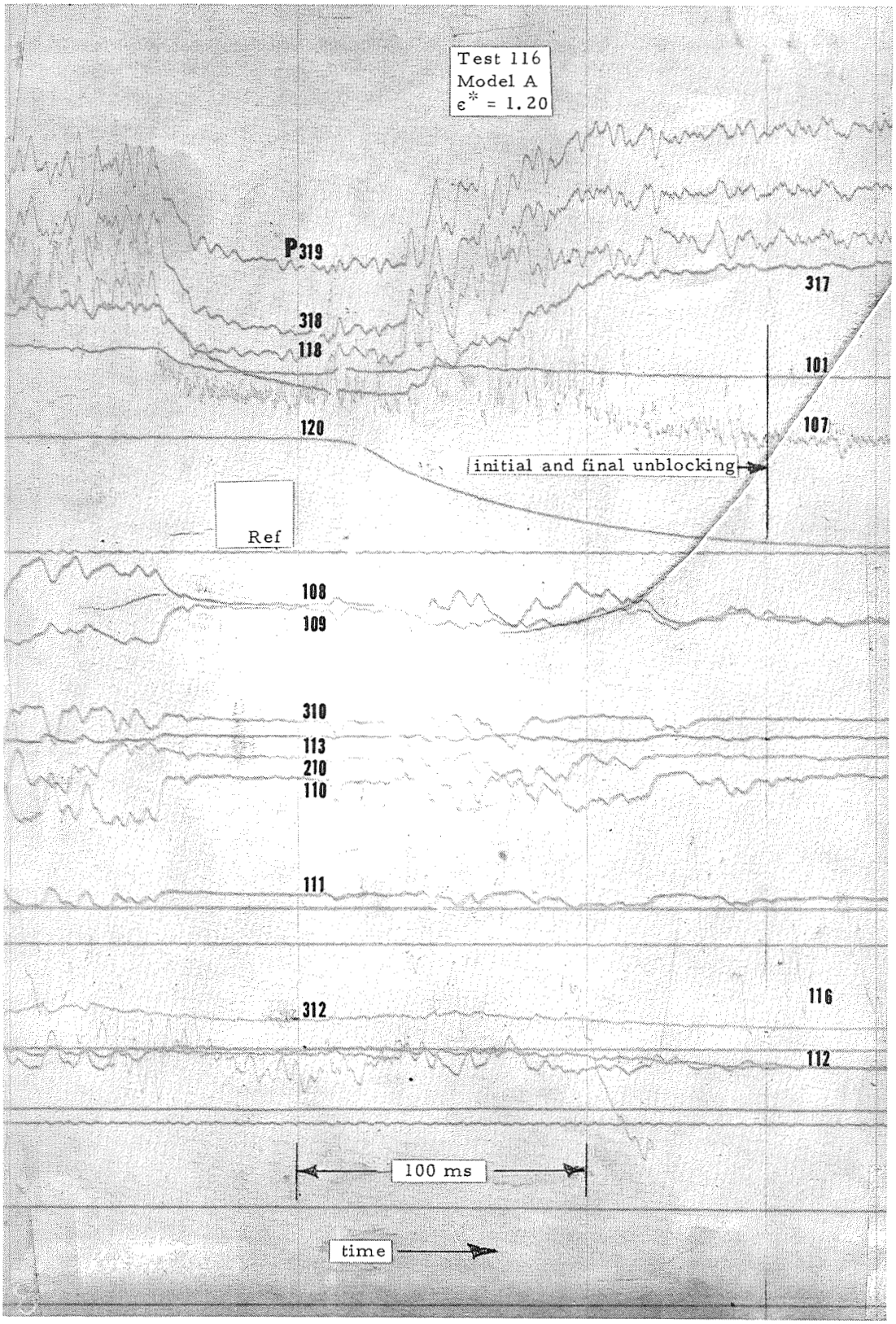

Figure 19. Aligned Model A Test Data, $\epsilon^* = 1.20$

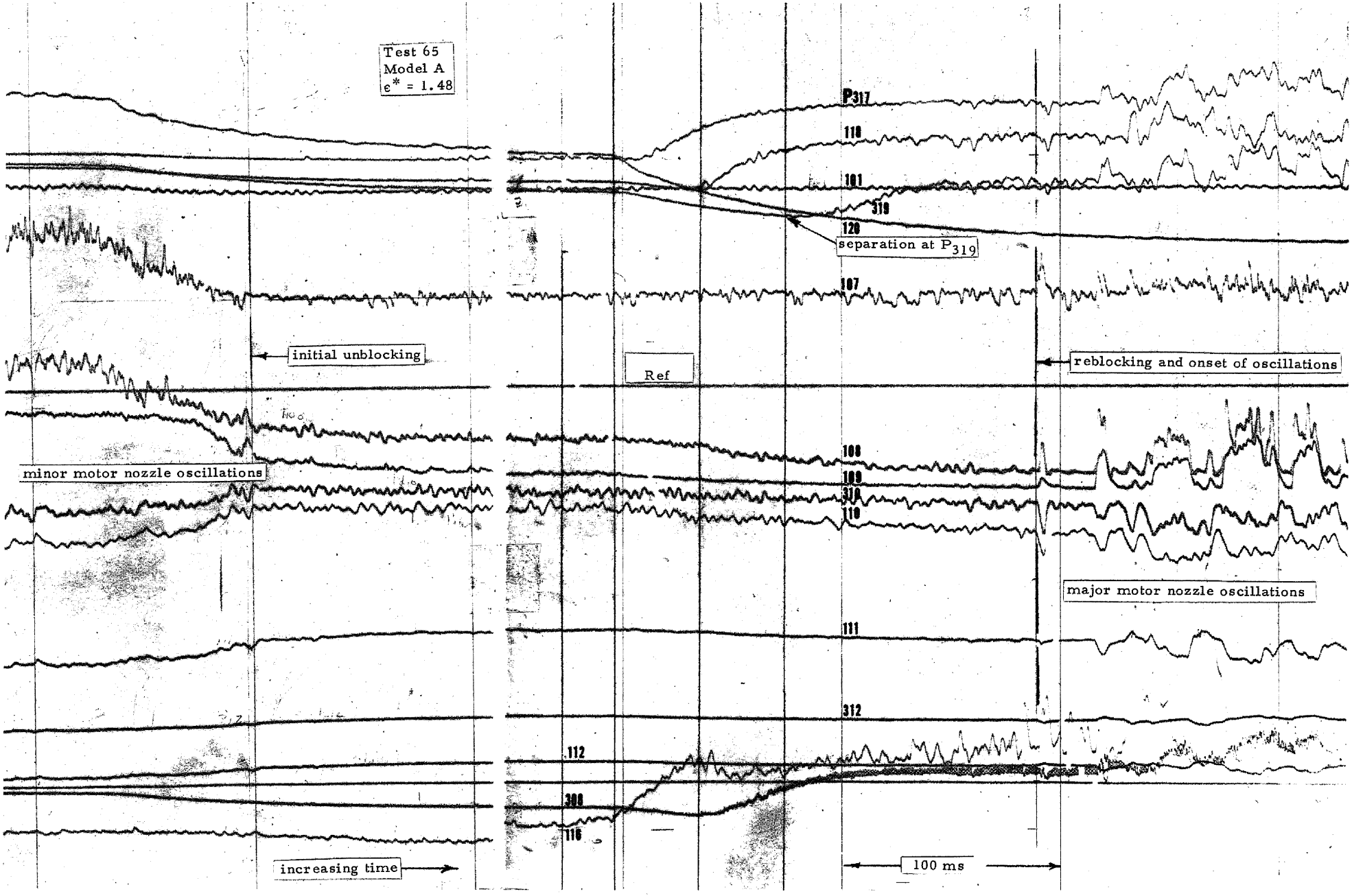

Figure 20. Aligned Model A Test Data, $e^* = 1.50$

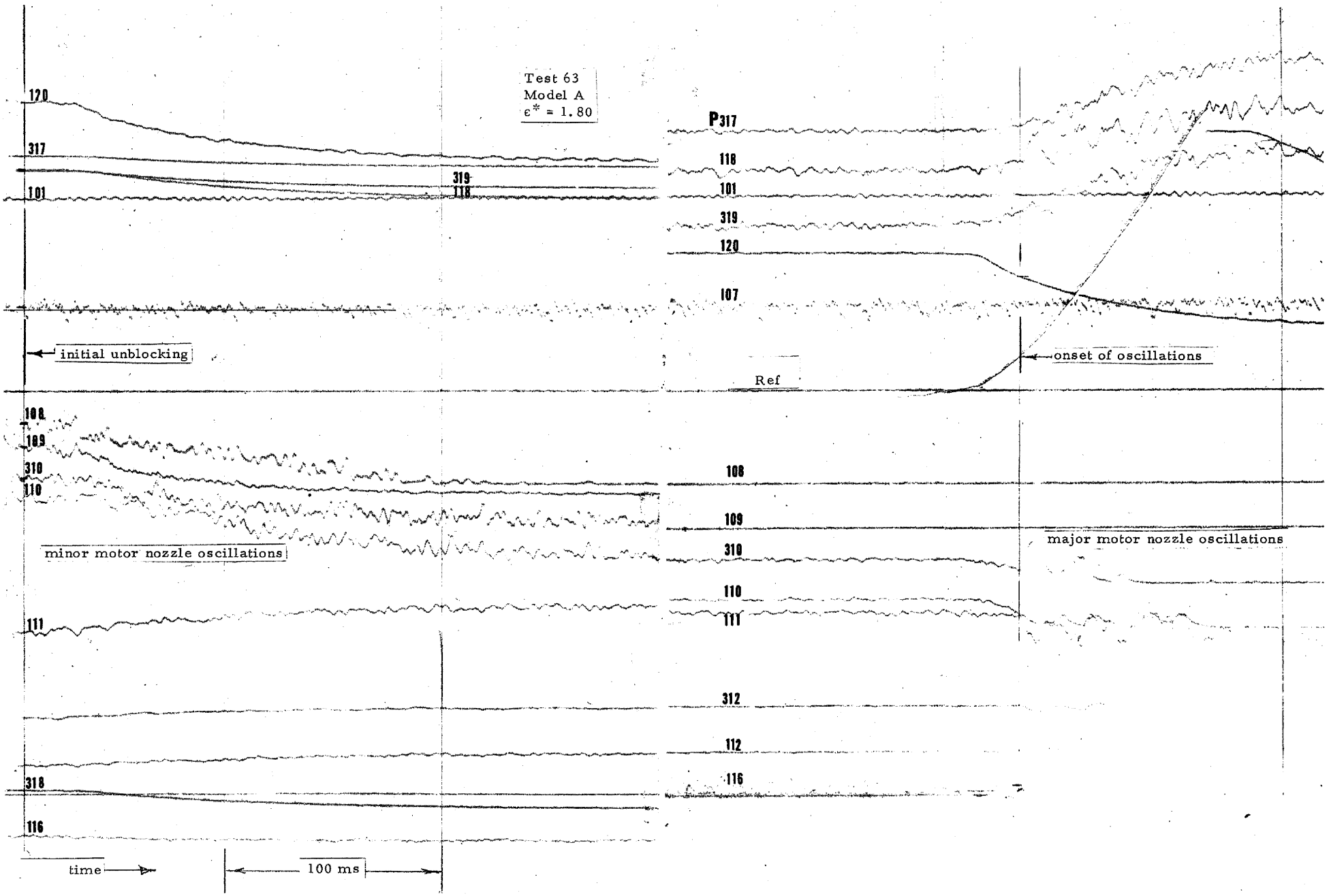

Figure 21. Aligned Model A Test Data, $\epsilon^* = 1.80$

At high ϵ^* values the motor-nozzle throat unblocked at relatively high chamber pressure ratios and did not reblock at any lower pressure ratio. After an unblocked PR range during which the flow was moderately stable, large-amplitude igniter and motor oscillations began and continued until igniter flow was terminated. Typical pressure behavior in the igniter and motor nozzles and chambers is shown in Figure 21 for $\epsilon^* = 1.8$.

Oscillations

Severe motor-nozzle pressure oscillations appeared only in conjunction with similar igniter-nozzle pressure disturbances. Although it was common for the characteristic pressure disturbances to display lateral or rotational components, the longitudinal component in most cases was predominant.

The techiques tested to suppress or eliminate motor-nozzle pressure oscillations were unsuccessful with one exception. Igniter nozzle Model AS3, which contained the largest step tested, significantly suppressed the amplitude of both igniter- and motor-nozzle pressure oscillations as shown in Figure 22.

The behavior of Models AB1 and AB2 was generally similar to that of the unmodified nozzles. However, some atypical pressure characteristics were noted particularily for nozzle AB2, which produced a bi-stable stepped pressure fluctuation in the motor nozzle for some test conditions.

Misalignment

Simple lateral and angular misaligned tests produced data which were nominally similar to the aligned tests. Combined angular and lateral misalignment showed a tendency toward alternate asymmetrical attachment of the igniter jet to opposite sides of the igniter wall. Figure 23 shows typical data from a test with combined lateral and angular misalignment.

Lift-Off

Lift-off test data indicated a decrease in the motor-nozzle pressure oscillations with increasing ϵ^*. At $\epsilon^* > 2.5$, motor-nozzle oscillations were not significant. Also at $\epsilon^* > 2.5$, no motor-nozzle blockage was experienced, due to a limitation on the maximum PR which could be obtained with the experimental apparatus.

3.2.4 Data Reduction

The test data were reduced to engineering values by application of scale factors determined from pre-test and post-test calibration of each instrumentation transducer.

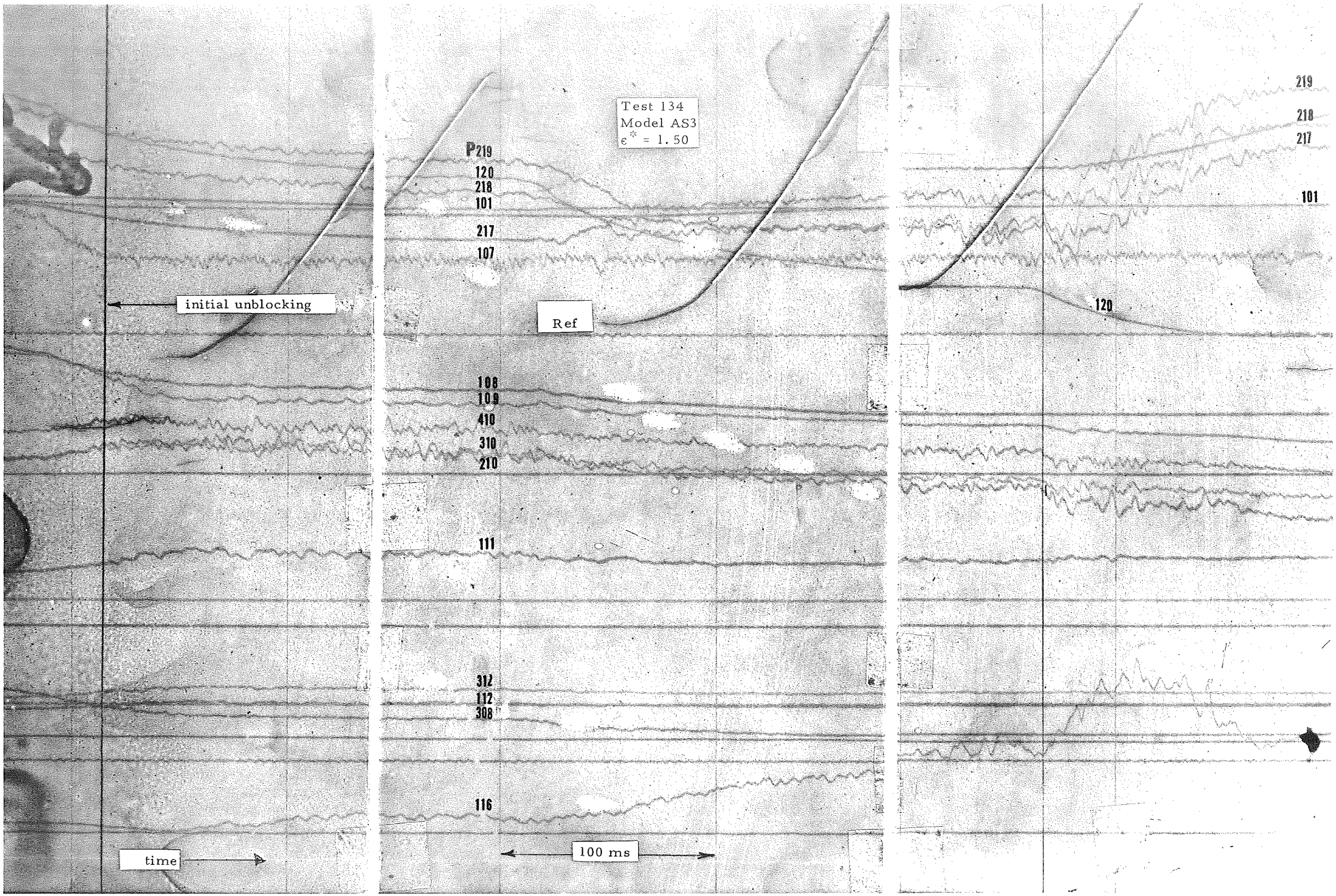

Figure 22. Aligned Model AS3 Test Data

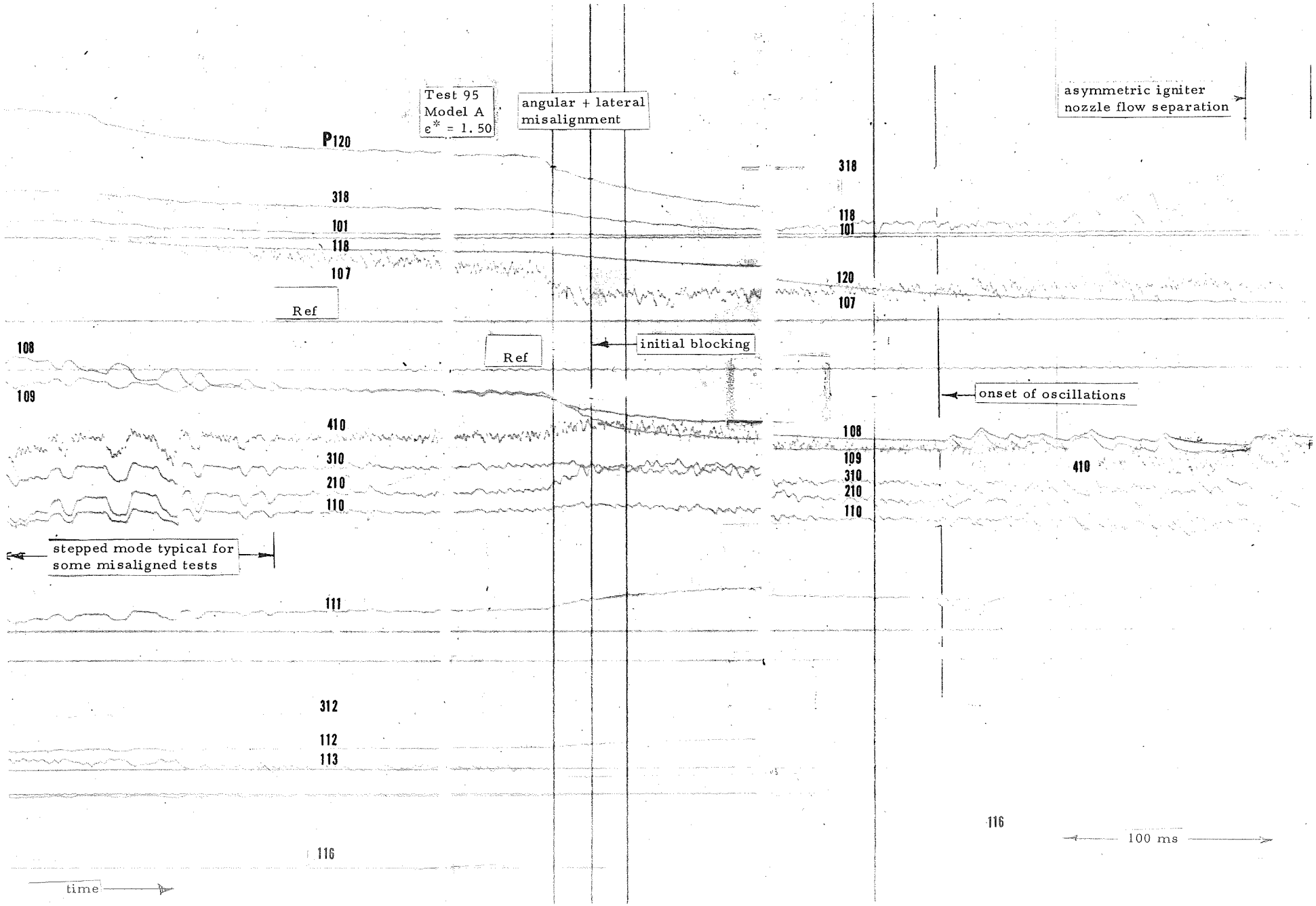

Figure 23. Test Data for Misaligned Test

The change in ϵ^* value with misalignment was small. Hence for misaligned tests, the ϵ^* value was assumed to be equal to the ϵ^* value for an aligned igniter located at an equivalent axial distance from the motor throat plane.

A principal problem in reducing the data was the difficulty in determining when the motor throat flow was unblocked, particularly at initial and final unblocking. Previous experience indicated that the cessation of the propagation of motor-nozzle pressure disturbances up-stream to the motor-nozzle throat-pressure tap was the easiest and most reliable determinant. However, during the current program nozzle throat oscillations were observed to occur at all times. These oscillations appeared to be a characteristic of the specific throat geometry (constant area section) of the motor nozzle. It is believed that the oscillations resulted from a shift of the choking location along the constant area section of the throat flat in response to low-level fluctuations in the motor chamber flow.

Analysis of the oscillations indicated a change in character during blocked or unblocked flow. When the nozzle was clearly blocked or unchoked, the oscillations appeared to be above a constant baseline pressure level. When the throat was clearly unblocked, the pressure fluctuated below the apparent baseline. At initial or final unblocking these pressure fluctuations changed from intermittently upward to intermittently downward. This characteristic frequently required subjective interpretation to determine the exact point when unblocking occurred.

3.3 DATA EVALUATION AND ANALYTICAL MODEL DEVELOPMENT

The primary purpose of the contract effort was to develop design criteria which could be used to design an aft-end ignition system for a given solid-propellant motor satisfying the following requirements:

(1) Satisfactory ignition.

(2) No motor overpressure.

(3) Control or minimization of the flow-field oscillations.

The previous program was successful in establishing techniques which can be used to control ignition characteristics. The program reported herein was oriented entirely toward the latter two requirements. Consequently, the development of analytical models of the flow fields occurring during initial unblocking and at the onset of oscillations was undertaken. The goal was that these models should be sufficiently rigorous to provide generality for conical and contoured nozzles, different gas properties (propellant formulations), and nozzle size.

The existence of several characteristic flow-field structures during the post-ignition period was confirmed. The general rationale of the behavior of the system, as described in Section 3.1, was found to be correct. The initial and final unblocking events occurred as expected, with flow-field structures which were peculiar to each event, as discussed in Section 3.3.1. That type of flow field which prevailed during initial unblocking has been called Mode A. The Mode B of structure existed during final unblocking. The major oscillations were identified to result from unstable igniter flow separation, with the igniter flow field rapidly alternating between Mode A and Mode B.

The flow-field models have been formulated largely through inductive reasoning based upon the measured pressure distributions and the sparce literature available on opposed supersonic flows. In a sense, the evidence regarding the flow-field structures can be considered circumstantial and has required a great deal of intuitive interpretation. Because of the time required, it was not possible to reduce and evaluate all the expermental data concurrent with the experiments. However, the general behavior and the variations of each model were evaluated currently with the tests, and the operating maps were plotted for each test to ensure that any apparent anomalies could be examined with additional test points. The performance and operating behavior of the slotted nozzle configurations were also evaluated on a current basis to support modifications which could result in positive control of the flow-field oscillations.

Following completion of the test program, the data were intensively studied and the development of the analytical models proceeded generally in the following fashion: First, an attempt was made to construct a rational flow-field model wich produced wall pressure distributions in the igniter and main motor nozzles reasonably similar to the measured distributions for specific test conditions, and then for more general conditions. However, this was categorically and uniformly unsuccessful. In no case was it possible to build a model for initial unblocking, onset of oscillations, or final unblocking which reproduced the experimentally measured pressure profiles, and which satisfied the equations of conservation of both mass and momentum. The assumptions used throughout the analytical study were, apparently, considerable oversimplifications in some cases, and were dictated by the extreme complexity of the interacting, confined flow fields, and the limited time available within the scope of the program. Furthermore, the lack of visual observation of the flow fields was a serious handicap to thorough understanding of the flow field process.

The basic assumptions used in all of the models to be discussed later are as follows, unless otherwise noted:

(1) Motor and igniter streams are identical gases having identical properties and equal total temperatures.

(2) The flows are adiabatic.

(3) Both streams are inviscid.

(4) Both streams always behave as ideal gases.

(5) The igniter-flow total pressure adjusts to the motor-flow total pressure, which may also adjust through the bow shock, so that the combined streams, following adjustment, are everywhere at a uniform total pressure.

(6) The flows are axi-symmetric and without swirl or rotation around the axis of symmetry.

(7) The flows at both igniter and motor throat are one-dimensional.

Following the initial attempt to construct reasonably rigorous models, the second efforts were directed toward the development of analyses, which although not correct in the sense of correlating with all the physical evidence, at least satisfied the mass and momentum balances, and provided satisfactory answers in terms of the physical geometric and pressure ratio conditions at which the major events occurred.

3.3.1 General Behavior - Bimodal Operation

Biomodal operation was clearly evident for all models tested. It is convenient to discuss the typical behavior in terms of the PR versus ϵ^* plots of the combined blocking and oscillations maps (see Figure 3) as shown generally in Figure 24.

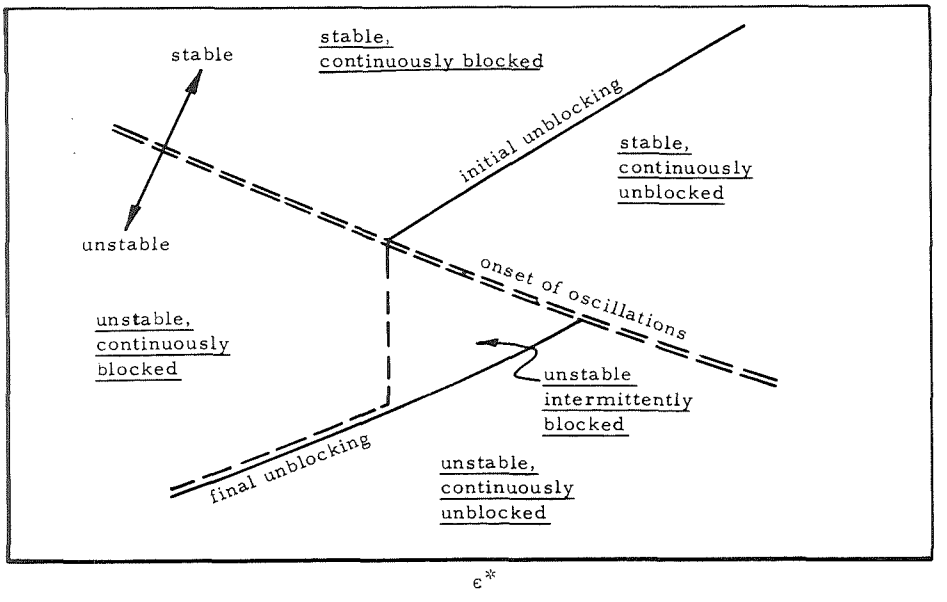

Figure 24. General Operating Map

In general, Mode A was observed to exist and unblock at higher PR values than Mode B. It was thus concluded that Mode A produces the greater total pressure loss in the igniter stream. This allows the motor flow to force the igniter flow away from the motor throat at a higher PR for Mode A than for Mode B. Only Mode A exists at high PR, above the onset of oscillation boundary, and tends to be a stable flow field. Mode B, with its lower igniter total pressure loss, exists only at a lower PR, below the onset of oscillations, and can itself be unstable. Below the onset of oscillations, Mode A unblocks only to the right of the intersection of the initial unblocking and onset of oscillations lines. In this region, the flow clearly alternates between Mode A and Mode B. The transition from Mode A to Mode B can cause reblocking, because the reduced igniter total pressure loss in Mode B produces an imbalance in stagnation pressure between the igniter and motor flows at the contact surface which forces the contact surface forward until it interferes with the motor throat flow.

The exact structures of the two types of flow are not clear. In Mode A it appears that the igniter flow passes through a family of oblique waves which adjust the jet boundary static pressure to the cavity pressure and that a terminal normal shock occurs at high Mach number, which adjusts the igniter total pressure to the main flow total pressure at the contact surface. Mode B features a one-shock system (normal or triple-point type) which produces both the separation and total pressure adjustment. This will be discussed in detail in the following sections, along with the constraining conditions of igniter nozzle placement which give rise to these types of flow structures.

Operating Maps

The operating maps for the basic (aligned, non-modified) cold-air models A, B, C, D, and E and for the hot-firing tests are shown in Figures 25 through 30. In all cases there is a region in which the motor throat is blocked (unchoked), then it unblocks at a high pressure ratio, remains unblocked and stable until the onset of oscillations, at which point the throat may or may not reblock, depending upon ϵ^*.

The unblocking points shown in the figures, both initial and final, were taken to be the pressure ratio at which the last upward throat pressure spike occurred (see Section 3.2.4 for a discussion of other criteria for unblocking). In most cases initial unblocking was actually observed before the last upward pressure spike. In a larger sense, and contrasted to "final" unblocking, "initial" unblocking is really the final termination of blocking in the flow mode which exists at that time.

Expected significant hysteresis was not observed in the tests. There was a trend toward the major events occurring at a slightly lower pressure ratio for decreasing igniter pressure, and vice versa, but this trend was so fragmentary that it was considered insigificant.

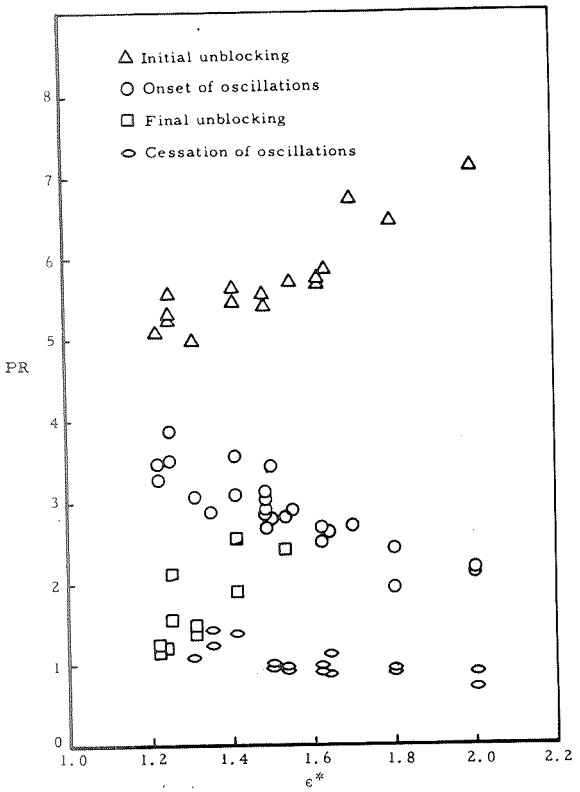

Figure 25. Model A Operating Map

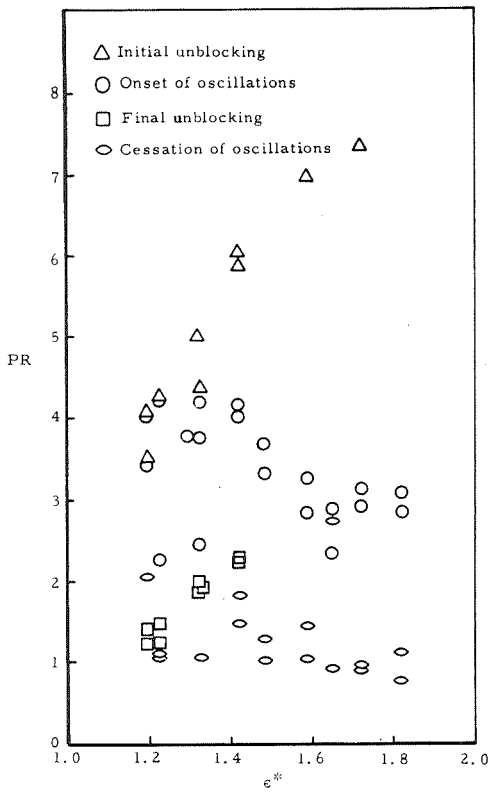

Figure 26. Model B Operating Map

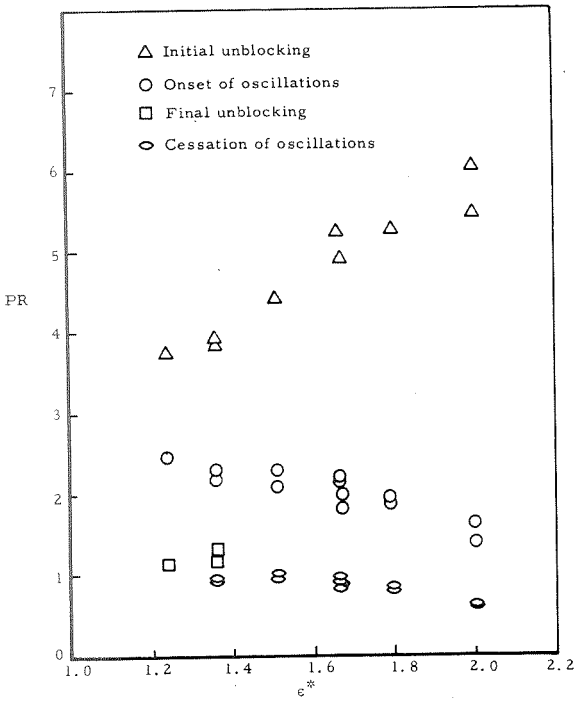

Figure 27. Model C Operating Map

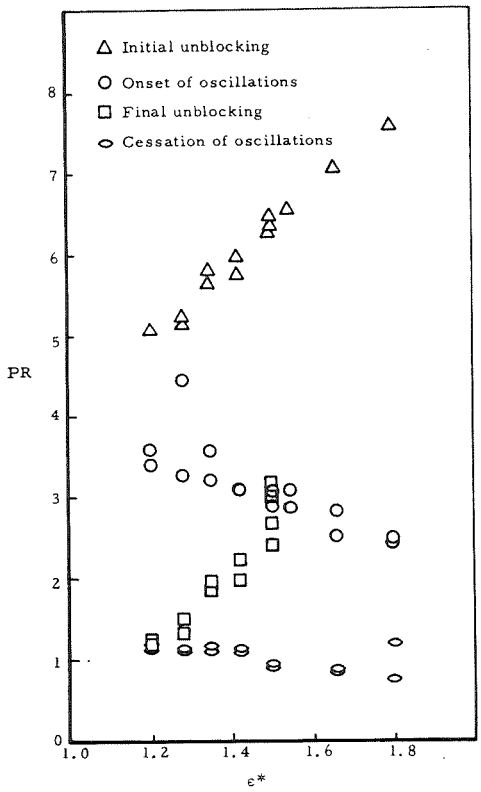

Figure 28. Model D Operating Map

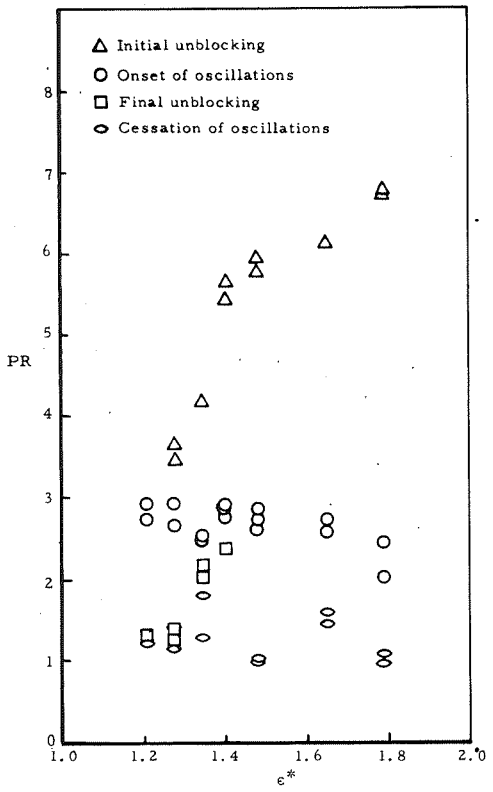

Figure 29. Model E Operating Map

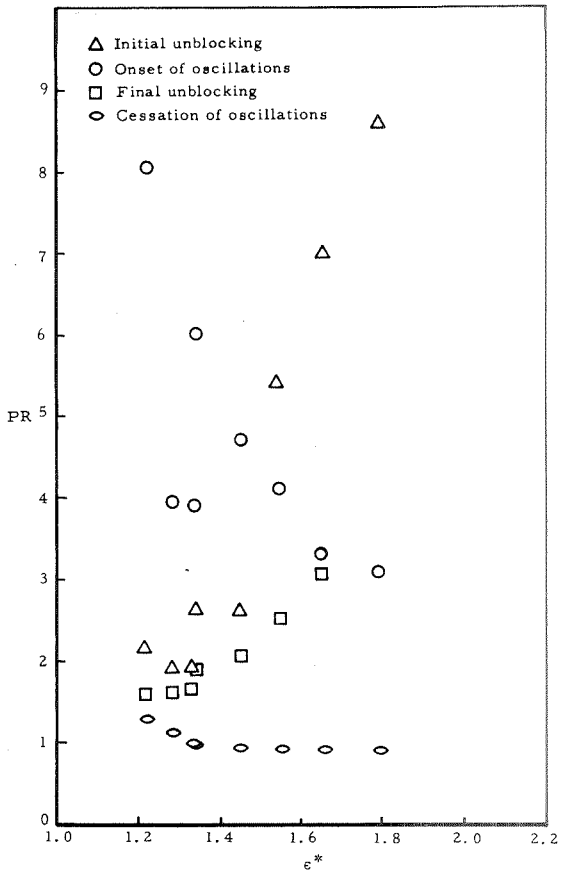

Figure 30. Hot-Firing Operating Map

One peculiarity was noted for all cold-flow tests at and below the ϵ^* where the initial unblocking and onset of oscillations occur simultaneously. Here the scatter is very great. Some of the data suggest that alternate choking mechanisms and accompanying flow fields result. At any rate, the pattern is quite perplexing and allows considerable speculation with little rational understanding.

Pressure Distribution

Figure 31a is a plot showing the history of the wall pressure distribution for Test 124 (Model A, $\epsilon^* = 1.35$) for a descending igniter total pressure profile starting before initial unblocking and ending with the igniter flow termination. Profile A is clearly before initial unblocking. Profile B is when the average throat pressure becomes decoupled from the igniter flow, but while the upward spikes still exist, and B' is just after the last upward spike and the throat is clearly and finally unblocked in Mode A. Profile C is immediately prior to the first of the oscillations. Profiles D and F are of the same flow field as A, B, and C, taken milliseconds apart, just before and after a transitory jump to the alternate flow field, shown by Profile E.

Notice that the igniter flow has jumped forward toward the motor throat with sufficient strength to unchoke or reblock the throat. At higher ϵ^* similar behavior exists, but without reblocking the throat.

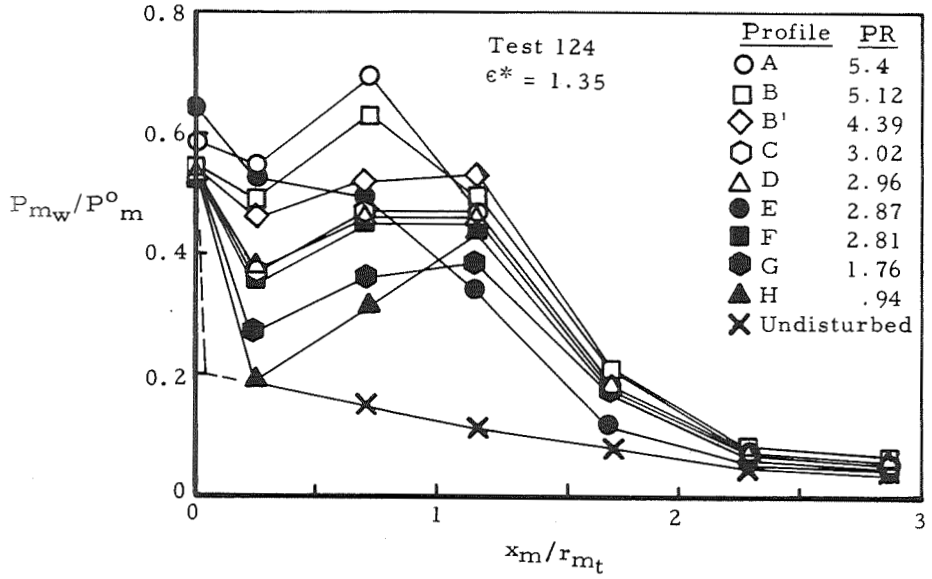

(a) Motor

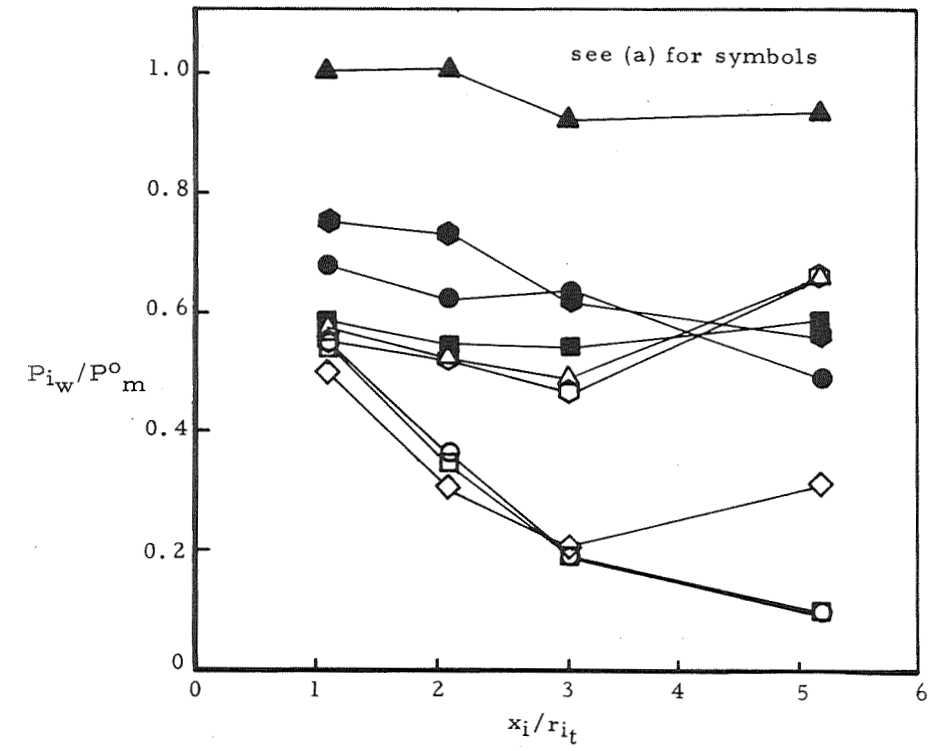

(b) Igniter

Figure 31. Typical Nozzle Pressures (Model A)

Figure 31b shows the igniter nozzle pressure distribution (ratio of igniter wall static pressure to motor chamber pressure) corresponding to the motor nozzle pressure ratios of Figure 31a. The nozzle initially flows full at Profile A in Mode A. As the igniter chamber pressure decreases, the nozzle becomes overexpanded, and the flow separation moves forward toward the igniter throat. At the jump to Mode B at Profile E, the igniter wall pressure distribution also experiences a jump, then returns to the lower pressure level at Profile F. It should be noted that the pressure level at Profile E is lower than that which is characteristic of Mode B, because the oscillations selected here as an example, i.e., Profiles D to E to F, were of such short duration that the Mode B structure did not fully develop before alternating back to Mode A.

Flow Field Models

It is virtually impossible to categorize and even to identify all of the different behavior patterns and characteristic flow structures which exist in this extremely complex and frequently unstable flow-field interaction. This appears to be especially true in the vicinity of the intersection of the initial unblocking and onset of oscillation lines. Figure 32 depicts the flow fields which are believed to be characteristic of Modes A and B. These greatly simplified models are representative of the main features of the flow fields and do not entirely account for the interaction of the various waves within the igniter jet. The two sketches of Mode A show different structures, which apply to conditions of low and high igniter-nozzle static back pressures (with respect to igniter total pressure). The key features of the flow fields are the same, however. The total pressure adjustment to the main stream total pressure occurs primarily through a normal shock, while the separation adjustment to the static back pressure or cavity pressure occurs through a different oblique wave system. These may be either expansion waves when the nozzle is underexpanded or shock waves from the lip or within the nozzle when it is overexpanded. This is in distinct contrast to Mode B in which the flow both separates and adjusts total pressure through a single normal shock. These flow fields, and the conditions during which they occur, will be discussed in greater detail in following subsections.

It is emphasized that blocking associated with the flow fields pictured in Figure 32 occurs from the gasdynamic constriction in the nozzle exit cone, in the absence of penetration of the motor throat. This happens at relatively high ε^* values where there is room for the igniter flow to adjust. At the lower ε^* values, however, there is considerable evidence to indicate that penetration of the motor throat plane by the igniter jet accompanies the second constriction of the main flow in the nozzle. In this situation it is believed that viscous interactions between the streams become more significant.

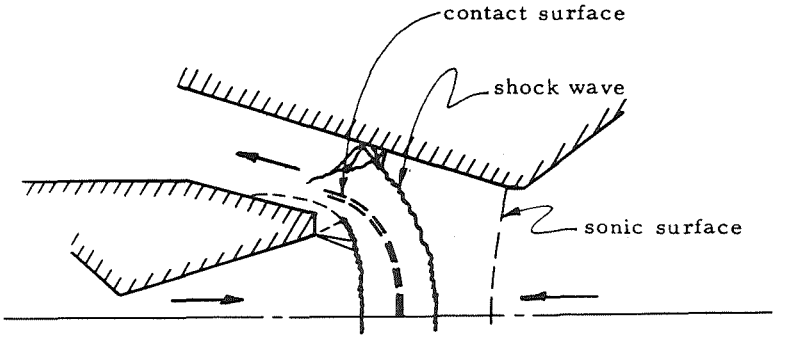

(a) Mode A, Igniter underexpanded

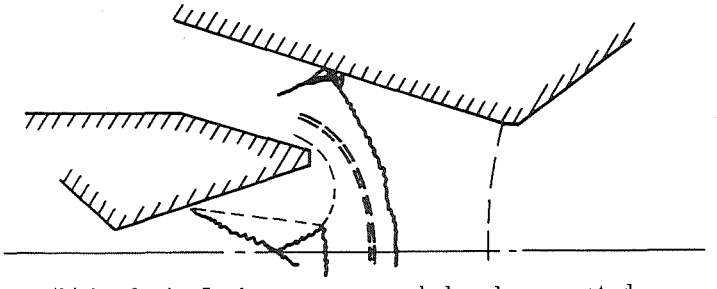

(b) Mode A, Igniter overexpanded and separated

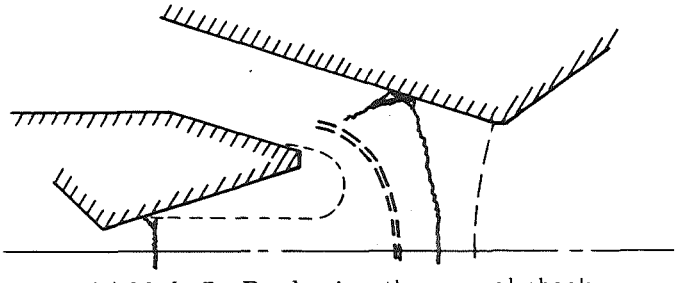

(c) Mode B, Predominantly normal shock

Figure 32. Representative Flow Fields

3.3.2 Initial Unblocking

There are several factors which aid in understanding and simplify the modeling of the initial unblocking event, in contrast to the other events:

(1) The flow condition is stable (except for the small-scale motor-throat oscillations previously discussed).

(2) At the moment of unblocking the main-motor flow suffers no significant total pressure loss because the interactions are near the throat and the Mach number of the stream is everywhere near sonic.

(3) At the high ϵ^* values the igniter nozzle flows full, so that the total pressure adjustment of the igniter flow occurs wholly outside of the nozzle.

For most of its span, the initial unblocking line is regular and nearly linear, even though the igniter flow in Mode A transitions from underexpanded at a high ϵ^*, to overexpanded at a lower ϵ^*. Therefore, it was decided to model the high ϵ^* condition as being the most straightforward and representative of the whole ϵ^* span of initial unblocking.

In the absence of visual observations of the interacting flows, the modeling is based upon the measured pressure distributions in the motor nozzle and upon the work of Charwat[11] with opposed unconfined supersonic streams.

Nozzle Pressure Distribution

Figure 33 is a plot of the nozzle-pressure distributions for Test 42 (Model A, $\epsilon^* = 1.62$) spanning the initial unblocking event. The throat is clearly blocked, or unchoked, at Profile A. The pressure ratio is greater than 0.6, and it increases to 0.73 at tap 9, being obviously subsonic. Profile B is also subsonic, but the pressure ratio is slightly reduced. It appears that the choke point for these flows is in the area of tap 10, where the pressure ratio is approximately 0.528. Profile C shows a change in pressure distribution, with the pressure ratio at tap 8 slightly below that at the throat. This suggests that the throat flow is choked, but only partially in the sense that it could be choking only during the lower portion of the minor throat-pressure oscillations discussed in Section 3.2.4. Furthermore, the pressure at tap 9 is greater than at the throat, indicating that the flow has passed through another sonic point, and passes through yet another throat in the vicinity of tap 10. Profile D progresses in the same fashion, with the secondary throat near tap 10 being of nearly equal effect (equal area) to the geometric motor throat. At Profile (1), the motor throat flow appears to have been stabilized, with the throat pressure ratio having reached a lower limiting value. Also, the pressure ratio at points downstream equals, but never exceeds, the pressure ratio at the throat. Therefore, the secondary throat, generated by gasdynamical constriction of the main stream against the nozzle wall by the igniter flow field, is of equal effect on the flow as the motor throat. As the igniter flow continues to tail off, in the absence of oscillations, the motor throat is now independent of the opposed flow interactions and the constricting effect of the igniter jet. Profile (1) is the initial unblocking point selected from examination of the traces, using the criterion previously described, that final unblocking occurs when the upward throat pressure spikes have ceased to exist. Note, however, that the actual pressure ratio is about 0.55, instead of the theoretical value of 0.528. It is the rule, rather than the exception, that frequently there is considerable disagreement in the unblocking pressure ratios selected by use of the various criteria. Usually the disagreement is not significant, but it occasionally is, making interpretation of the data difficult.

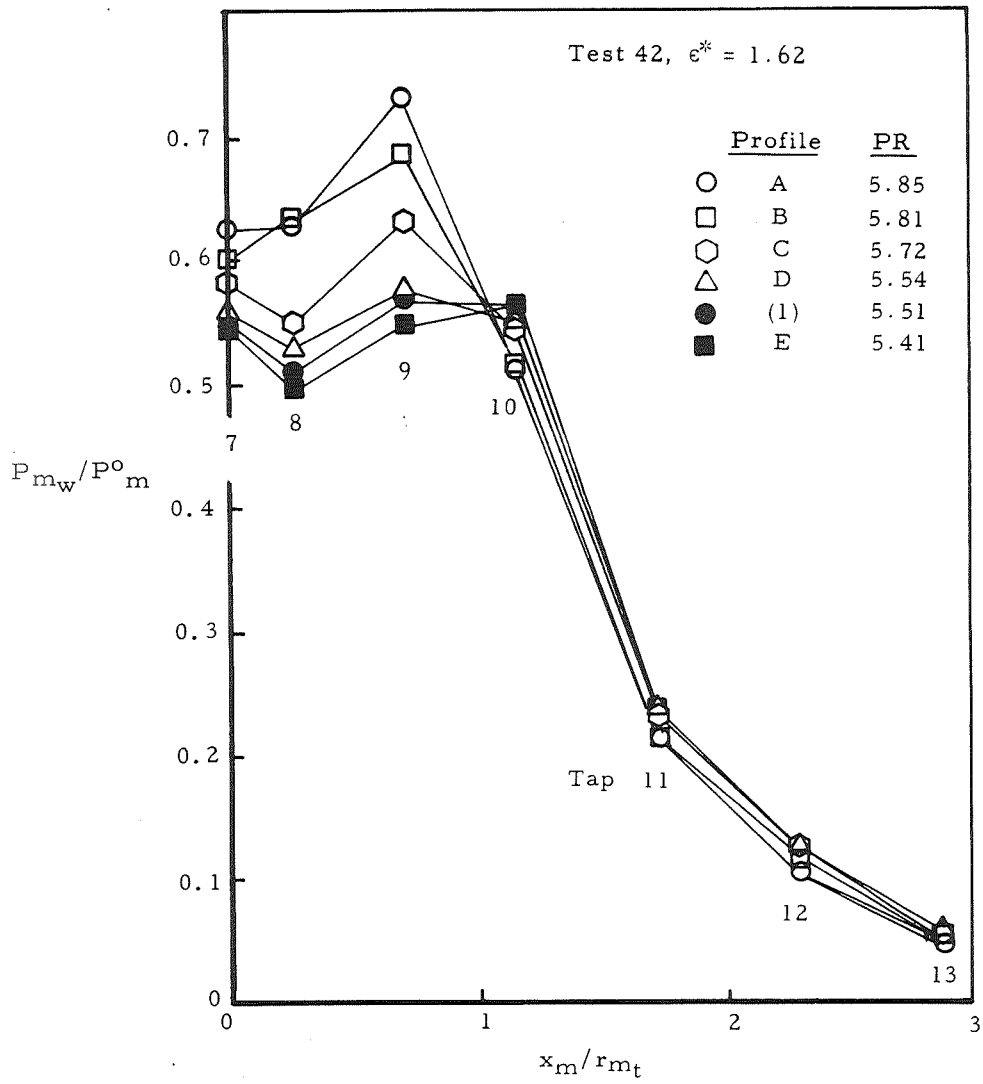

Figure 33. Initial Unblocking Pressure Distribution

Figure 34 shows the nozzle pressure-ratio distributions for all of the cold-flow models at initial unblocking points selected from the pressure spike criterion. The most important feature of these plots is the relative constancy and uniformity of the pressure distributions for all models and all ϵ^* values greater than about 1.5. This strongly indicates that, at least for the higher ϵ^* values, the flow at the termination of initial blocking is characterized by the double throat system described in the previous paragraph, and with the qualification that the throats are of equal area (in the absence of main stream total pressure loss). Additionally, from the constant axial position of the distributions, and hence the second choke point, it can be assumed that the flow fields from the throat to the contact surface with the igniter flow are nearly identical for all models and all ϵ^* greater than some lower limit around 1.50. It is also worthy of note that the pressure is nearly constant between the throats.

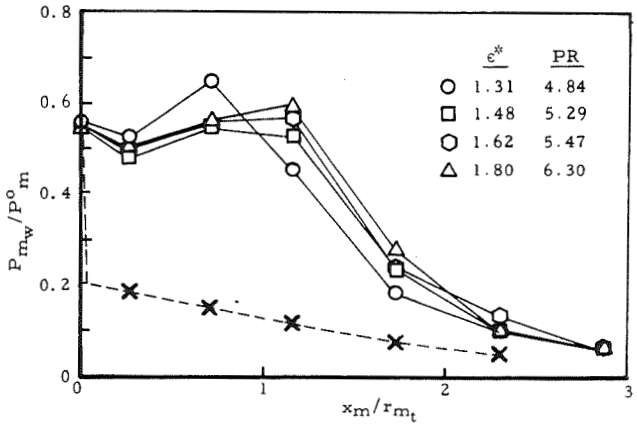

(a) Model A

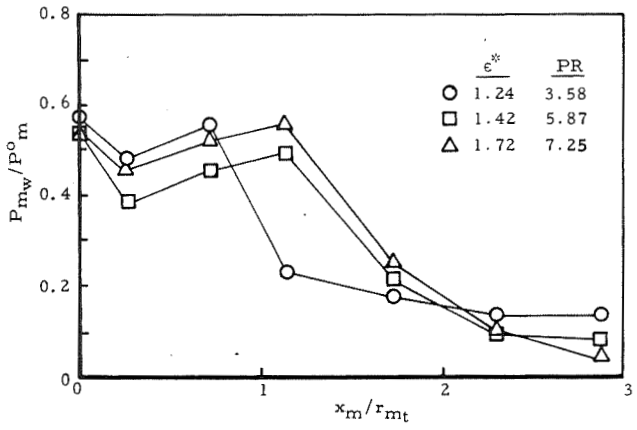

(b) Model B

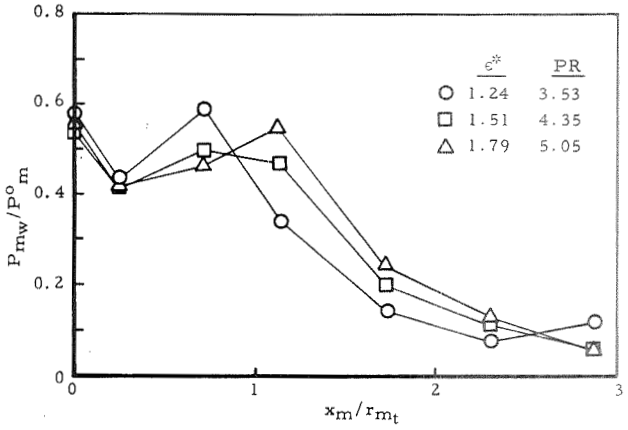

(c) Model C

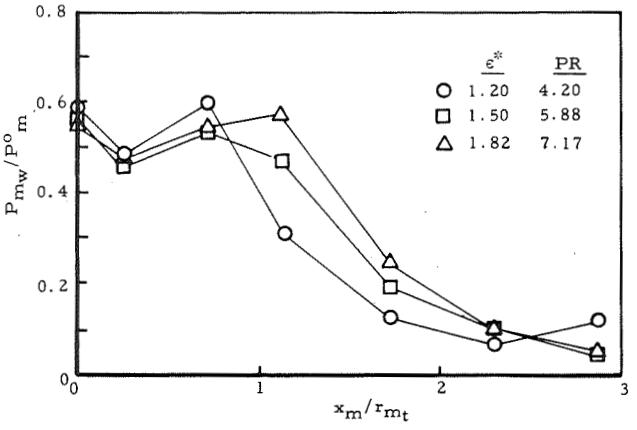

(d) Model D

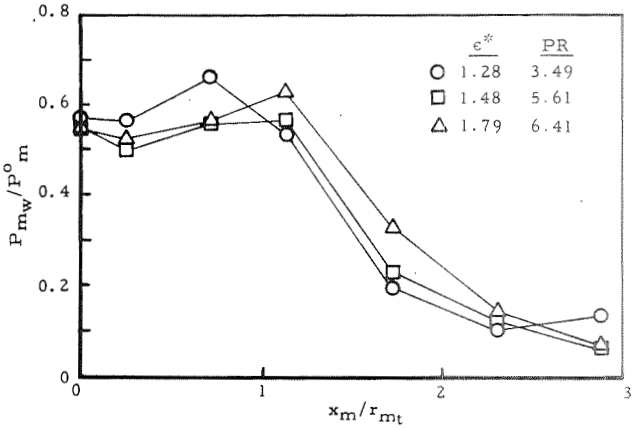

(e) Model E

Figure 34. Initial Unblocking Pressure Distributions

Flow-Field Model and Analysis

In accordance with the above observations and interpretations, a model of the flow-field structure has been proposed and used as the basis for the analysis of the initial unblocking event. The general features of the model are as shown in Figure 35. The main flow issues from the throat, which is sonic, and passes through the second throat formed by the contact surface and the nozzle wall. The igniter flow issues from the jet exit, flowing full and undisturbed. It then passes through a normal shock sufficient to adjust the total pressure to the main flow total pressure, turns subsonically to the sonic point, and continues to expand supersonically. The behavior of the igniter jet is generally modeled after the observations of Charwat[11] of supersonic jets issuing into a counterflowing supersonic stream.

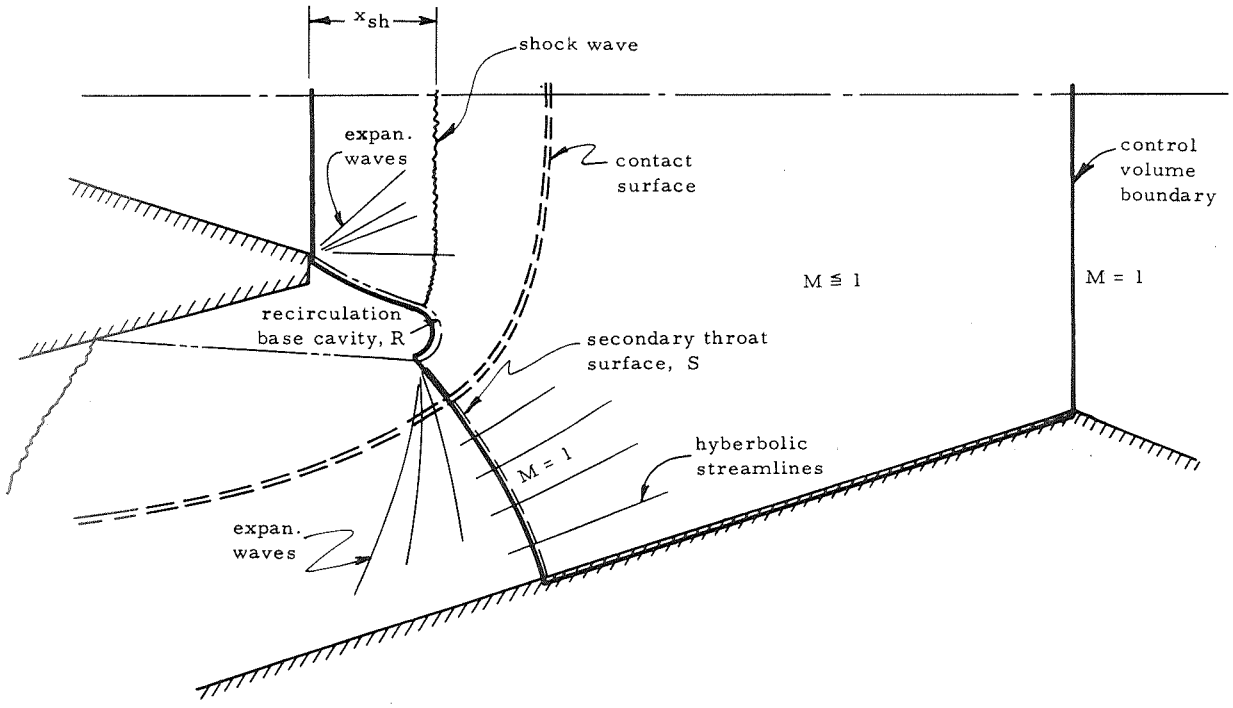

Figure 35. Analytical Model—Initial Unblocking

In addition to the assumptions listed at the beginning of this section which apply to all the analytical models, the following are key features of the initial unblocking model:

(1) The igniter flows full at its exit and issues as source or radial flow which persists until the normal shock (within the portion of the jet which is undisturbed by expansion or compression waves from the nozzle exit).

(2) The igniter flow adjusts to the total pressure of the main flow through a single normal shock. Even though the Mach number

of the stream is not uniform, owing to expansion or compression waves entering into it from the jet exit, it is assumed that the effects of such non-uniformity on the total pressure are negligible.

(3) Regardless of flow structure between motor throat and contact surface, the nozzle wall pressure between the motor throat and secondary choke point is constant and equal to the theoretical critical pressure.

(4) The total pressure of the main stream in the nozzle is constant and equal to the chamber total pressure.

(5) The flow at the secondary choke point is not parallel to the nozzle wall, but rather the streamlines follow a family of hyperbolas satisfying the condition that, at the sonic point, the derivative of the area of each stream tube along its flow direction is equal to zero.

(6) The igniter normal shock is planar out to a radius equal to the jet exit radius, whence it follows a circular arc whose center is the jet exit lip.

(7) The free subsonic boundary of the jet, behind the shock wave intersection with the boundary, may undergo a turn of finite radius, without a change in pressure along that free boundary.

Additional details of the model and description of the analysis are given in the Appendix. The calculations are performed by setting the desired geometric variables, including ϵ^*.

A trial PR is selected and the location of the shock and its shape are calculated, followed by selection of a trial cavity pressure. The free boundary is determined, along with the area of the secondary throat. The calculation procedure is repeated, iterating on both PR and the cavity pressure, until the conservation of mass and momentum and the condition of sonic flow at the secondary throat are simultaneously satisfied.

Three variable factors were used to adjust the calculated results to achieve the best correlation with the experimental results: the radius, R, of the subsonic turn; a multiplier on x_{sh} to adjust the shock standoff distance; and a multiplier less than 1.0, to account for loss of axial momentum at the second throat due to swirl of the flow field about the axis of symmetry or to other non-normal inclination of the flow direction to the surface, S.

Correlation of Analytical Results with Experimental Data

In general, agreement between the analysis and the experimental results is good. Figure 36a shows a comparison between the experimental data of

Model A and calculated points. Two sets of test data points are shown. One set represents the termination of the initial blocking points, while the other set consists of the points at which unblocking, even though temporary, first occurs. It appears that, for ϵ^* greater than 1.4, the initial unblocking pressure ratios may be approximated by a straight line, and that neither the scatter nor the difference between the two sets of data is great. However, at lower ϵ^* values, the behavior appears to be different, probably resulting from an altered flow structure. Analytical data are also shown generated with the combination of factors which gives the best correlation with the map of Figure 36a and also with the cavity pressure. The values of these factors are:

$$R = 0.1\ D_{i_e}$$

Shock standoff factor = 1.5

Secondary throat momentum factor = 0.95.

The individual effect of these parameters is shown in Figure 37.

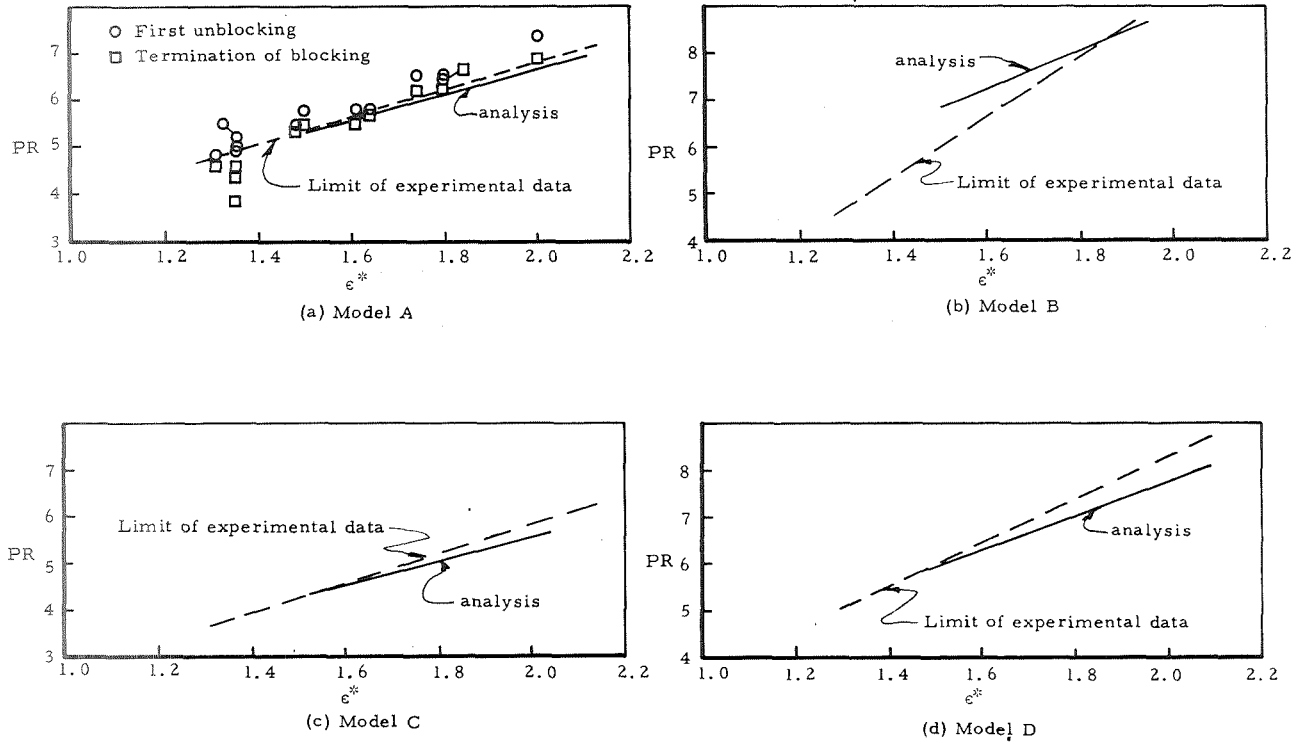

Figure 36. Comparison of Initial Unblocking Analysis and Experiment

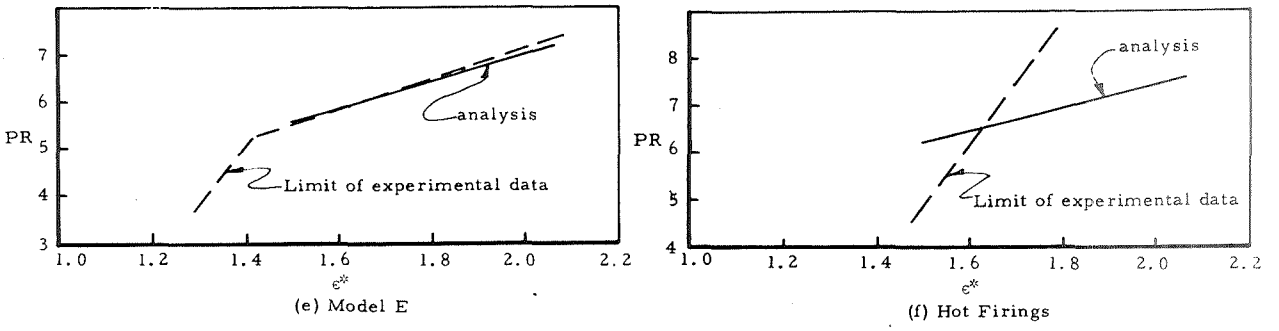

Figure 36. Comparison of Initial Unblocking Analysis and Experiment (concluded)

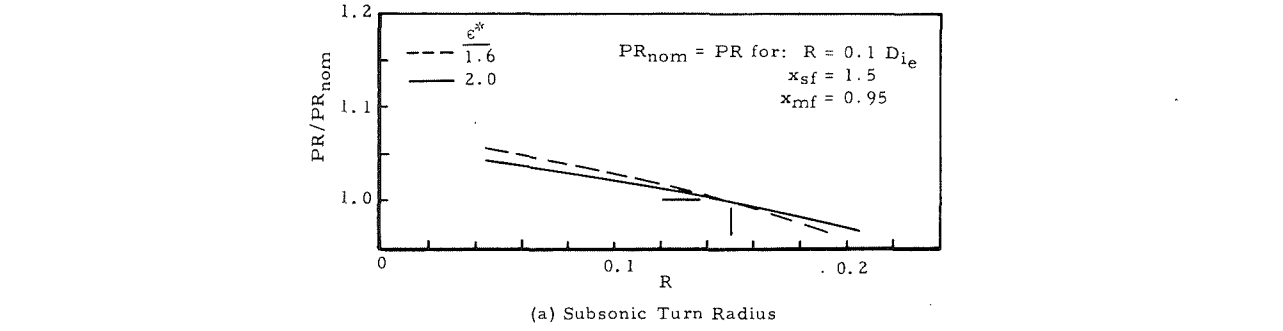

Figure 37. Effects of Analytical Model Parameters

The only one which produces a significantly altered slope of the curve is the shock distance factor.

The reconstructed flow fields for ϵ^* of 1.5 and 2.0 from the curve of Figure 36a are shown in Figure 38. Note that, although the shock standoff distance adjusts as ϵ^* varies, this adjustment is insufficient to keep the secondary throat position the same for all ϵ^*. This is a slight departure from the experimental results as shown in Figure 34a.

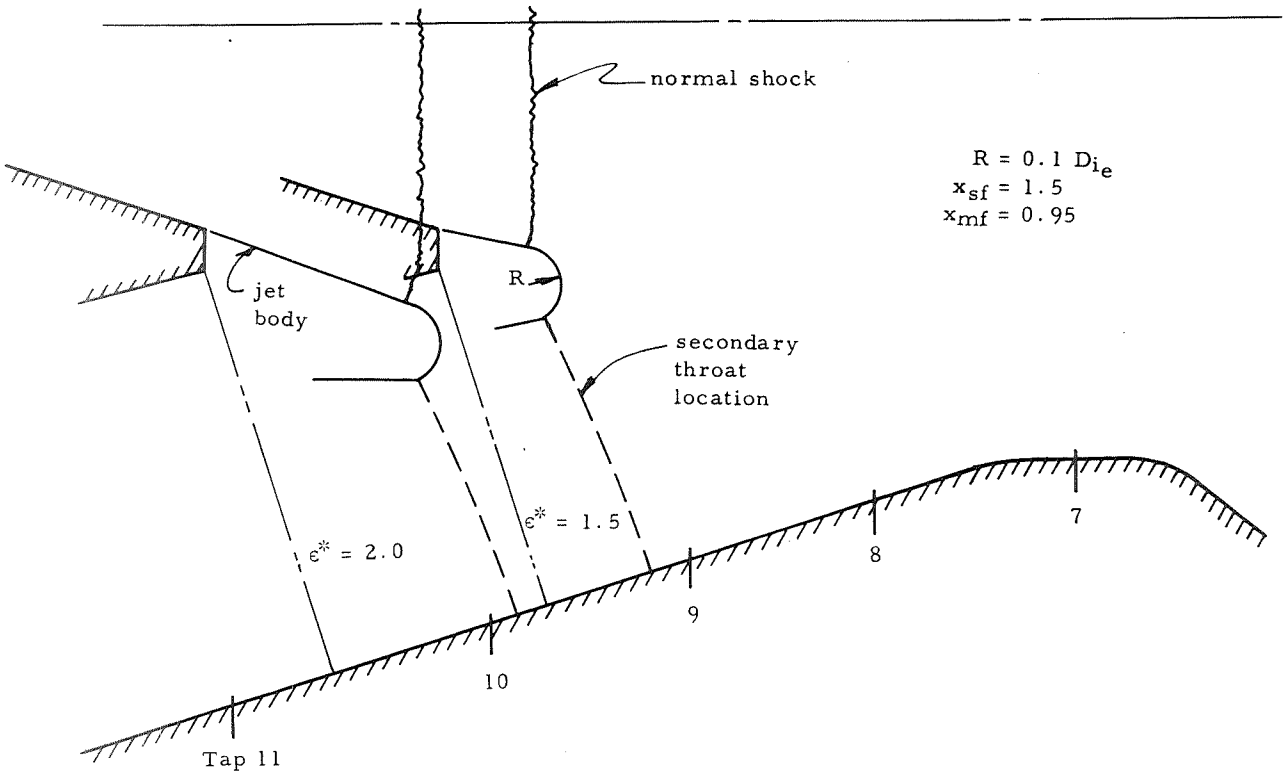

Figure 38. Calculated Flow Fields at Initial Unblocking, Model A

A comparison is shown in Figure 36b through f between the transposed experimental data and analytical results, using the same factors enumerated above for all other models. Correlation is good for Models C, D, and E. Both the slope and position of the curves agree. However, the slope of the curves for Model B and the hot-firing (HF) test are considerably incorrect. The only difference between Model B and Model D is the igniter-nozzle expansion ratio (9.2 and 7.0, respectively). The HF model has an even greater expansion of 10.0, but also has greatly different gas properties (γ = 1.18 vs 1.4). It appears likely that the effect of gas properties is less than that of igniter expansion ratio because of the behavior of Model B (γ = 1.4). Therefore, it seems that the analytical model becomes less valid at some ϵ_i greater than 7.0. An attempt was made to correct this deficiency by incorporating a curved jet boundary consistent with the data of Love, et al.[12]. However, wide variations in the radius of curvature of the boundary produced an effect only on the cavity static pressure, but not on the unblocking pressure ratio.

It is believed that a better definition of the centerline igniter Mach number distribution would improve the validity of the model at the higher expansion ratios. Also the assumptions of the shock shape and uniform total pressure distribution are obviously contradictory. However, time allowed within the program did not allow for even superficial evaluation of these factors or others which perhaps could also result in the error noted.

3.3.3 Final Unblocking

Studies were conducted to update the final unblocking model developed under Contract NAS-3-10297. That unblocking model was based upon a mass and momentum balance for a control volume similar to that shown in Figure 39. The model featured a single normal-shock igniter-flow separation and total pressure adjustment mechanism (Mode B) and predicted initial unblocking PR values which agreed reasonably well with experimental data. There was disagreement between assumed model control volume boundary conditions and corresponding experimental values. Initial efforts during the current program were directed toward changing the previous model by incorporating more accurate boundary conditions. This included more accurate modeling of the igniter-nozzle shock configuration and the use of experimentally derived motor-nozzle pressure distributions.

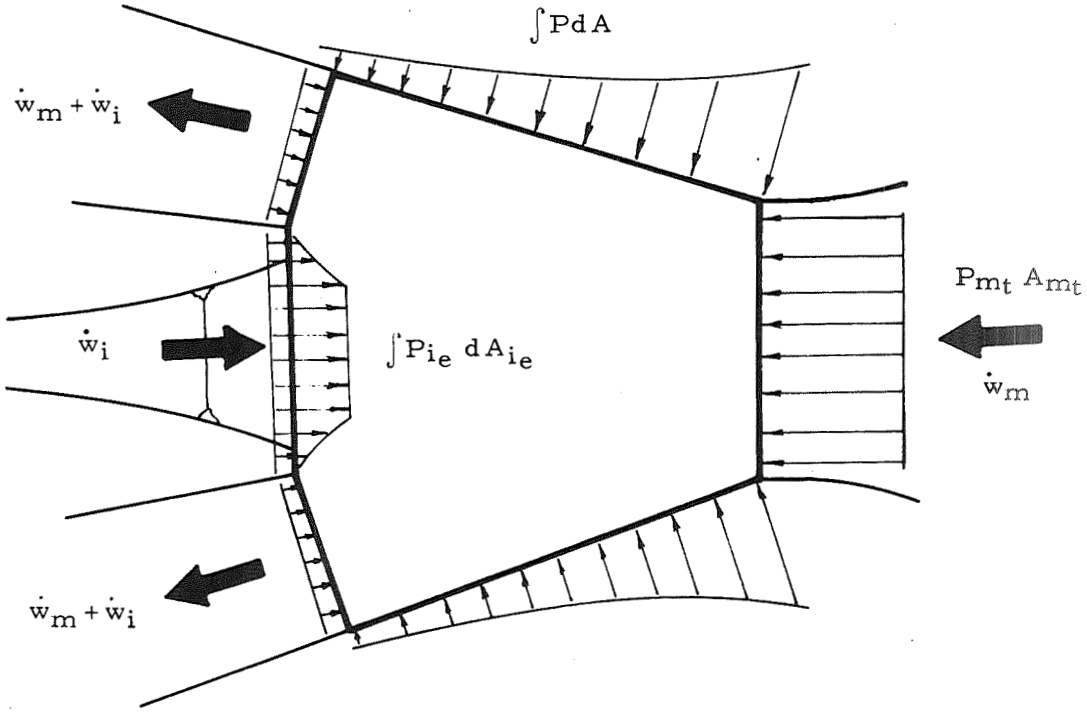

Figure 39. Final Unblocking Control Volume

The initial modeling efforts were not successful because of an inability to accurately define conditions at the slant area. Analysis indicated that the slant momentum vector contained a significant component not normal to the slant area. Studies to analytically model the slant area flow did not provide results which could be rationally justified with the limited motor- and igniter-nozzle pressure data.

Subsequent studies were directed toward modifying the previous model by using more nearly correct igniter pressure and momentum terms. This modified model provided a conservative approximation of the unblocking pressure ratios for all cold-flow model configurations and the solid-propellant motor data. However, there were disagreements between the experimental and model boundary values for some conditions. The fact that the model did give approximately correct values is attributed to the fact that: (1) gross features of model in general agreed with the experimental results, (2) the model was internally consistent, and (3) failures to exactly model conditions at one control volume boundary were off-set by a compensating error on another boundary.

The following sections present observed experimental conditions at final unblocking and an analysis of the modified final unblocking model.

3.3.3.1 Flow-Field Analysis

Igniter Nozzle

Final unblocking occurred at relatively low pressure ratios after a period of unstable flow during which the motor alternately unblocked in Mode A and reblocked in Mode B. Figure 40 presents typical igniter nozzle pressure data at the point of final unblocking (Mode B) for ϵ^* locations of 1.20, 1.35, and 1.50. Figure 41 shows three distinct flow structures which are believed to correspond to the pressure distributions at these ϵ^* values. For low ϵ^* values (1.20) the igniter throat was either choked or unblocked with subsonic flow separation. For this case the required igniter total pressure loss occurred through viscous mixing. For intermediate ϵ^* values (1.35) a strong shock exists within the igniter exit cone with flow separation immediately downstream of the shock. At high ϵ^* locations (1.50) it appeared that a triple-point shock or similar configuration exists.

Motor Nozzle

Motor-nozzle wall pressures were in an oscillatory state at the time of final unblocking. Consequently the pressure distribution corresponding to the limiting unblocking mode was difficult to select. Figure 42 presents pressure data for three ϵ^* values. The only significant feature of these profiles was the fact that the slant area exhibited a sonic or nearly sonic pressure ratio for all ϵ^*.

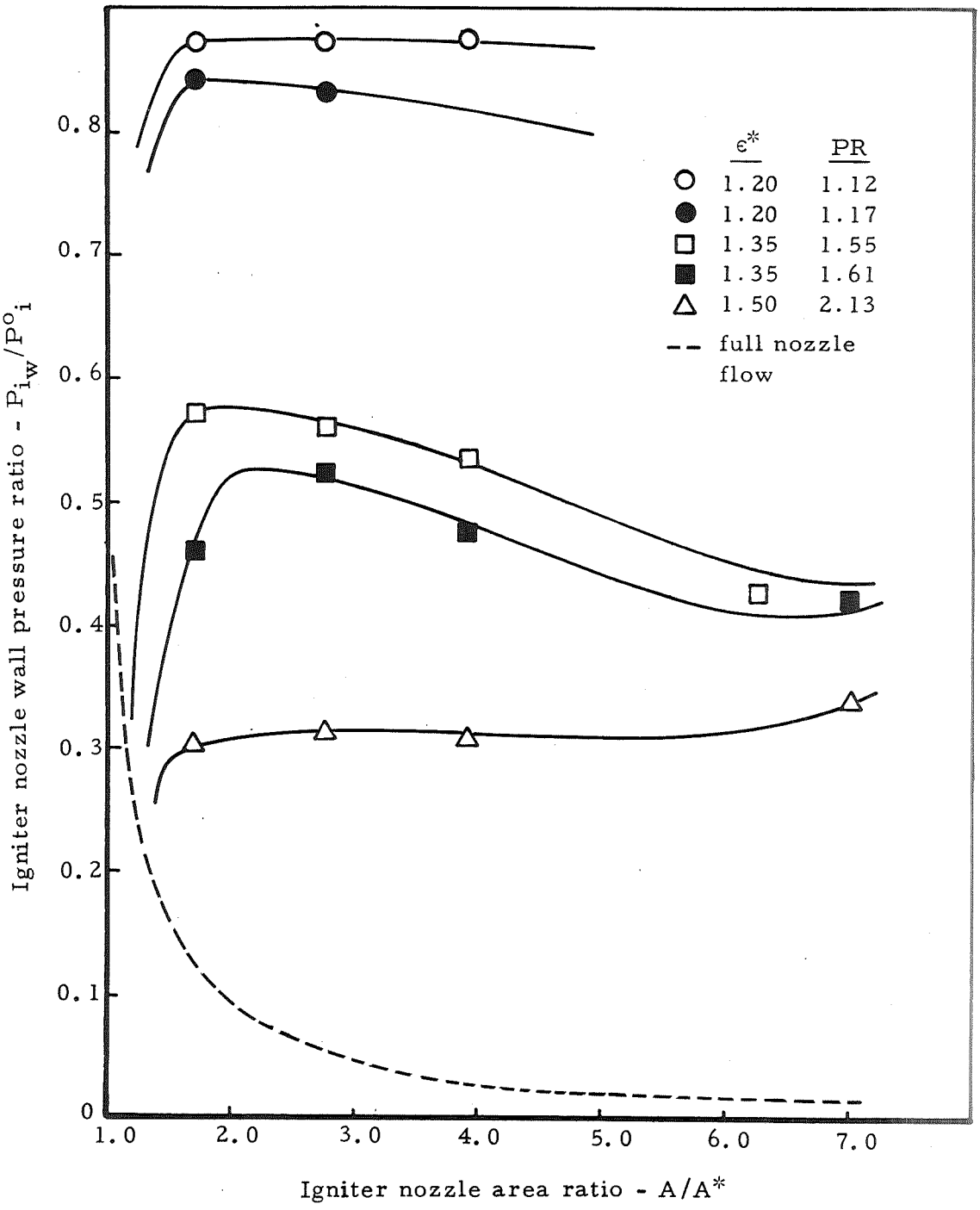

Figure 40. Final Unblocking Igniter-Nozzle Pressure Data

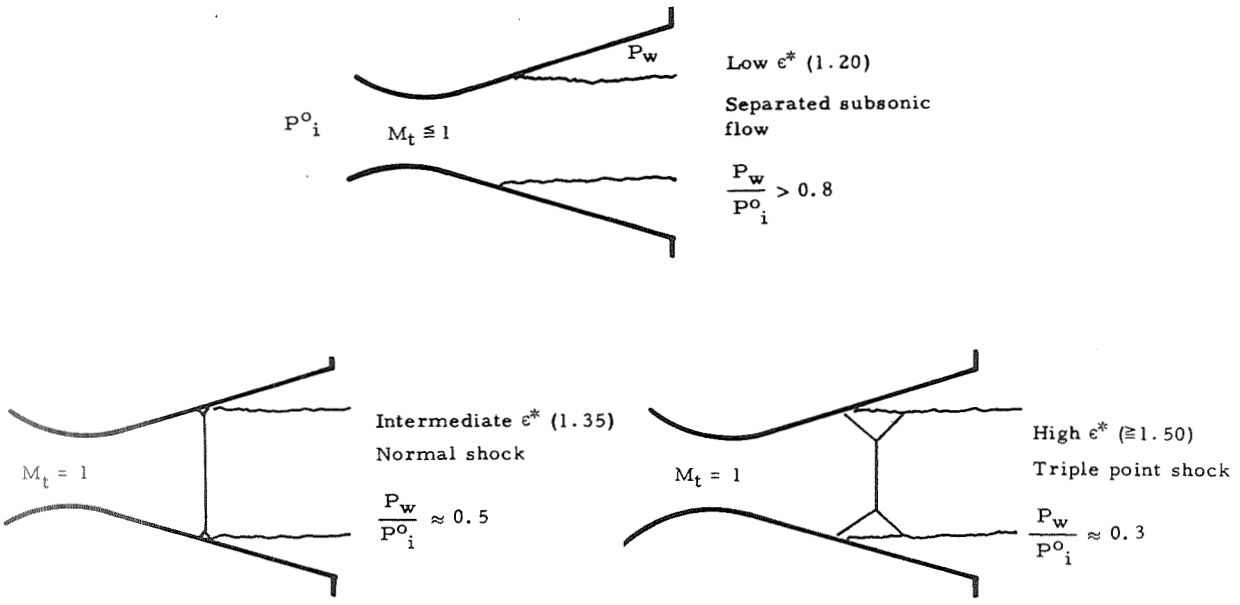

Figure 41. Final Unblocking Igniter-Nozzle Flow Structures

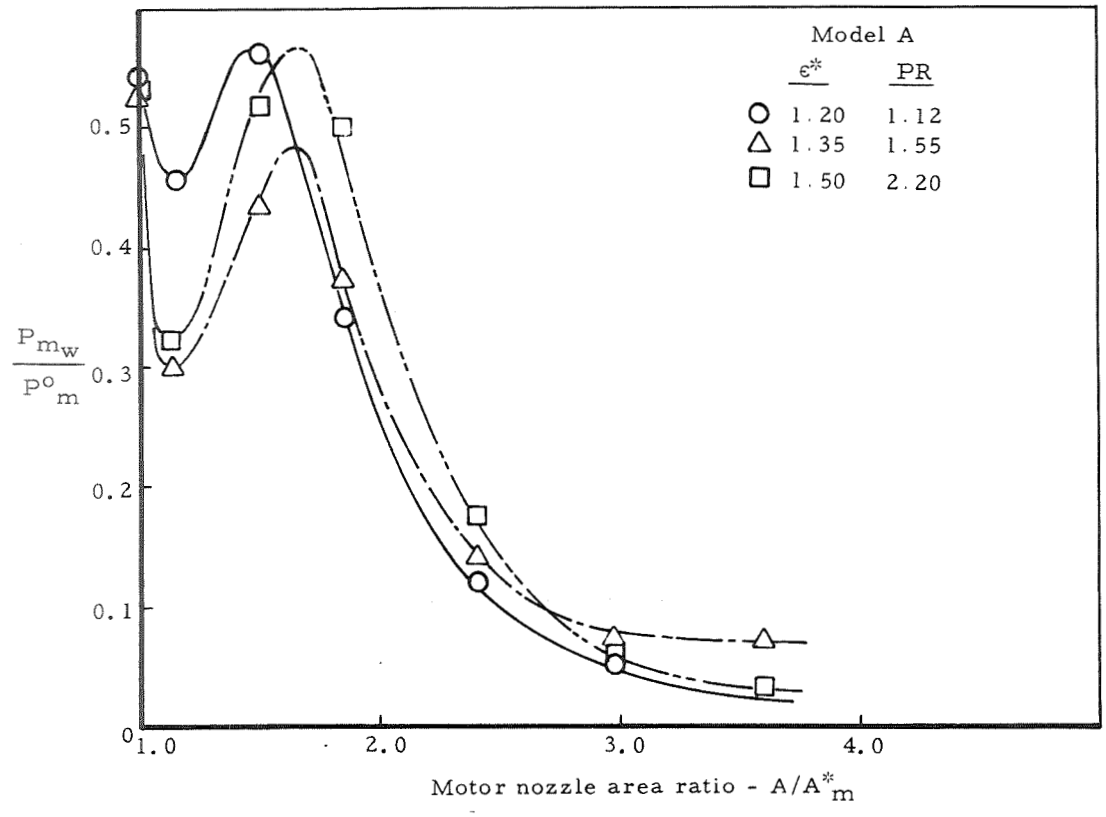

Figure 42. Motor-Nozzle Pressure Distribution in Final Unblocking

Analytical Model

The analytical model was based upon a mass and momentum balance taken on motor and igniter control volume as shown in Figure 39. Assumptions made in constructing the model were:

(1) Flow entering and leaving the control volume may be described by axisymmetric and isentropic flow relations.

(2) Pressures are constant across main-motor throat and slant area.

(3) Pressure distribution along the main-motor exit cone assumes a parabolic shape.

(4) Any main-motor flow shocks occur at sufficiently low Mach numbers so that the total pressure losses may be neglected.

(5) A normal shock occurs within the igniter-nozzle exit cone at an approximate igniter jet area such that the igniter total pressure is equal to the main motor pressure.

(6) The igniter flow separates immediately after the normal shock and it may be described by a constant area stream with constant boundary pressure.

(7) Pressure forces across igniter exit are constant across the stream tube and are parabolic in shape from the stream tube to the igniter lip.

(8) The slant area flow is full and supersonic.

To establish the applicability and accuracy of this model, it is necessary to first compare model predictions with experimental results and finally to compare the model with experimental data to find out the degree of agreement of the basic assumptions.

Comparison of predicted model values with experimental results with the cold-flow tests indicated good agreement for low ϵ^* values, with less accuracy at intermediate and high ϵ^* values, as shown in Figure 43.

This behavior of the analytical model holds for all the igniter models. Comparison of the model with solid-propellant motor data revealed a conservative prediction with a moderate disagreement for all ϵ^* values.

Model assumptions which exhibited the greatest disagreement were the motor nozzle pressure distributions and the igniter nozzle pressure and momentum distribution terms. The motor wall pressure integral in all cases was lower than the experimental values. However, this error was probably

offset by a compensating error in the slant area momentum term which was necessary to obtain mass and momentum balance. The model igniter shock configuration agreed fairly well with the experimental values at moderately low and intermediate ϵ^* values. However, at high ϵ^* locations experimental data indicated that a triple-point shock structure probably existed instead of modeled normal shock. This is probably the reason for the major disagreement between model and experiment at high ϵ^* values.

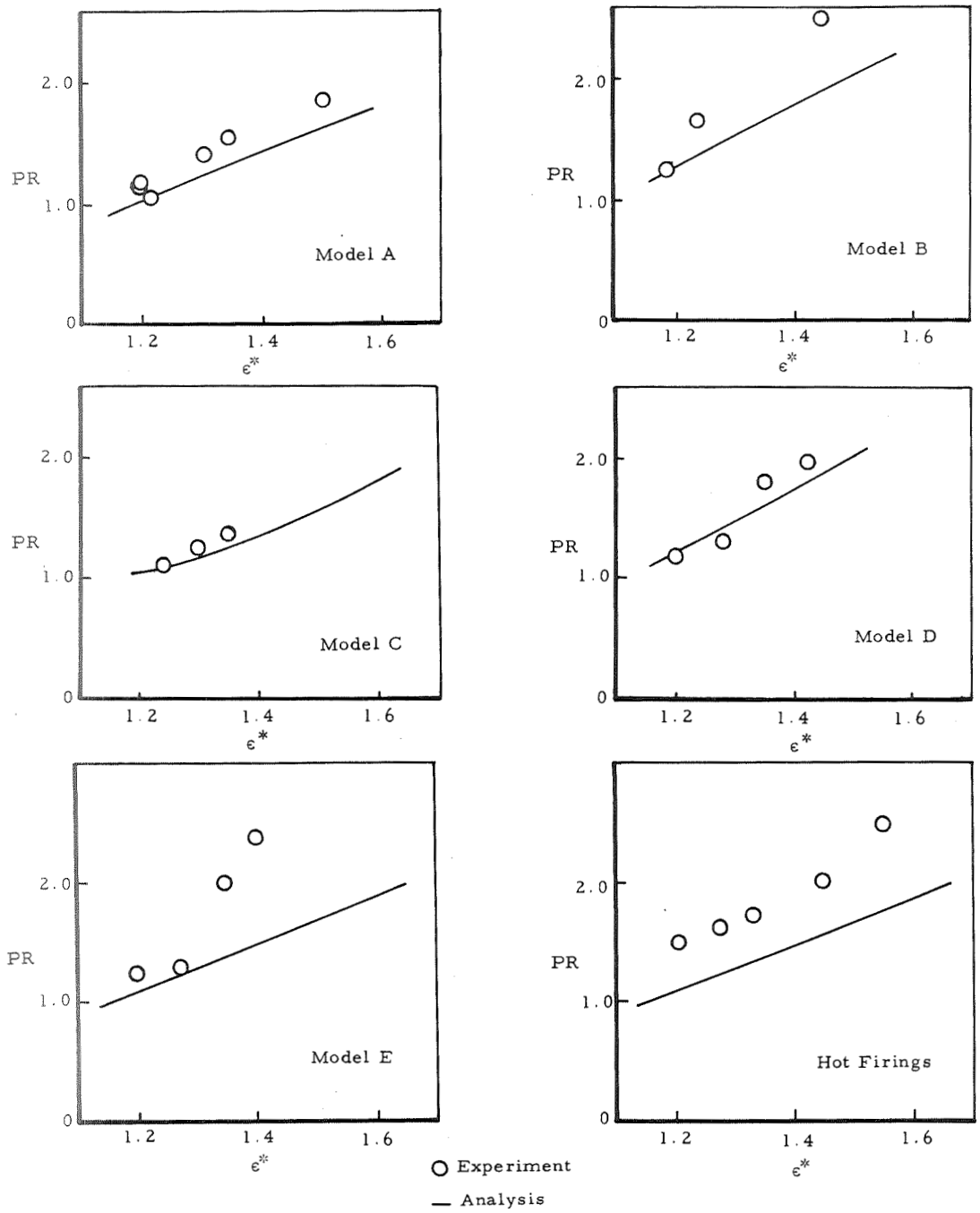

Figure 43. Comparison of Experiment and Analysis in Final Unblocking

3.3.4 Oscillations

The data evaluation and analytical modeling of the oscillatory behavior were oriented toward achieving two specific goals: determining the PR and ϵ^* conditions and flow-field structure which produced the onset of oscillations themselves and their effects on the motor-nozzle pressure distribution. Two types of oscillations were found to exist. Major oscillations occurred, as have been previously described, as the result of alternation between two distinctly different flow fields, Modes A and B, and variations of these types. Secondly, minor oscillations were frequently, although not always, observed early in the post-ignition period. Efforts were concentrated almost entirely on the major oscillations and the conditions under which they develop.

It appeared that the major flow-field oscillations were produced by inherently unstable separation of the overexpanded igniter nozzle flow. Consequently, the major emphasis was placed upon evaluating and modeling the igniter nozzle flow, independent of the nozzle flow field and the interactions between the two.

The first attempt to identify the igniter flow-field structures just before and during the oscillations was to construct flow-field models which produced the observed igniter-nozzle pressure distributions and the associated PR values. This approach failed, universally, apparently because of the simplifying assumptions which were required.

The second approach was to develop a series of three different types of separation and total pressure adjustment models whose general behavior under varying conditions could be compared with experimental results. This approach was successful, to the degree that the flow field qualitatively behaved in a fashion similar to that of the Mode A model before oscillations. During oscillations, the flow field alternated between the Mode A type (oblique shock) and the Mode B structure behaving more nearly like a typical normal shock with or without lambda feet.

Modeling of the overall motor-nozzle flow field was unsuccessful, apparently because of insufficient knowledge of the combined flow conditions in the slant area.

3.3.4.1 Analysis of Experimental Data

General Characteristics

The igniter- and motor-nozzle pressure oscillations were generally similar in nature for all igniter model configurations. The minor oscillations were characterized by moderate motor-nozzle pressure oscillations with basically stable igniter nozzle flow. The major oscillations were characterized by high-amplitude pressure oscillations in both igniter and motor nozzles.

Igniter-nozzle pressure oscillations during periods of unstable separated igniter-nozzle flow were predominately longitudinal in character. However, lateral and rotational components were often noted, especially during misalignment tests. Motor-nozzle pressure oscillations appeared to result from response of the motor-nozzle flow field to the pulsating movements of the igniter jet. Like the igniter nozzle, the predominant oscillations were longitudinal in nature with some asymmetric behavior.

The minor nozzle pressure oscillations were not always observed and then only before the onset of (major) oscillations. The amplitudes were largest when the motor nozzle was blocked. After initial unblocking, the motor-nozzle oscillation amplitudes were attenuated and sometimes ceased altogether before the onset of oscillations. The igniter-nozzle flow varied between full and stable, separated and stable or separated and stable with occasional moderate perturbations. Because of the random existence of the minor oscillations and their relative insignificance, with respect to the major oscillations, they will not be discussed further. All references to oscillations will be understood to mean major oscillations unless otherwise noted. References to stable or unstable flow will mean operation either without or within the region of major oscillations, respectively.

The time-dependent behavior of the (major) oscillations was significantly affected by the level and rate of decay of PR. When the PR reached a plateau level at the oscillation onset boundary, or was decaying slightly, the pressure oscillations were intermittent. Sometimes this intermittency was characterized by momentary unstable pressure pulsations and at other times by alternate periods of stable and unstable flow. (See Figure 18.) When the igniter chamber pressure decayed into the region of unstable PR, the oscillations were continuous. The magnitude of the oscillations were proportional to the PR, i.e., for relatively stronger igniter flow fields the oscillations were larger in amplitude. Typical continuous oscillations are shown in Figure 20.

3.3.4.2 Igniter-Nozzle Flow-Field Analysis

Igniter Nozzle Pressure Distribution

Typical igniter-nozzle wall-pressure distributions at various igniter to motor pressure ratios are shown in Figure 44 for Model A. At the highest pressure ratio of 5.09 the nozzle was flowing full. As the pressure ratio (igniter chamber pressure) decreased, the igniter nozzle flow became more overexpanded and began to separate. The separation point moved progressively upstream to lower nozzle area ratios until it reached the last stable pressure profile at PR = 2.66. After the onset of oscillations the pressure profiles appeared to oscillate between two extremes as illustrated by the two different pressure distributions at PR = 1.59. The lower pressure-distribution curve at PR = 1.59 corresponds to supersonic pressure ratios while the upper curve is predominately subsonic.

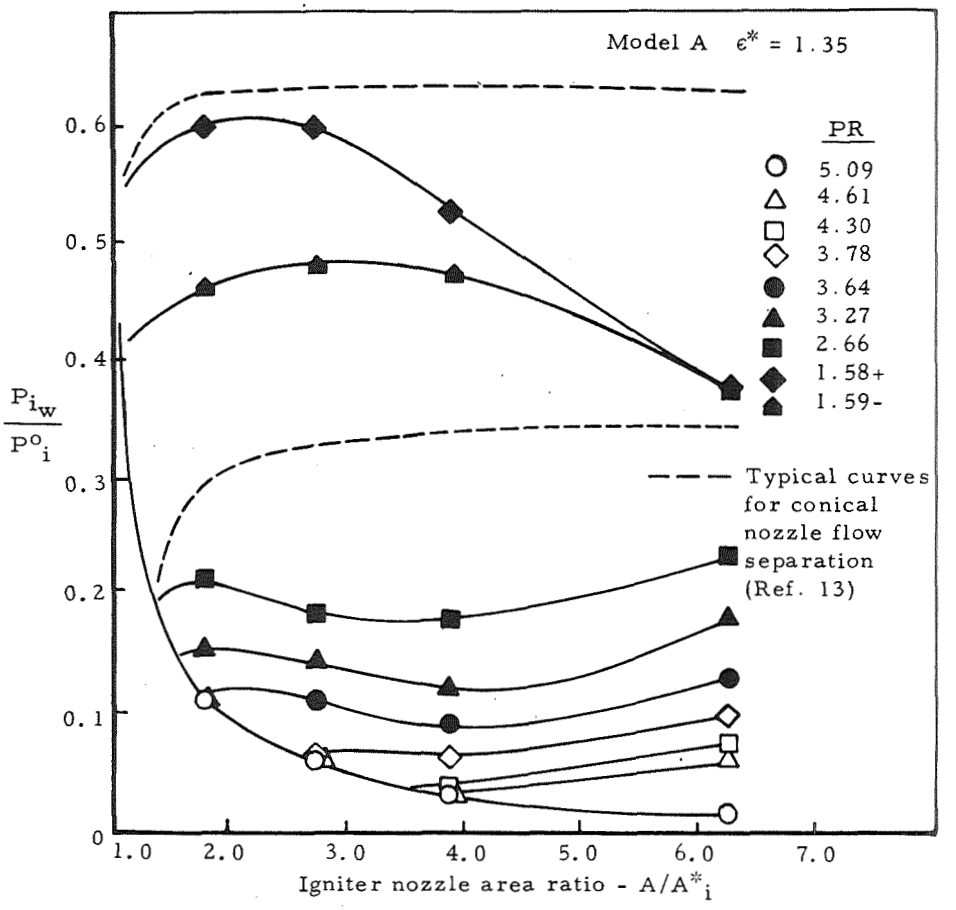

Figure 44. Igniter-Nozzle Wall-Pressure Distributions

The igniter-nozzle pressure distributions did not agree with the monotonically increasing wall pressures after separation which are normally expected of overexpanded conical nozzles[8, 9, 10, 13]. Attempts to identify igniter flow fields which would produce these typical pressure distributions were not successful. These unusual distributions probably result from distortion of the igniter flow field by the external flow-field structure and pressure field, or by oscillations of such high frequency that no flow field could develop fully.

Igniter-nozzle pressure-ratio distributions for various ϵ^* locations at the onset of oscillations are shown in Figure 45 for Models A through E. These data indicate that at the onset of oscillations the igniter-nozzle pressure-ratio distribution for a given model is independent of ϵ^* location. This pressure profile uniformity indicates that the igniter-nozzle flow field within the nozzle is identical for all ϵ^* locations, and suggests that the external igniter jet flow shape is likewise constant. In this eventuality the change of PR for onset of oscillations with ϵ^* would depend only upon the motor total pressure adjustment across the igniter bow-shock, assuming that the contact surface position is fixed with respect to the igniter.

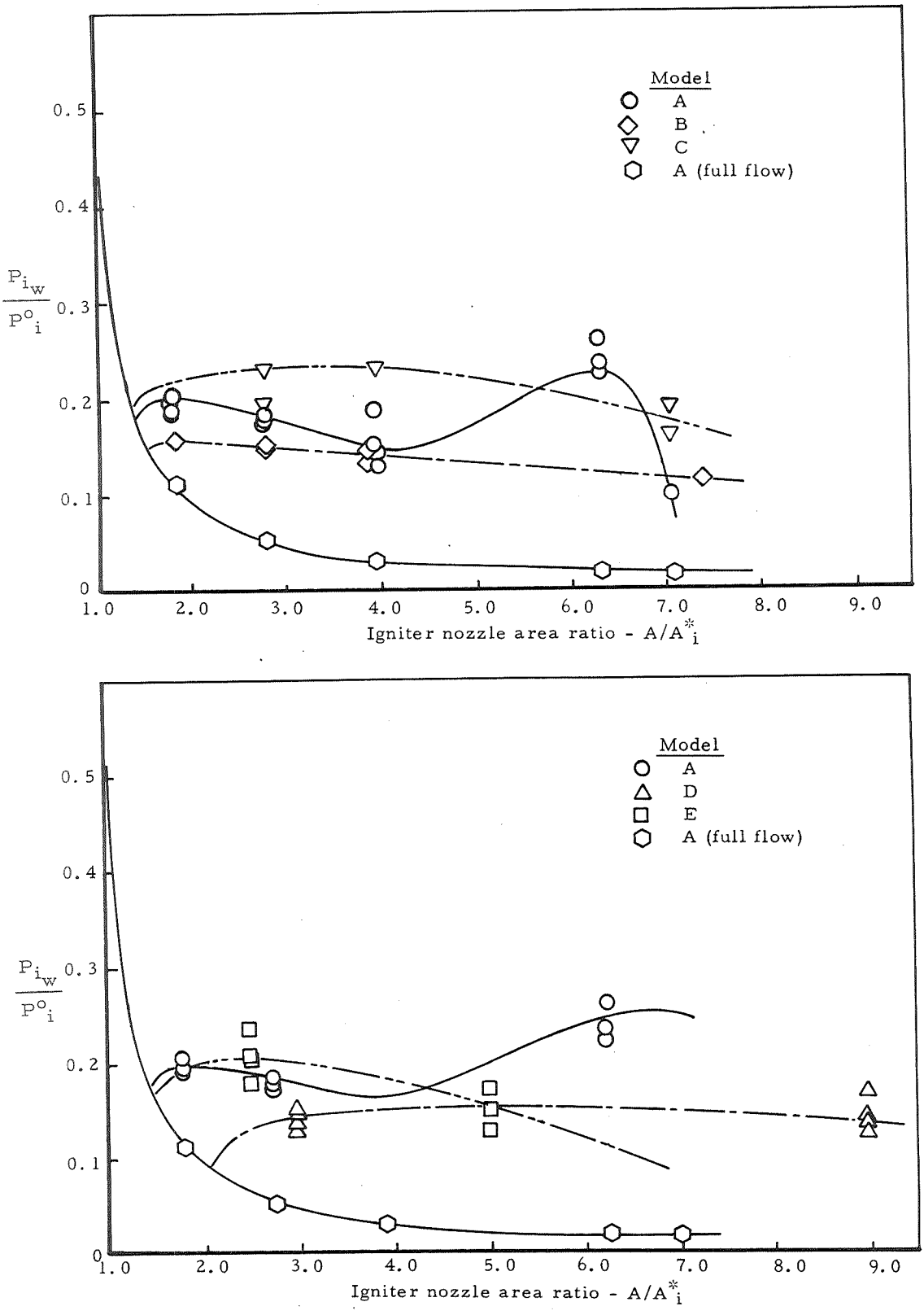

Figure 45. Igniter-Nozzle Pressure Distributions at Onset of Oscillations

Igniter Flow Field Structure

The initial approach to reconstruct the Mode A and B flow fields from the experimental wall-pressure distribution failed because of an inability to define the igniter-nozzle flow separation point and flow-field total pressure loss. A second approach was the selection and analysis of three plausible flow fields from other separated nozzle flow studies. The three configurations studied were (1) a normal shock, (2) a triple-point shock, and (3) an oblique shock with a regular reflection terminating in a normal shock. The modeled flow fields corresponding to these three shock structures are shown in Figure 46.

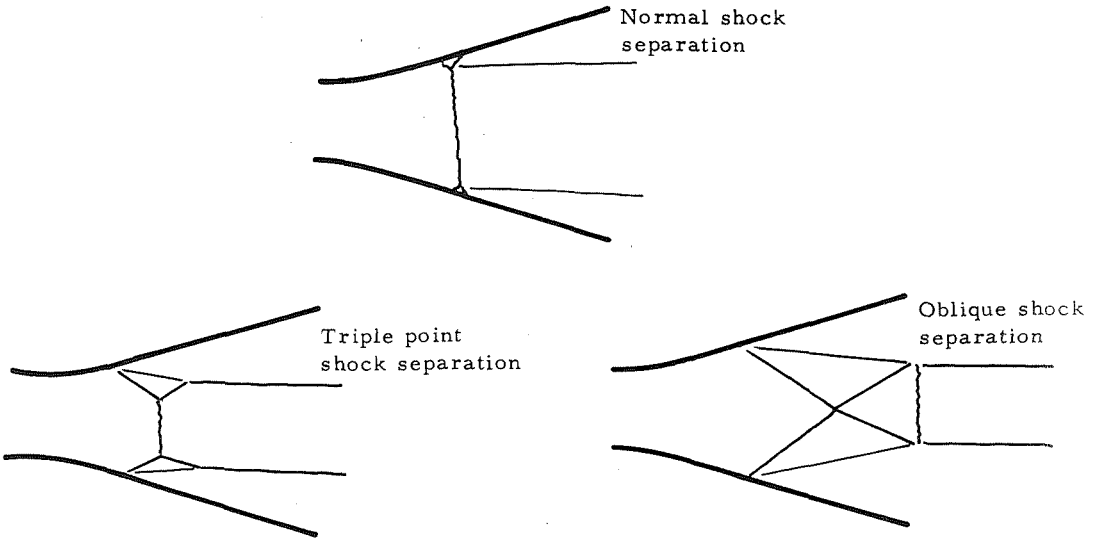

Figure 46. Igniter Flow-Field Models

In constructing the analytical models it was assumed that the nozzle flow field could be described by theoretical inviscid isentropic and shock relationships. Further assumptions which were consistent with observed nozzle wall pressure data were:

For normal shock—

The igniter flow separates immediately after the normal shock and flows parallel to the nozzle axis.

For triple-point shock—

(1) The shocks are straight.

(2) The static pressure downstream of the second oblique shock is equal to the static pressure downstream of the normal shock.

(3) The flow direction downstream of the second oblique shock is parallel to the streamline passing through the triple-point.

For oblique shock—

(1) The shocks are straight.

(2) The oblique shock reflection is regular.

(3) The terminal normal shock occurs at the Mach number of the flow immediately downstream of the reflected shock.

Two parameters were used to assign numerical values to each flow-field structure study. These were the static wall-pressure ratio across the separation point and the igniter total pressure loss across the modeled igniter shock structure at the nozzle axis.

Results of the parametric study for the three shock configurations are plotted in Figure 47 as a function of the two characteristic pressure-ratio parameters. The locus of states for the normal shock and triple-point shock configurations each represent a unique solution for separation at a given nozzle area ratio. Each curve for the oblique shock configuration represents solutions at a distinct separation area ratio, but for varying initial oblique shock turning angles. These oblique shock curves in turn define two constraining boundaries. The first is the locus of conditions for which the oblique shock becomes a Mach line at the nozzle center line and beyond which the model has no solutions. The second corresponds to the limiting conditions at which the initial oblique shock becomes a strong shock.

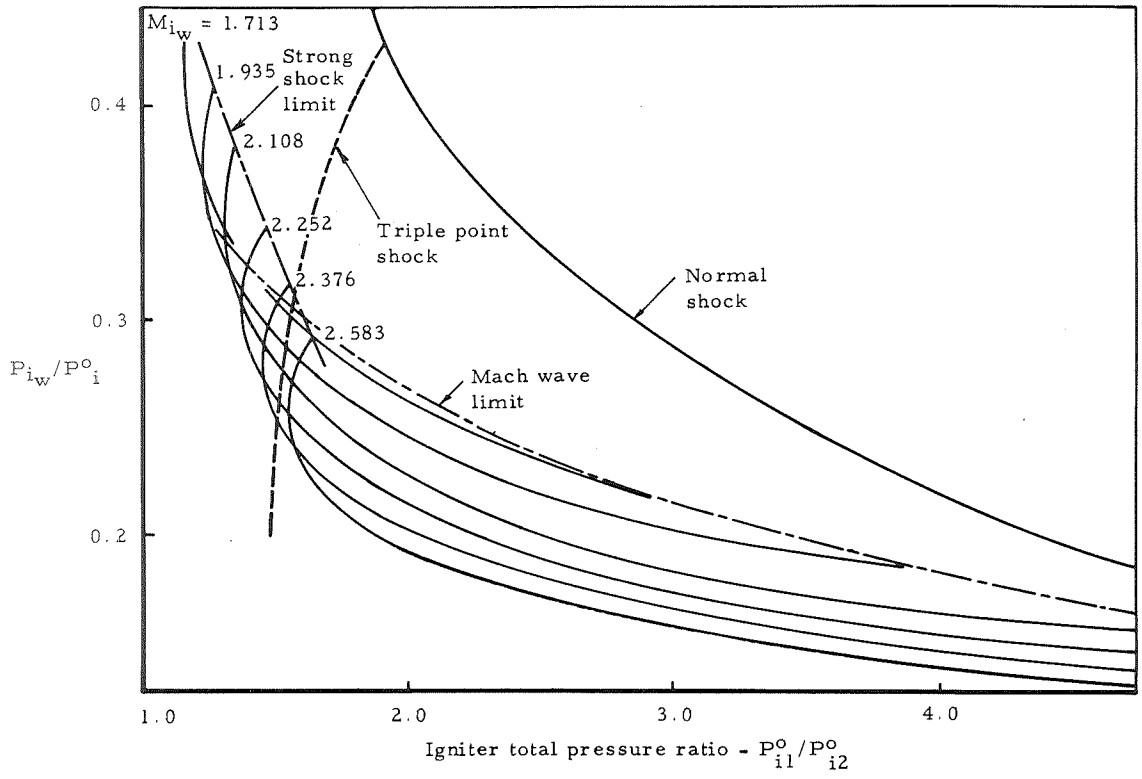

Figure 47. Igniter Flow-Field-Model Operating Characteristics

The igniter flow models were evaluated by comparing experimental data with the three theoretical shock configuration solutions. The experimental points were chosen for a low ϵ^* position to avoid accounting for the total pressure loss across a main flow bow-shock. At low ϵ^* values the motor-nozzle flow upstream of the slant area remains subsonic so that with the exception of viscous losses the igniter to motor chamber pressure ratio should be approximately equal to the reciprocal of the igniter jet total pressure recovery. Experimental points selected for Model D at $\epsilon^* = 1.35$ are shown in Figure 48 for continuously decreasing PR. The igniter flow is stable for points DO1, DO2, and DO3, with point DO3 being the last condition for which the flow is entirely stable. Points DN1, DN2, DN3, and DN4 are a sequence of points taken at the peaks of the igniter-nozzle pressure oscillations, based upon P_{118}. Conversely, points DO4 through DO7 are taken at the valleys of the oscillations, where the flow appears to return to the flow mode which existed before the oscillations began.

The wall-pressure ratio versus PR of these data, along with data from Model A, are plotted in Figure 49 with the theoretical curves of Figure 48.

The bimodal nature of the oscillations is clearly evident. The behavior of the flow leading to and during the oscillations is apparently as follows:

(1) Although only one point, DO1, is shown on the figure, Curve I is the locus of states during separated operation in Mode A at high PR. The points progress upward along Curve I until they reach Curve II.

(2) Upon reaching Curve II, which apparently is the limiting condition that the oblique separation shock degenerates to a Mach wave at the centerline, the points then move to the left along Curve II.

(3) After passing through point DO3, the flow jumps to the conditions represented by point DN1 on Curve III.

(4) As PR continues to decrease, the flow alternates between Curves II and III.

(5) Curve II', upon which the left-most point lies, has been drawn as separate from Curve II, and as such, could represent a shift to the alternate limiting condition of the multiple-shock configuration, indicating that the oblique shock is strong rather than weak. However, it is equally possible that Curve II' is an extension of Curve II.

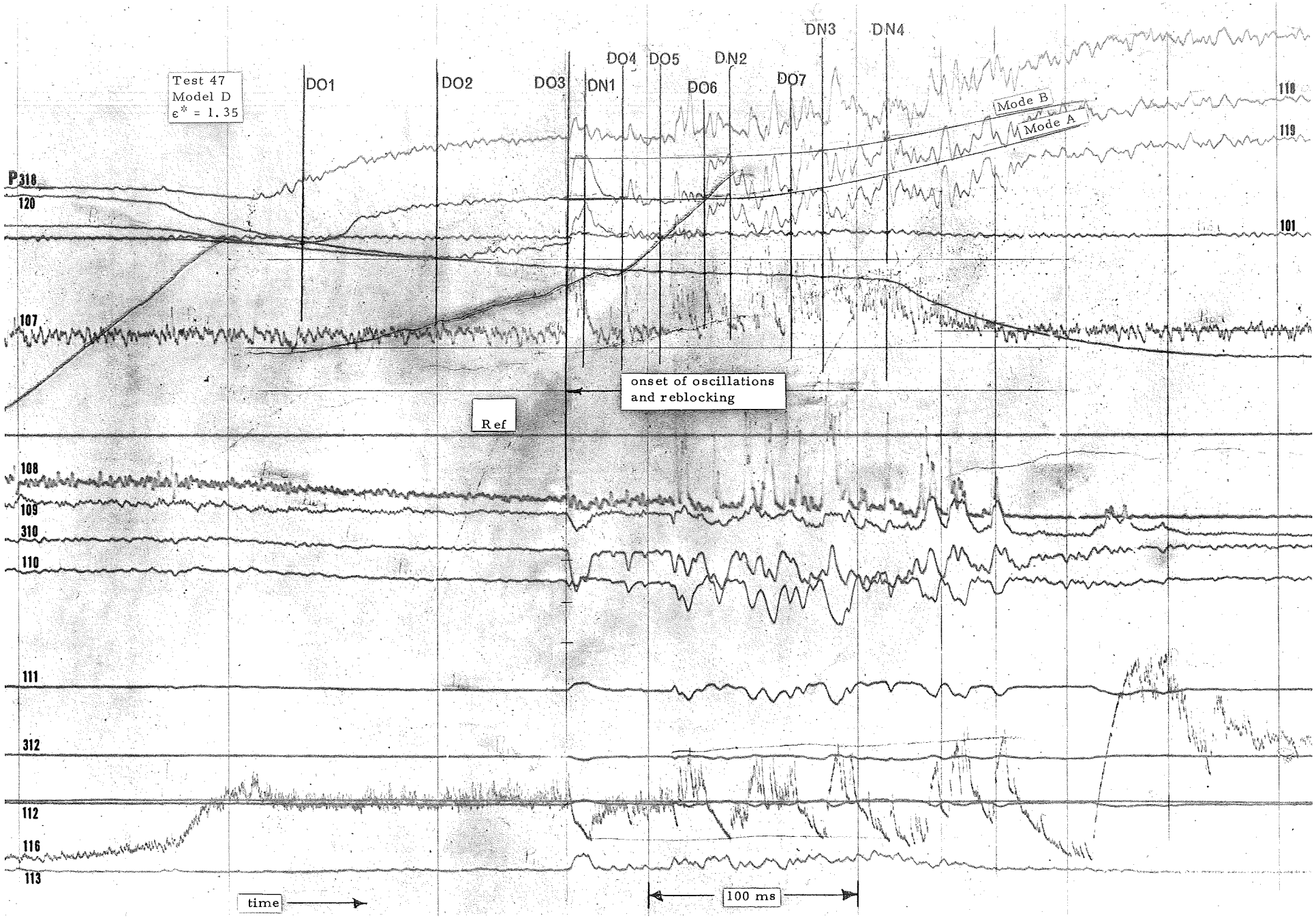

Figure 48. Oscillation Data, Model D

Although the experimental and theoretical loci do not coincide exactly, the general agreement is another piece of evidence to show that two different flow modes exist. Also, this agreement indicates that the actual and modeled igniter flow fields are similar in their essential features; i. e., that the Mode A flow field corresponds to a multiple oblique-normal shock configuration and Mode B corresponds to a normal shock structure or variations thereof (lamda feet, triple point, etc).

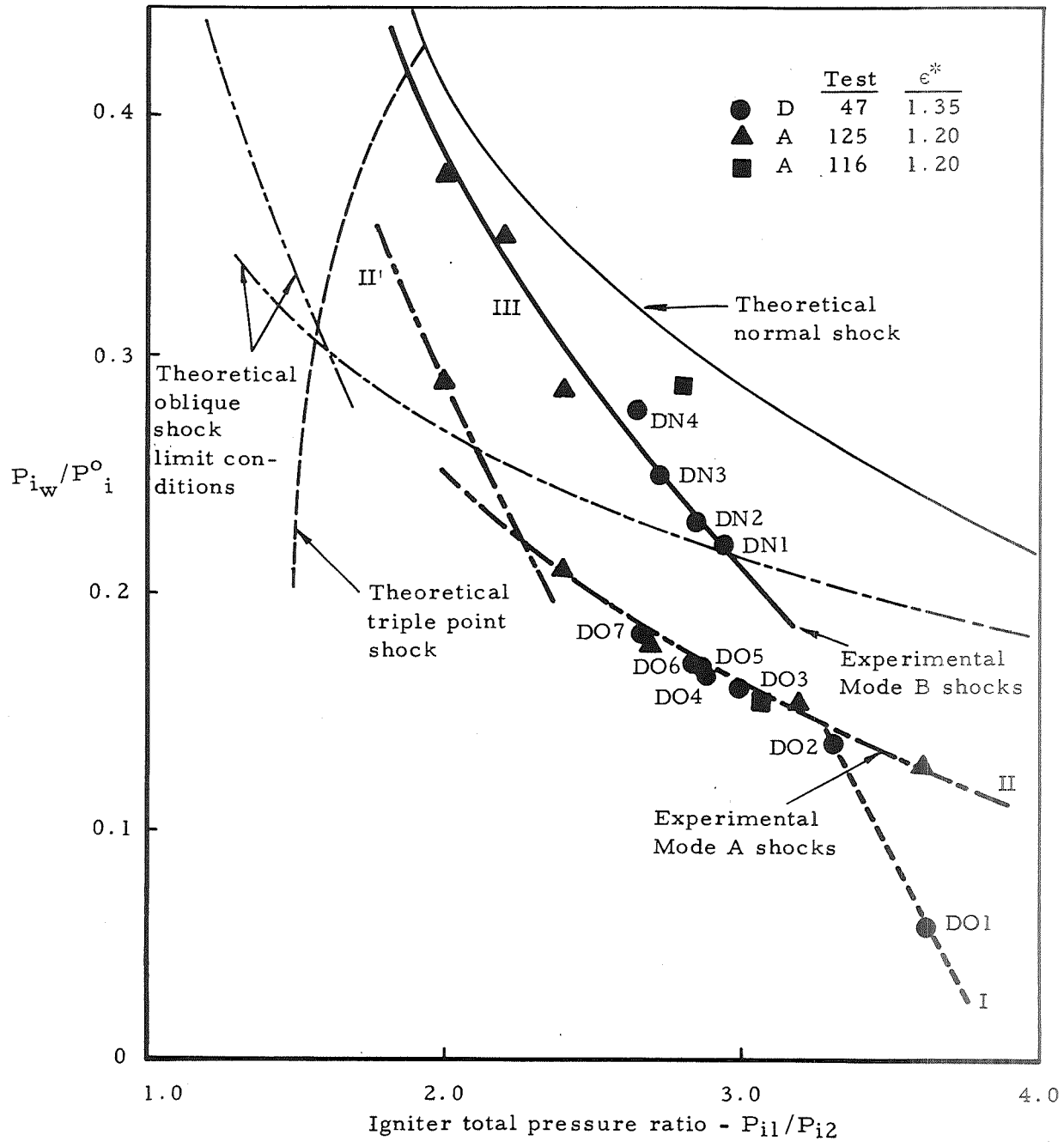

Figure 49. Comparison of Experimental and Theoretical Loci

While the data presented in Figure 49 does not prove the exact configurations of the oscillatory igniter jet flow fields, it supports previous conclusions that two distinct (Mode A and Mode B) flow structures exist and that the onset of oscillations represents the limiting conditions for which an oblique Mode A shock strucuture is the preferred stable configuration. It is possible that continued studies using the available nozzle pressure data might finally lead to some quantitative agreement between model and data. However, this would not necessarily confirm that the model configuration actually conformed to the physical flow field and that the agreement in modeled and physical results would extend to solid-propellant motor conditions. For these reasons it is believed that the oscillation onset conditions cannot be modeled (excepting experimental correlations) without flow visualization studies.

3.3.4.3 Motor-Nozzle Flow-Field Analysis

Motor-Nozzle Pressure Distribution

The motor-nozzle pressure distribution just prior to the onset of oscillations depend upon the igniter model configuration and ϵ^* location. For a given configuration at low ϵ^* values, peak pressures approximately equal to the throat pressure occurred well forward in the nozzle. The amplitude of the peak as well as the location moved downstream as the igniter ϵ^* location was increased (see Figure 50). Lesser pressure variations were noted for different models at equivalent ϵ^* locations as shown in Figure 51 for $\epsilon^* = 1.5$. The decreasing peak pressures correlated with decreasing values of the igniter nozzle lip diameter.

A non-dimensional nozzle pressure integral (just prior to the onset of oscillations) taken over the nozzle surface to the intersection with the slant area was found to be a continuously smooth function of ϵ^* for a given igniter-nozzle configuration. However, the pressure integral at a given ϵ^* location was found to be significantly different for different igniter models as shown in Figure 52. Thus, it appears that it will be difficult or impossible to generalize the nozzle wall pressure integral.

Motor-nozzle pressure distributions after the onset of oscillations were cyclical in nature. Oscillations with the largest amplitude appeared to occur at moderate ϵ^* values (approximately 1.5). Data showing the pressure distributions corresponding to maximum, minimum, and intermediate peak pressures are shown in Figure 53 for ϵ^* values of 1.35, 1.50, and 1.80, respectively.

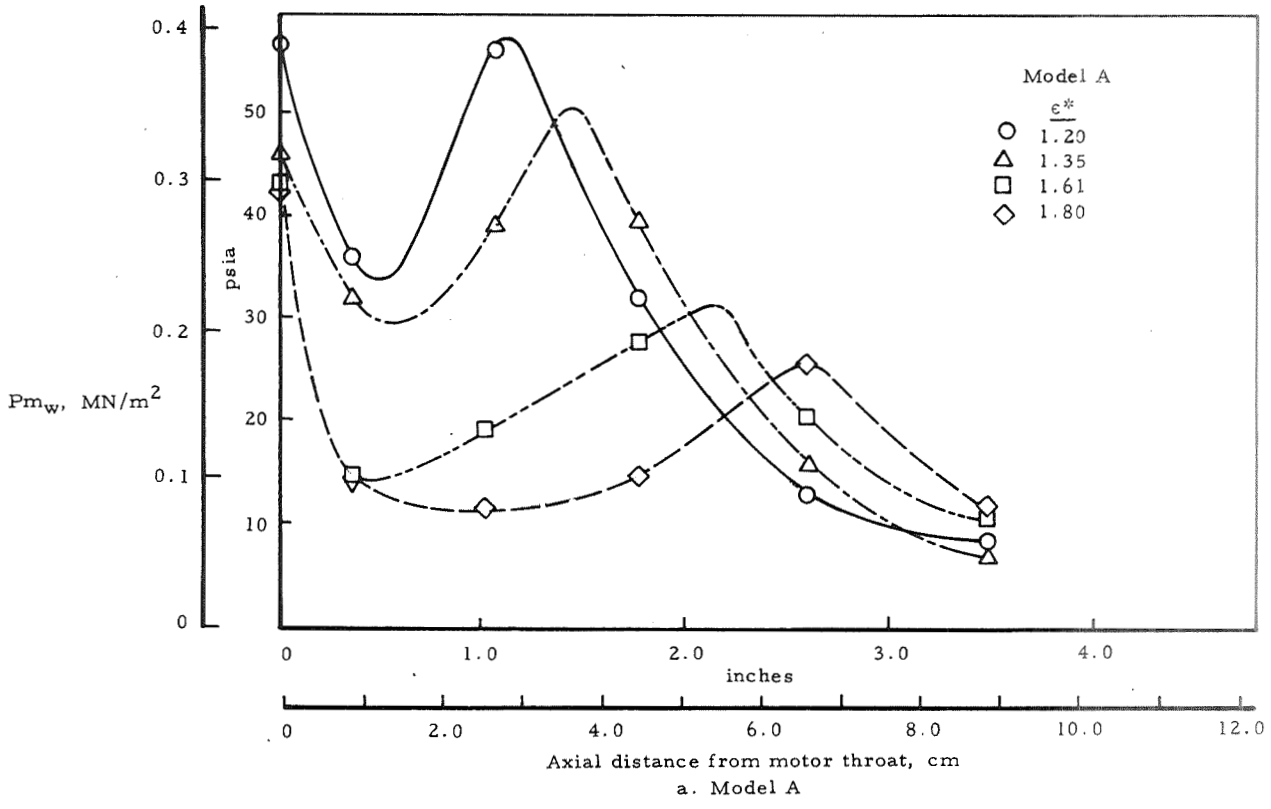

a. Model A

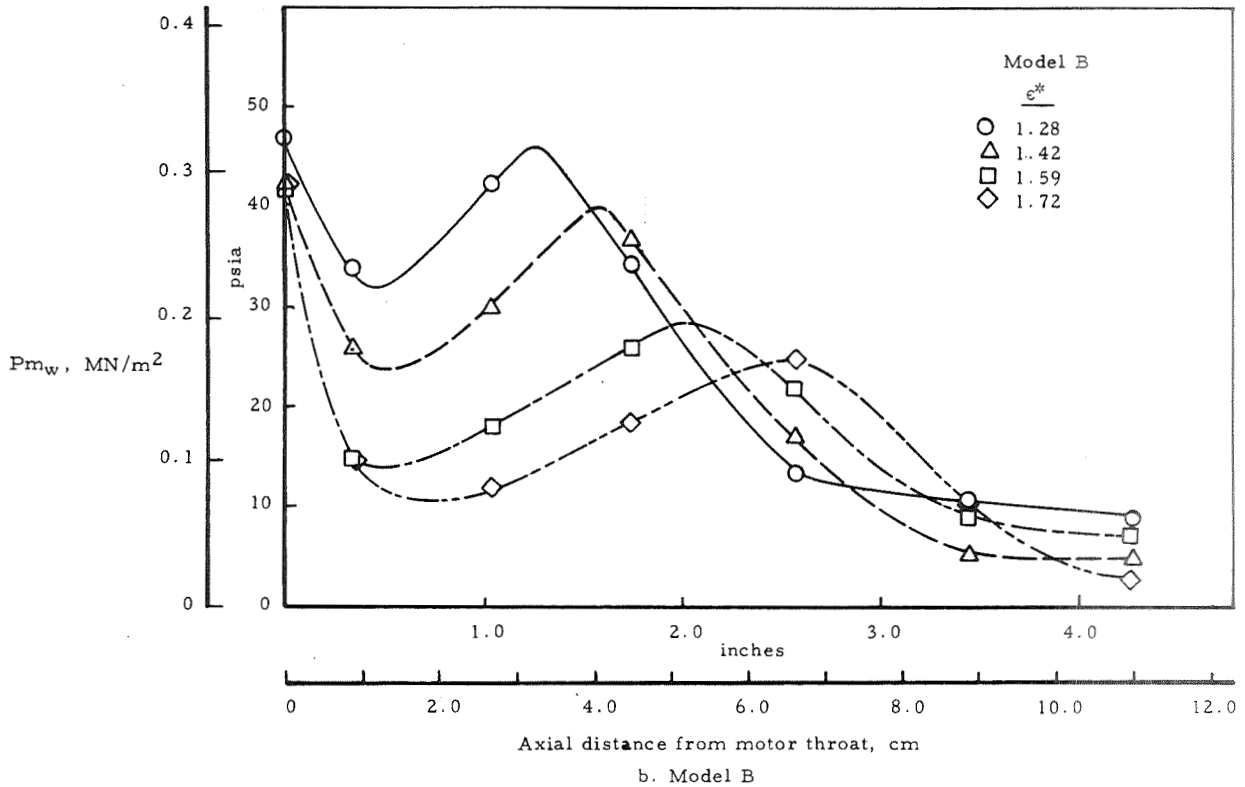

b. Model B

Figure 50. Motor-Nozzle Pressure Data at Onset of Oscillations

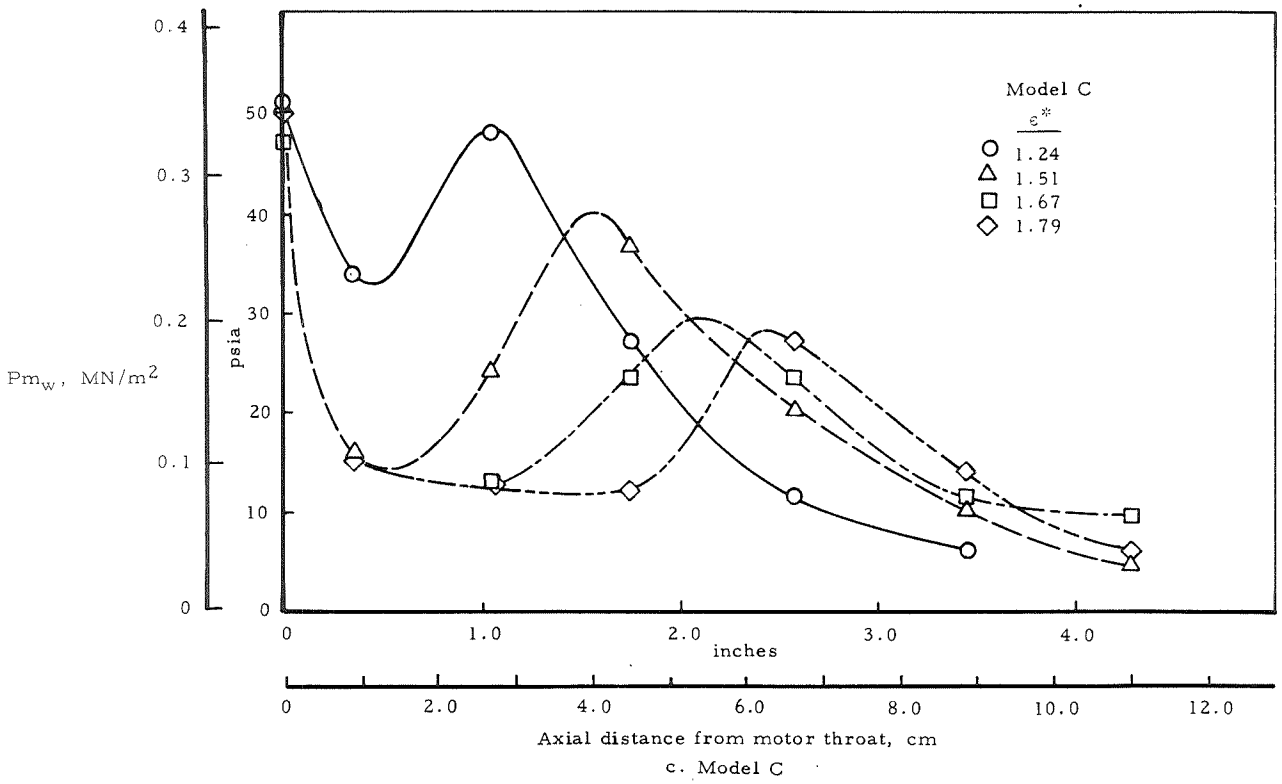

c. Model C

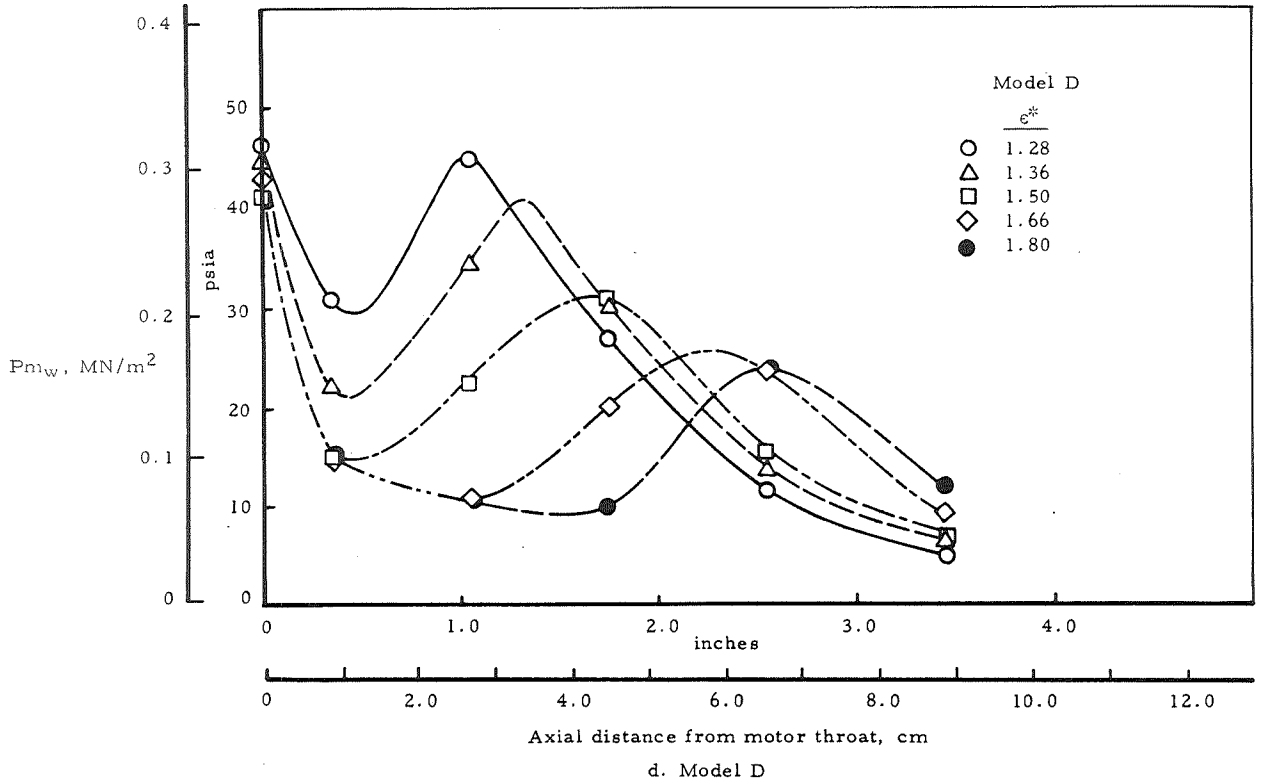

d. Model D

Figure 50. Motor-Nozzle Pressure Data at Onset of Oscillations (continued)

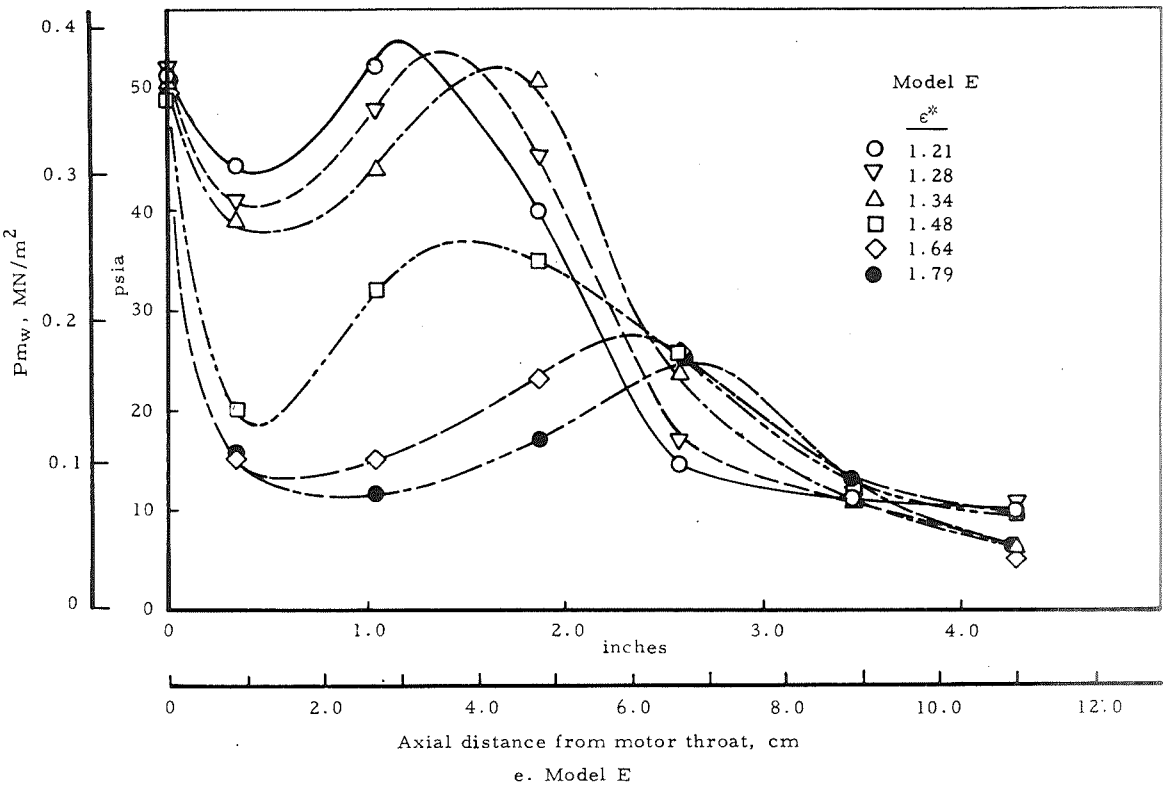

e. Model E

Figure 50. Motor-Nozzle Pressure Data at Onset of Oscillations (concluded)

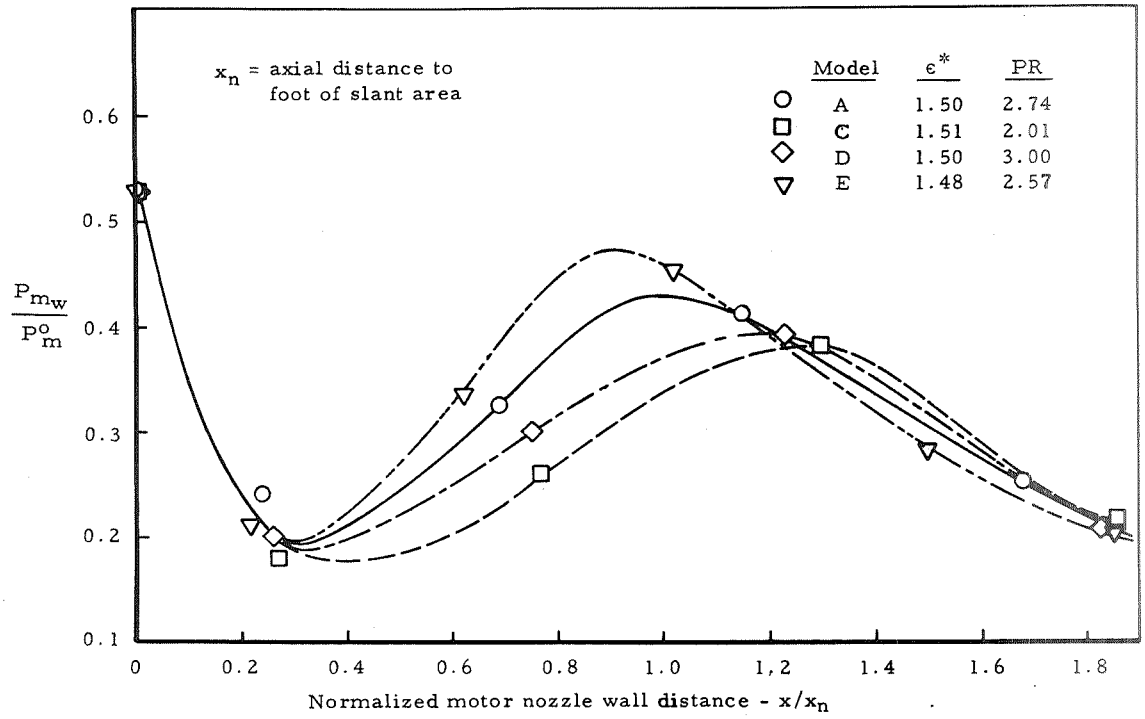

Figure 51. Effect of Model Configuration on Motor-Nozzle Pressure Distribution at Onset of Oscillations

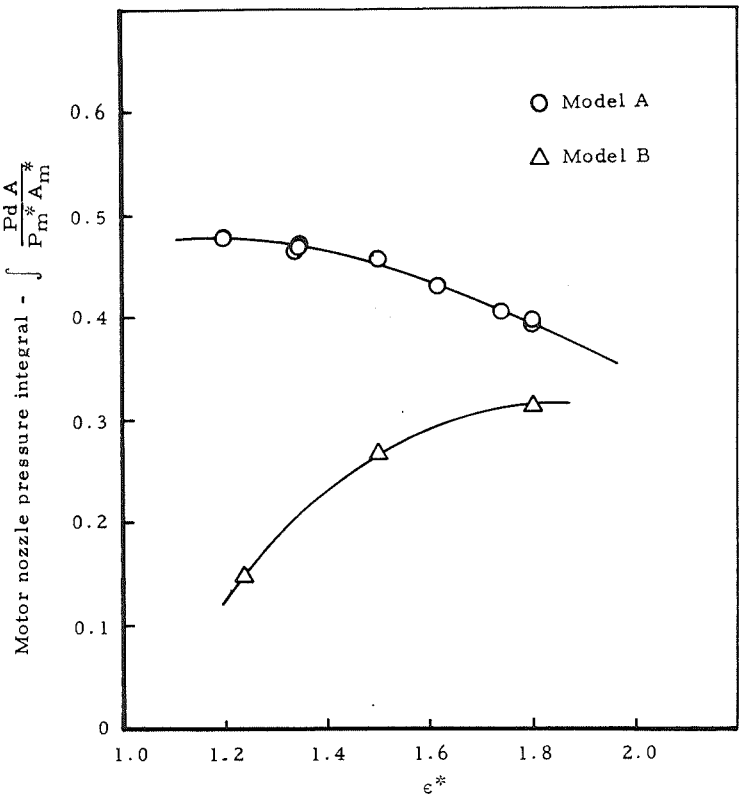

Figure 52. Motor-Nozzle Pressure Integral at Onset of Oscillations

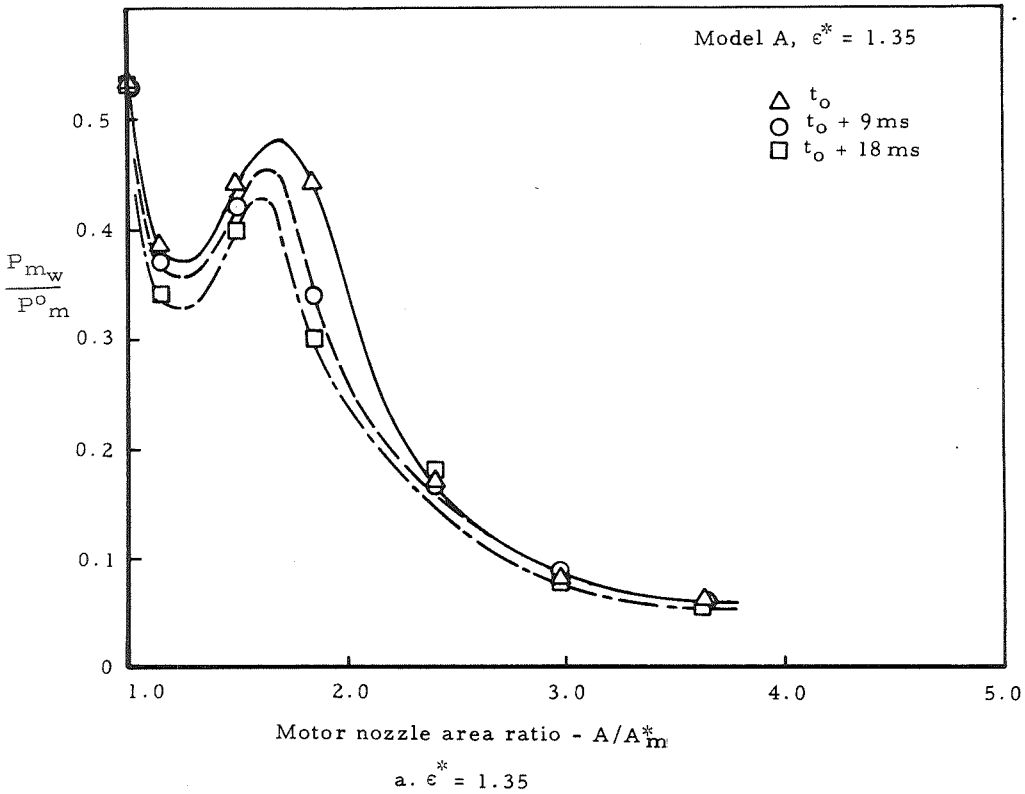

a. $\epsilon^* = 1.35$

Figure 53. Motor-Nozzle Pressure Distributions During Oscillations

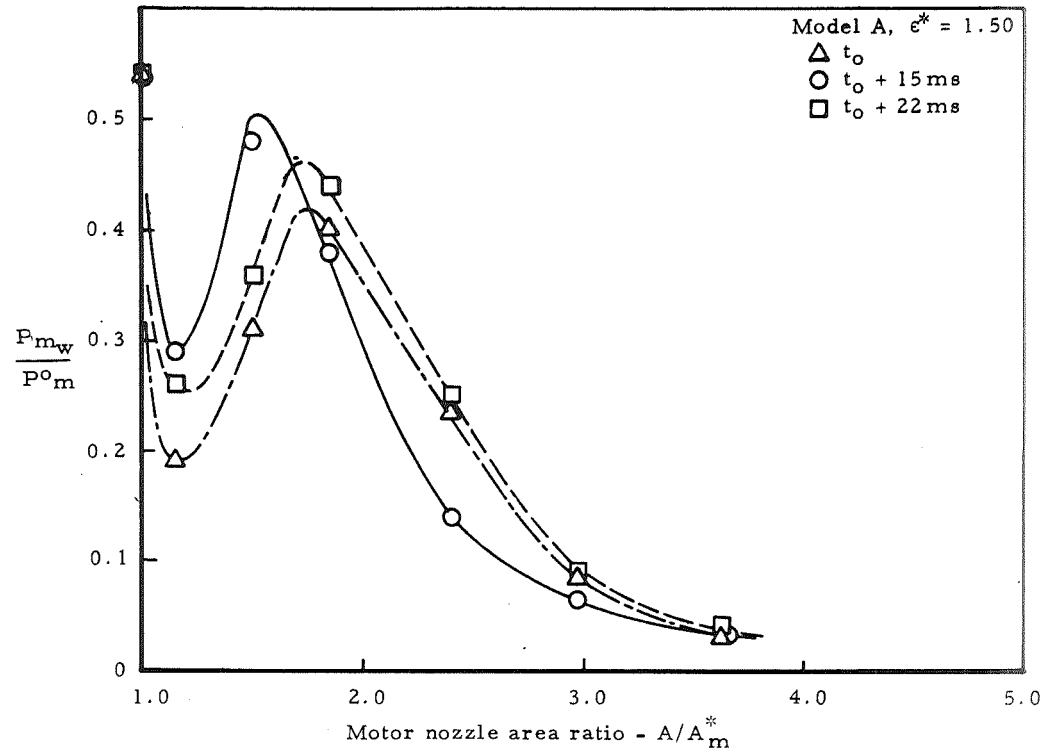

b. $\epsilon^* = 1.50$

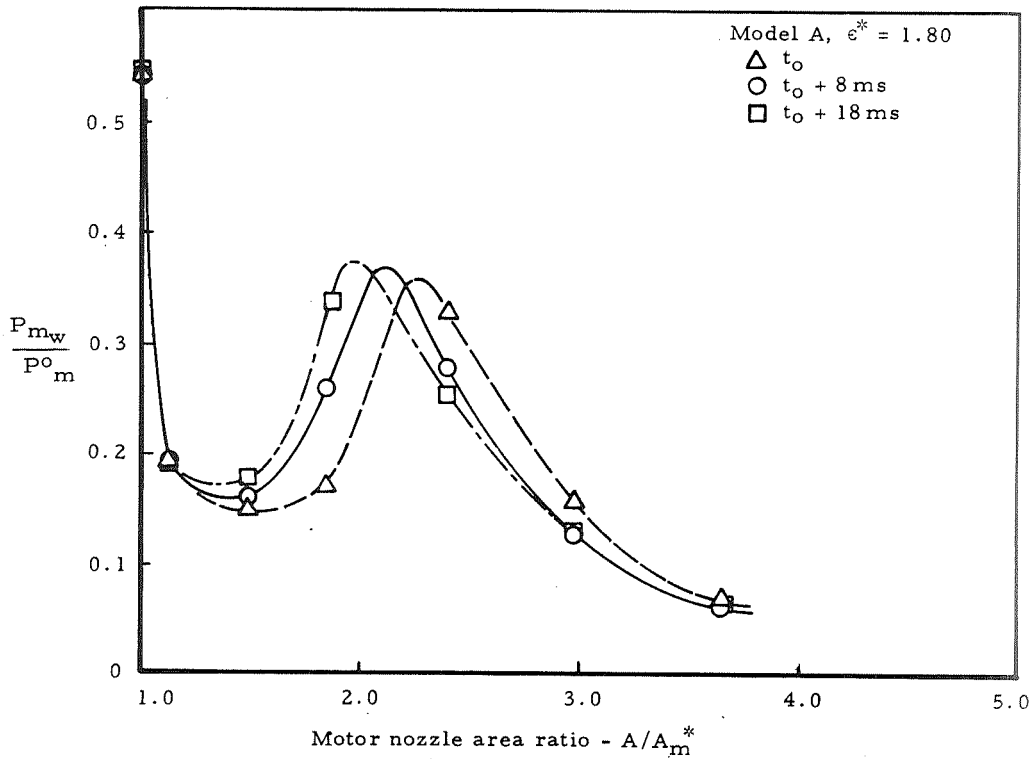

c. $\epsilon^* = 1.80$

Figure 53. Motor-Nozzle Pressure Distributions During Oscillations (concluded)

Motor Flow-Field Structure

Limited studies were performed to investigate essential features of the motor-nozzle flow field needed for analytical model development of oscillation onset. Features studied were the motor total pressure loss at the axis and the slant area flow properties. The slant area flow properties will be discussed under Section 3.3.4.4, Analytical Model studies.

Any satisfactory analytical model for a given igniter geometry and location must relate the oscillation onset conditions to PR. A necessary relationship which must exist is the equality of igniter and motor total pressure at opposite sides of the slip surface along the motor axis. If P^0_{i2} and P^0_{m2} are the igniter and motor total pressures at the slip surface along the axis, then:

$$PR = \frac{P^0_i / P^0_{i2}}{P^0_m / P^0_{m2}}$$

The equality of the normalized igniter-nozzle pressure distribution and igniter flow field at the onset of oscillations would imply that P^0_i / P^0_{i2} is constant and independent of ϵ^* location. If the constant value of P^0_i / P^0_{i2} can be found for a given geometry, then the solution of an analytical oscillation onset model would be reduced to defining the loss in motor total pressure along the axis to the slip-surface stagnation point.

The constant igniter total pressure loss ratio, P^0_i / P^0_{i2}, can be approximated by examination of experimental data at low ϵ^* values. If the motor nozzle is blocked, then the motor flow is subsonic and except for viscous losses, $P^0_m = P^0_{m2}$ and $P^0_i / P^0_m = P^0_i / P^0_{i2}$.

The motor total pressure loss along the axis can then be approximated as a function of ϵ^* by:

(1) Assuming that the igniter flow-field distance to the slip surface is independent of ϵ^* and that viscous motor-nozzle viscous total pressure losses are negligible.

(2) Determining this constant axial-igniter jet-slip-surface distance and bow-shock standoff distance.

(3) Assuming that, at each ϵ^* location, the motor total pressure loss is equal to the bow-shock loss. The bow-shock loss is calculated after determining the shock axial position and centerline Mach number from the known shock standoff distance.

This method of determining the motor total pressure loss was evaluated by utilizing experimental data to calculate igniter total pressure loss

and the bow-shock standoff distance. The resulting determination of igniter to motor chamber pressure ratio at the onset of oscillations for Model A is shown in Figure 54. Good agreement with the experimental data is observed for low ε^* values with increasing divergence of results for increasing ε^*. Part of the disagreement at high ε^* values resulted from the simplifying assumption that a bow-shock standoff distance remains constant as the igniter is withdrawn. In reality the bow-shock standoff distance would decrease with increasing ε^* and the subsequent motor total pressure losses taken at a higher Mach number would also increase. Therefore, if the movement of the bow-shock location were accounted for, the agreement between experimental and modeled results would be improved. In the absence of knowledge of the contact surface shape, it was impossible to calculate the bow-shock standoff distance as a function of Mach number.

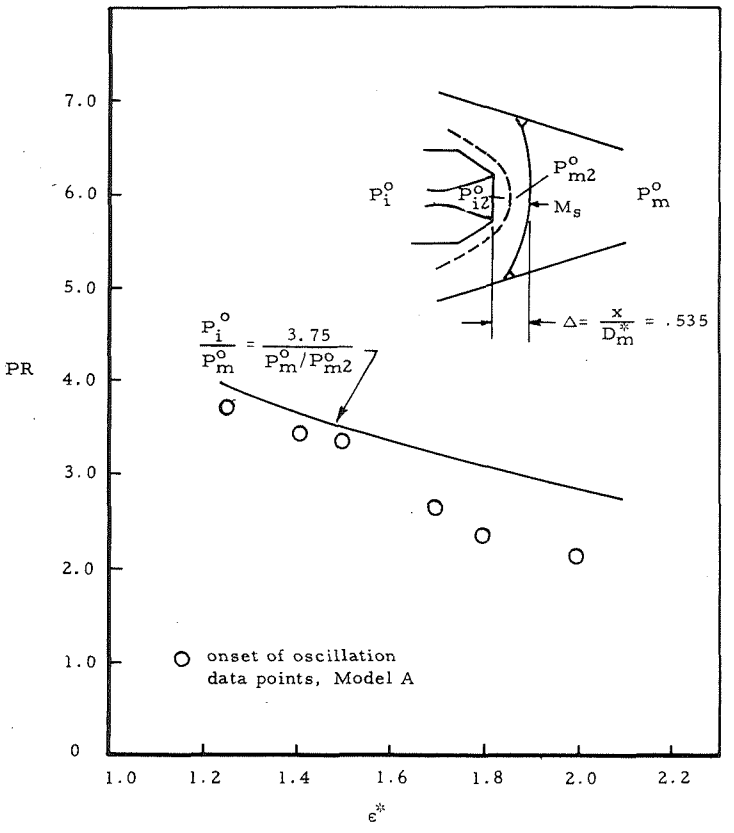

Figure 54. PR Calculated by Bow-Shock Total-Pressure-Loss Approximation

These results suggest that the foregoing may be a useful method for modeling the onset of oscillations. However, either an experimental correlation or an analytical method is needed to establish the igniter total pressure loss and the constant slip-surface standoff distance. (Experimental data exist for calculating the bow-shock standoff distance as a function of apparent stream Mach No.) Previous sections indicated possible methods for determining the igniter total pressure loss. Time limitations prevented determination of a satisfactory method of calculating the slip-surface standoff

distance. It is believed that the use of empirical correlations would be the easiest solution to this problem.

3.3.4.4 Analytical Model

The approach taken in attempting to develop a satisfactory analytical model was similar to that used for the blockage models. A control volume contained within the igniter and motor nozzles was established and solutions of the mass and momentum conservation equations were sought in terms of modeled boundary conditions.

The modeling study did not provide results which could be used to quantitatively determine motor and igniter conditions which result in unstable operation. This failure resulted primarily from an inability to model the flow field at the slant-area boundary. While not completely successful, the model studies did provide considerable insight into the flow-field structure and indicated data which must be obtained to develop a successful model.

Analysis of igniter and motor nozzle flow-field studies indicated a probable flow-field structure similar to that shown in Figure 55. A control volume with boundaries which incorporate basic flow-field features is shown in Figure 56. In writing generalized mass and momentum equations for the control volume, it was assumed that the flow at boundaries can be described by perfect gas isentropic relationships. This does not preclude shock or viscous interactions within the control volume. It was also assumed that heat transfer at the boundaries is negligible, that the motor and igniter total temperatures were equal, and that both igniter and motor had identical perfect gas properties. All equations were written in non-dimensional form by using the non-dimensional parameters which characterize motor and igniter design and flow conditions.

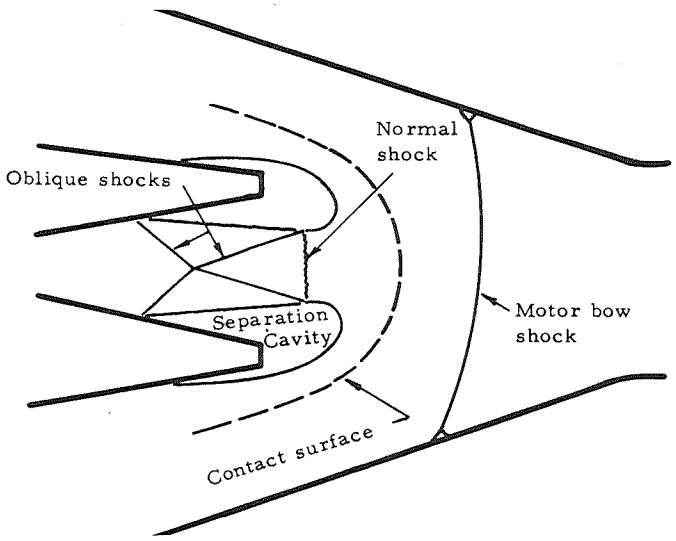

Figure 55. Flow-Field Structure at Onset of Oscillations

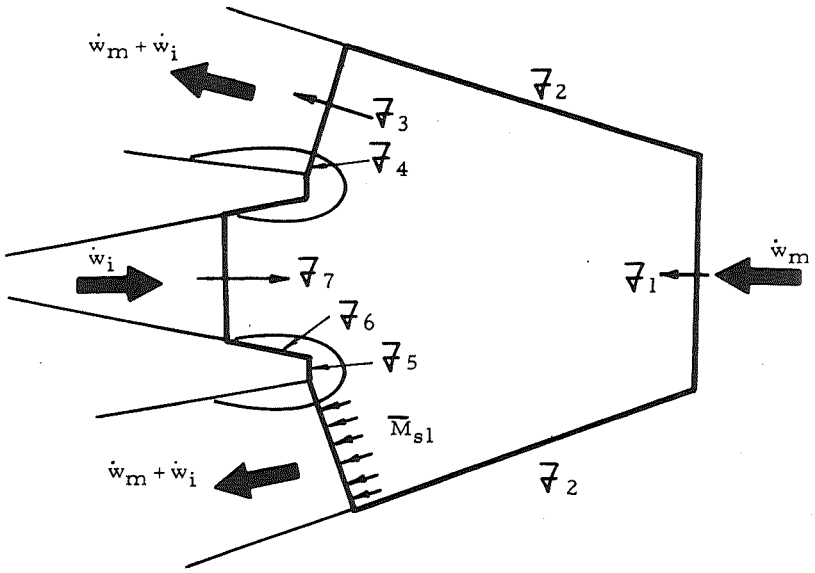

Figure 56. Control Volume at Onset of Oscillations

Conservation of momentum requires satisfaction of the non-dimensional momentum equation:

$$\Sigma F_x = F_{1x} + F_{2x} - (F_{3x} + F_{4x} + F_{5x} + F_{6x} + F_{7x}) = 0$$

By suitable expression of the momentum terms at each of the boundaries, i.e., by use of empirical correlations and by the application of mass conservation in the term for F_{3x}, the equation F_x was reduced to an equation in two unknown variables $\overline{M}_{sl}$ and PR. Thus to obtain a solution for $F_x = 0$, an empirical correlation or model of the form $M_{sl} = h\,(\epsilon^*, PR)$ was required to reduce the number of variables. In an attempt to find an empirical correlation for the average slant-area Mach number, experimental values for all unknowns were input into the mass-momentum equation. Also F_{3x} was solved as a function of M_{sl} for parametric values of PR and A_m^*/A_i^* (see Figure 57). It was found that the minimum calculated value of F_{3x} was greater than the algebraic sum of the other terms derived using experimental values, i.e.,

$$(F_3 \cos \theta_f)_{min} = (F_{3x})_{min} > F_{1x} + F_{2x} - (F_{4x} + F_{5x} + F_{6x} + F_{7x})$$

A systematic review of all assumptions used in deriving the model and an analysis of the effects of moderate variation in the experimental error was made. On the basis of this review, it was concluded that the assumption that the flow out of the control volume was normal to the slant area was the only factor which could produce the required discrepancy in results. The direction of the error indicated that the actual average flow angle θ_f at the slant area was greater than the nozzle half angle. This factor in essence added another unknown which must be modeled or experimentally determined

to define the slant area Mach number as a function of ϵ^* and PR. Further parametric studies of slant-area flow models could possibly be made to define $\overline{M}_{sl}$, but the postulated flow model would have to be verified by confirmation with visualization studies of the slant area. Some empirical correlation which would adequately model the onset of oscillations could possibly be obtained with the test results available if time permitted.

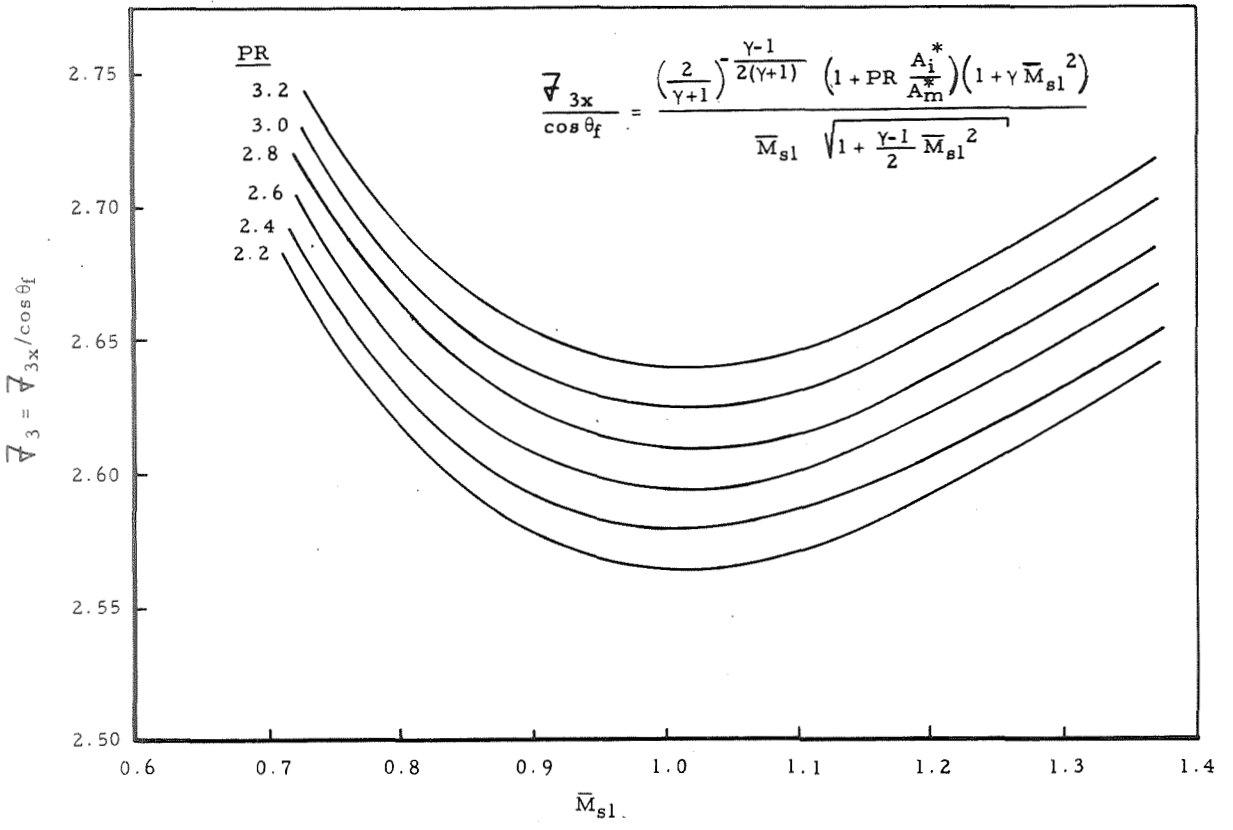

Figure 57. Parametric Solution of Oscillation Onset Model

3.3.4.5 Oscillation Control Techniques

Tests were conducted to survey possible oscillation control techniques. Comparison of data from these tests indicated that of the modified nozzles the only technique which satisfactorily reduced the oscillations was the stepped-nozzle configurations. Tests with conventional nozzles, but with rapid termination or decay of igniter chamber pressure, demonstrated that oscillations could also be avoided or reduced in magnitude by that method.

The general oscillation characteristic of the stepped nozzles was similar to that of the unmodified nozzles. However, the characteristic mapping regions were modified and amplitudes of the unstable igniter and motor nozzle oscillations were progressively reduced with increasing step size. Figure 58a presents mapping data for nozzle AS1 and comparative mapping curves for Model A. Although a similarity in mapping regions exists, the

desirable unblocked stable region is reduced for Model AS1. Mapping data for Models AS2, AS3, A, and C are presented in Figure 58b. This mapping indicated that the unblocked stable region is expanded for Models AS2 and AS3. The initial unblocking comes at higher pressure ratios and the onset of oscillations at lower pressure ratios. It is instructive to note that the oscillation onset pressure ratios for stepped nozzles AS2 and AS3 are reduced to values obtained for igniter Model C. The nozzle area ratio on Model C was 5.0 as compared to an area ratio at step of 2.27. This is consistent with an analysis of data from the other models. It was observed that for a given ϵ^* location the onset of oscillation occurred at increasingly lower pressure ratios for decreasing igniter-nozzle expansion ratios. In the case of the stepped nozzle, the effective back pressure is permitted to feed back into the step cavity, allowing the nozzle to operate as if the step expansion ratio was the nozzle expansion ratio. This lowering of effective expansion ratio allows the nozzle to operate stably at higher back pressures.

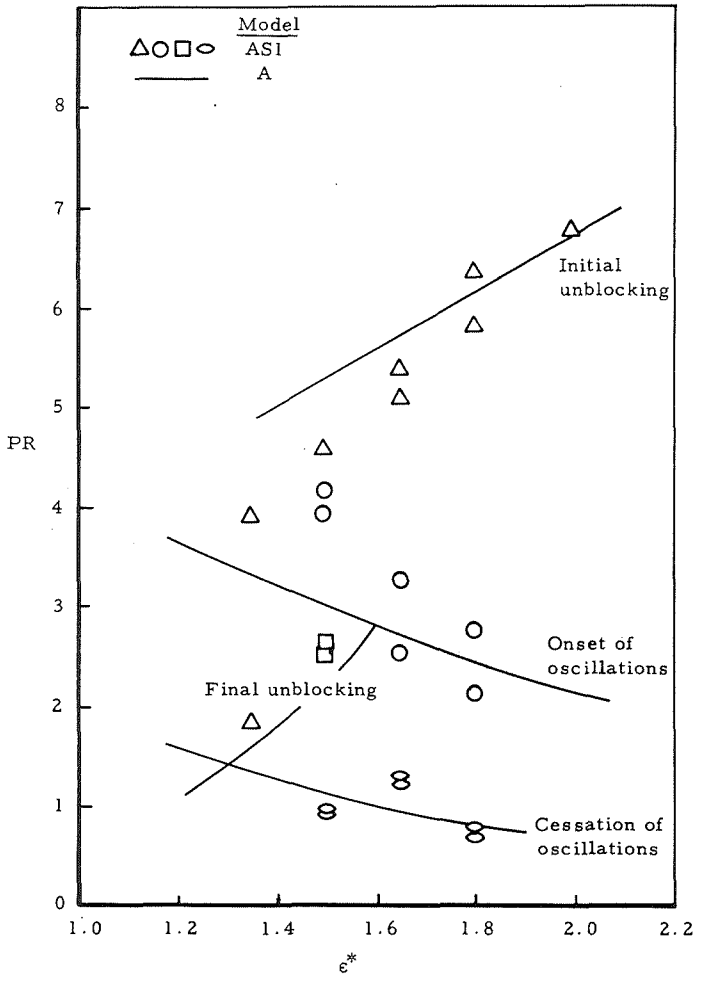

a) Model AS1

Figure 58. Operating Maps for Stepped Nozzles

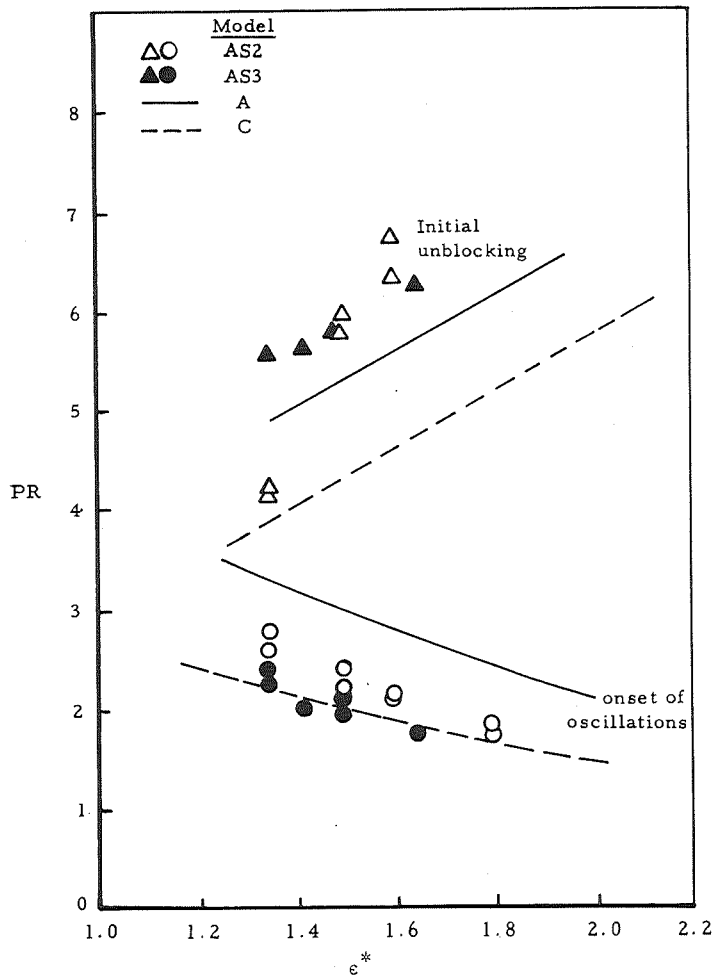

b) Models AS2 and AS3

Figure 58. Operating Maps for Stepped Nozzles (concluded)

The step nozzle, particularly AS3, significantly reduced the amplitude of the unstable and motor oscillations. Figure 22 shows data from nozzle AS3 for $\epsilon^* = 1.5$. As indicated, the pressure oscillations are much less severe than comparable oscillations for Model A shown in Figure 20.

Models AB1 and AB2 did not appreciably modify the oscillation characteristics or mapping region relationships. For some tests, the minor motor-nozzle pressure disturbances noted prior to the onset of oscillations were enhanced. However, in the majority of tests with Models AB1 and AB2, there did not appear to be any notable differences in oscillatory behavior as compared with that for nozzle A.

A mapping of tests for Models AB1 and AB2 (see Figure 59) indicated results which were almost identical with those of Model A, except for delayed initial unblocking points at $\epsilon^* = 1.50$ and 1.65. These changes apparently resulted from modified nozzle-shock configurations due to induced boundary layer separation.

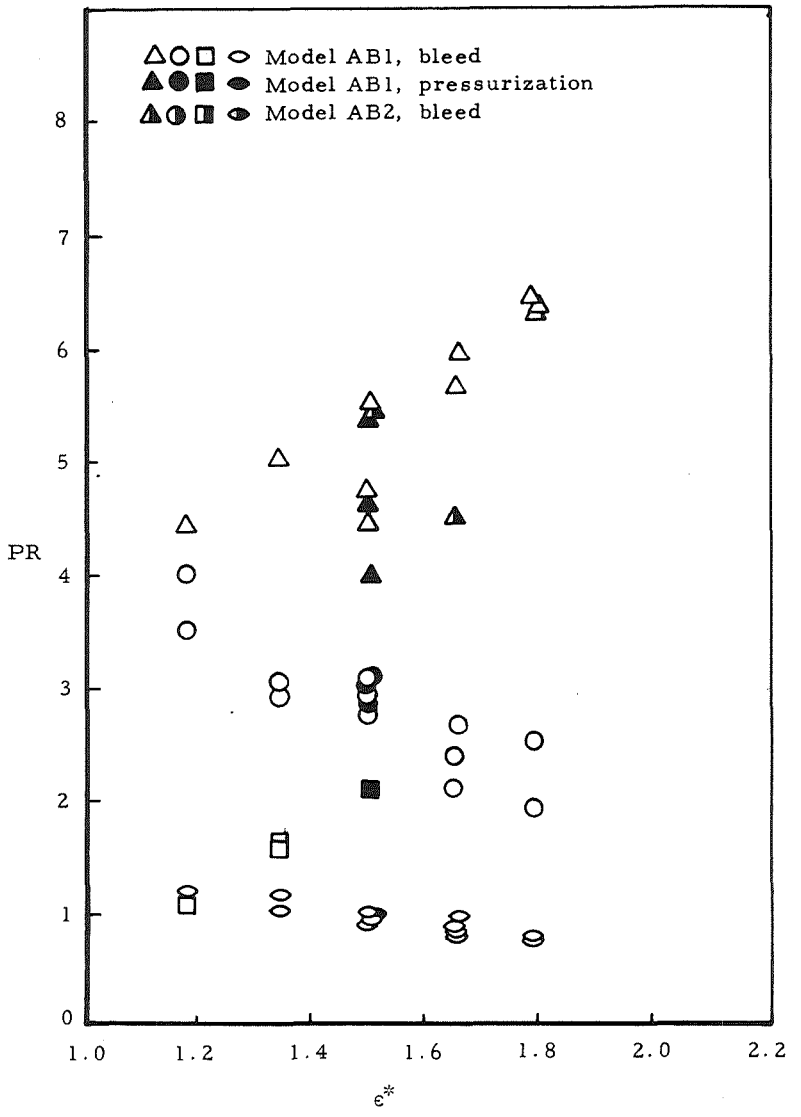

Figure 59. Operating Maps for Perforated Nozzles

3.3.5 Misalignment

Tests with only angular or lateral misalignment displayed characteristic oscillations which were quite similar to those observed for comparable aligned tests. Tests with combined angular and lateral misalignment displayed less stability and a tendency toward asymmetric motor- and igniter-nozzle flow behavior. This behavior was noted for both combined misalignment configurations which did not display any qualitatively dissimilar differentiating characteristics.

Data for a lateral plus angular misalignment configuration at $\epsilon^* = 1.35$ is shown in Figure 23. At high blocked pressure ratios, with a full-flowing igniter nozzle, a stepped behavior of the motor nozzle pressure traces was observed. This is characteristic of a lateral switching of the igniter jet.

After the onset of oscillations the igniter-nozzle pressure-phase relationship indicated moderately more asymmetric flow separation than the aligned tests. Combined misalignment tests at higher ϵ^* locations displayed tendency toward asymmetrical igniter flow separation with increasing ϵ^* values.

Misalignment did not change the mapping characteristics of the igniter nozzles tested. Figures 60 and 61 present misaligned mapping data for igniter nozzles A and B.

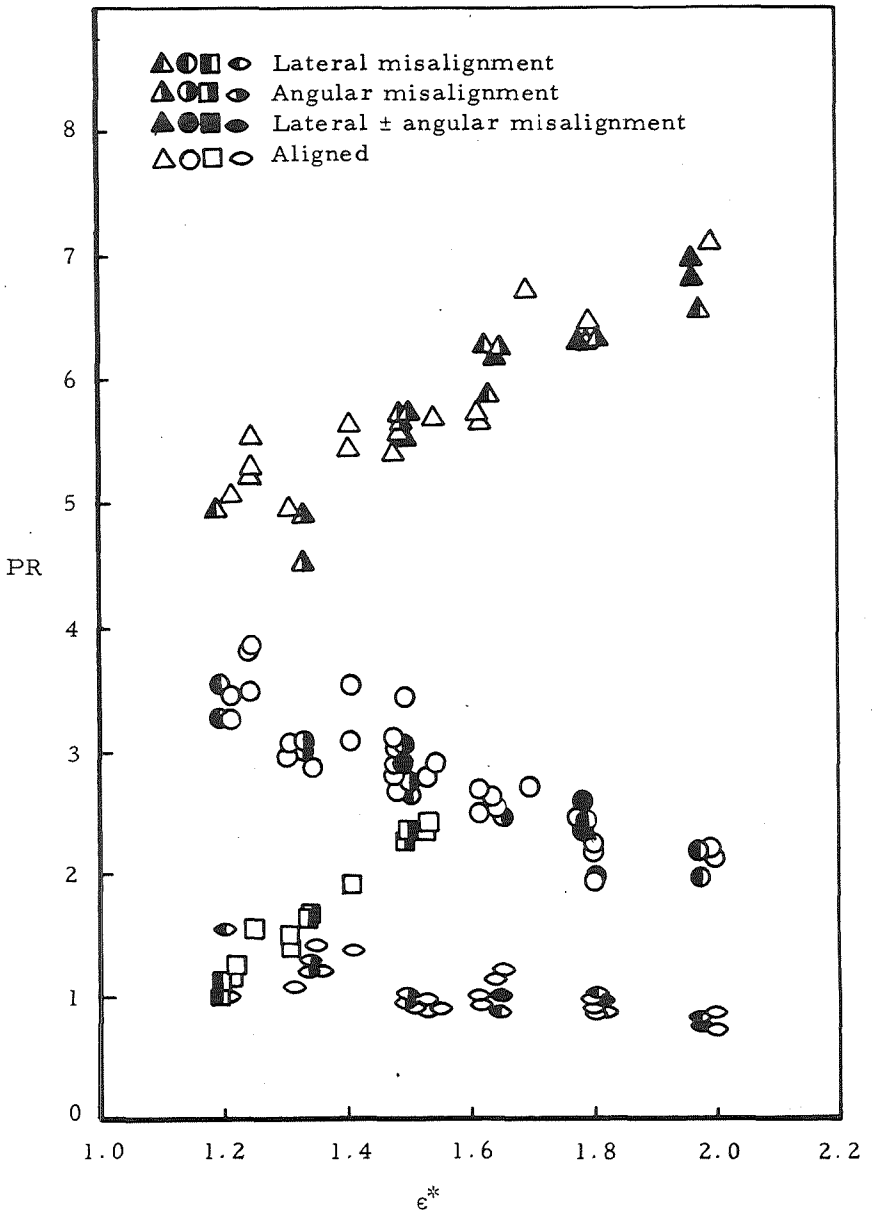

Figure 60. Operating Map for Model A Misaligned

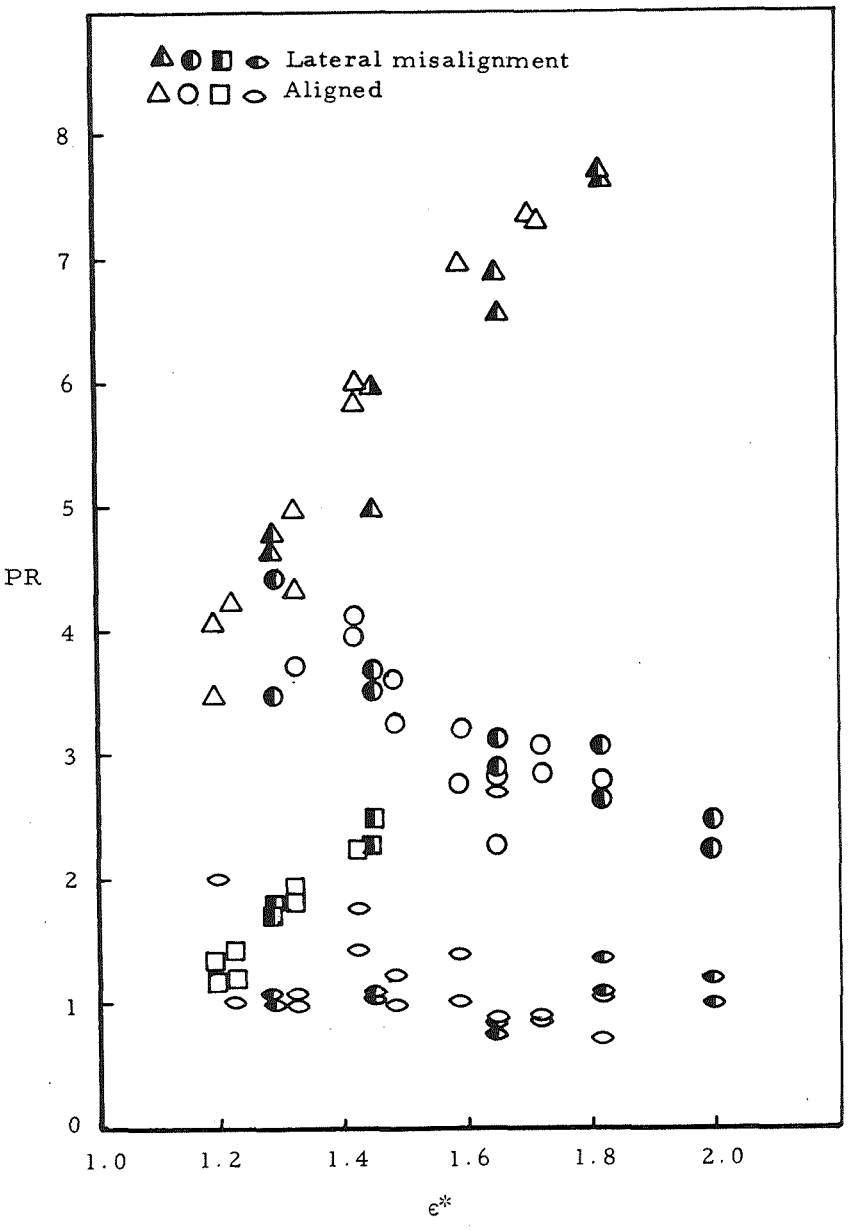

Figure 61. Operating Map for Model B Misaligned

Interpretation of the phase relationships of pressure measurements on opposite sides of the nozzles permitted a qualitative characterization of motor-nozzle asymmetric behavior. However, it was difficult to determine the distributional motor-nozzle asymmetry because only two measurements each were made in the quadrants other than the principal plane of measurement. All of the nozzle pressure taps in the principal quadrant were instrumented along with P_{210}, P_{310}, P_{410}, P_{312}, and P_{412}. In retrospect it would have been more desirable to instrument all of the pressure taps along two opposed quadrants to define two complete pressure profiles. Definition of the pressure distribution in the fully instrumented quadrant was possible, but construction of a pressure profile with the two pressure taps in any other

quadrant required considerable subjective interpretation and as such is open to question.

Lateral, angular plus lateral, and angular minus lateral misalignment data are presented in Figure 62 for ϵ^* values of 1.50 - 1.51. These data indicate approximately the same imbalance of pressure distribution regardless of misalignment configuration. The deviation from the aligned pressure distribution was not significant. Similar conclusions can be made about the aligned and misaligned data presented in Figure 63 for $\epsilon^* = 1.97 - 2.00$.

3.4 DESIGN CRITERIA

The primary purpose of this program was to develop design criteria applicable to the aft-end ignition of 260 inch (6.6 m) type of solid-propellant rocket motors. In this subsection the results of this program and the previous program, and the conclusions drawn therefrom, will be presented more in a general design philosophy to be used as guidelines in the design of a system. Although considerable experimental data have been generated in these programs, comparable analyses have been developed sufficiently to justify confidence in extrapolations to a large system. While it is believed that a large system will behave in the same general fashion as the test systems, the correctness of critical parametric values for which certain behavior occurs is open to question.

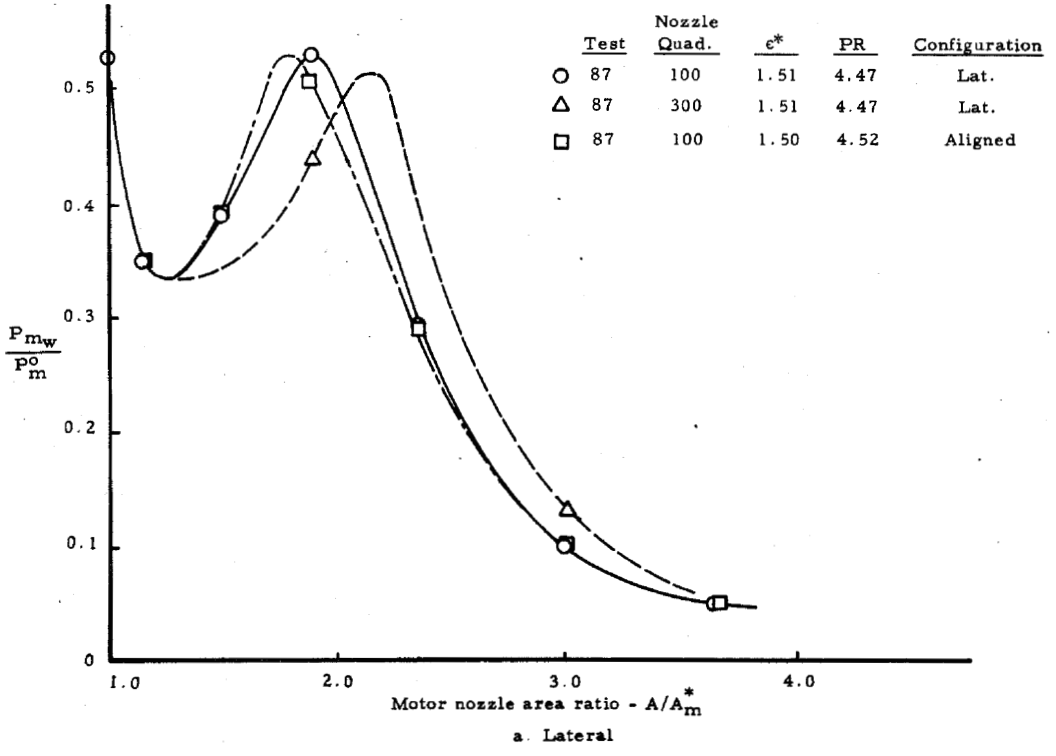

a. Lateral

Figure 62. Misalignment Motor-Nozzle Pressure Distribution $\epsilon^* = 1.50, 1.51$

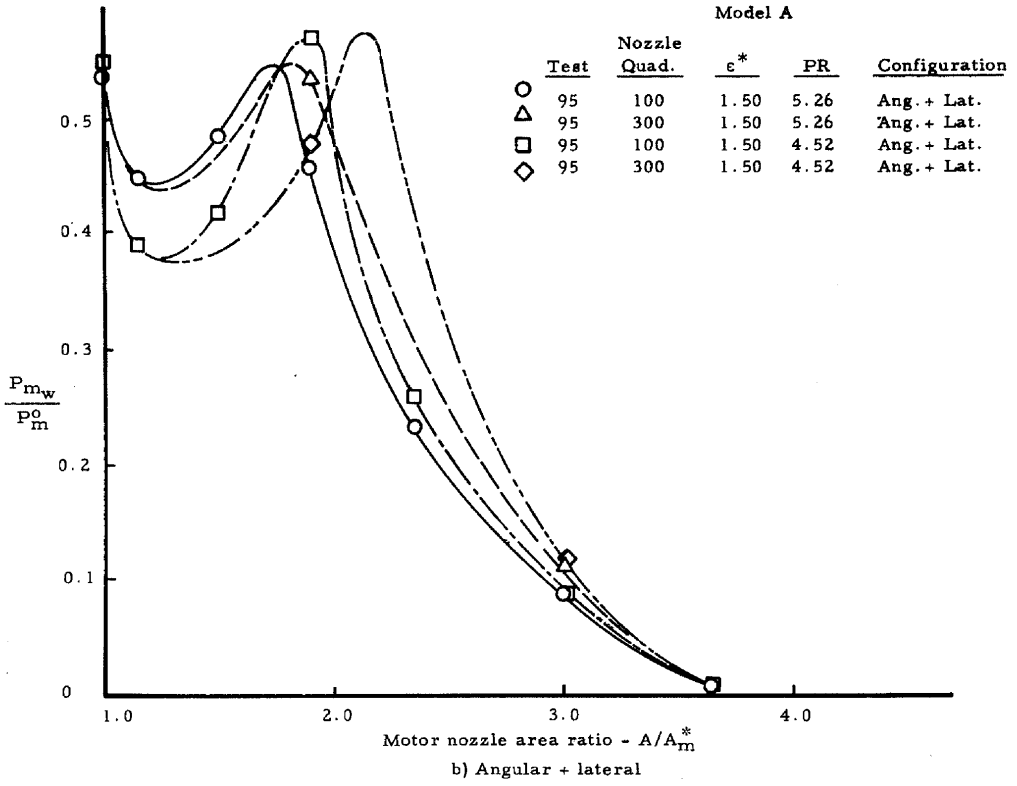

b) Angular + lateral

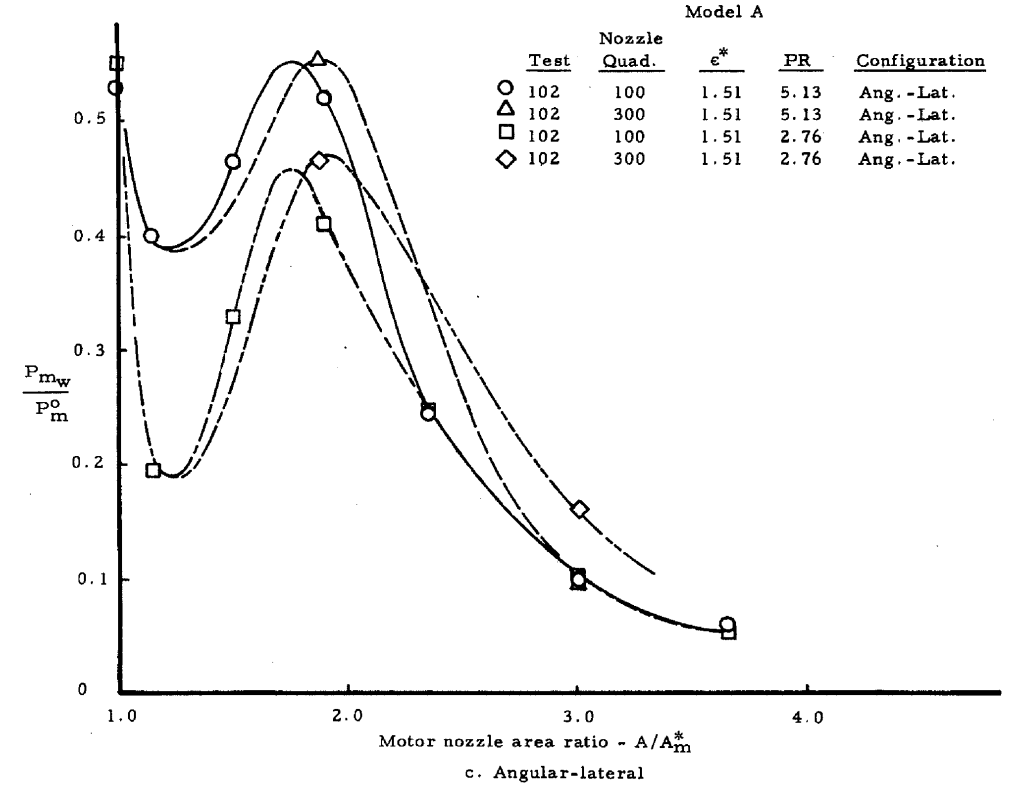

c. Angular-lateral

Figure 62. Misalignment Motor-Nozzle Pressure Distribution $\varepsilon^* = 1.50, 1.51$ (concluded)

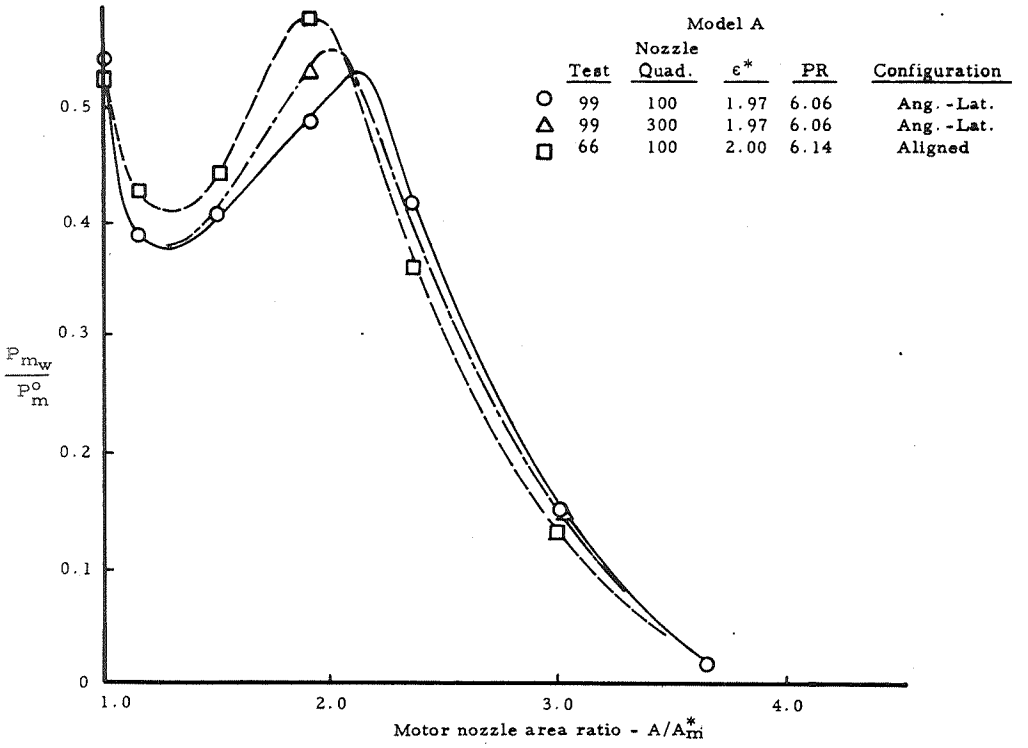

a. High ϵ^* and PR

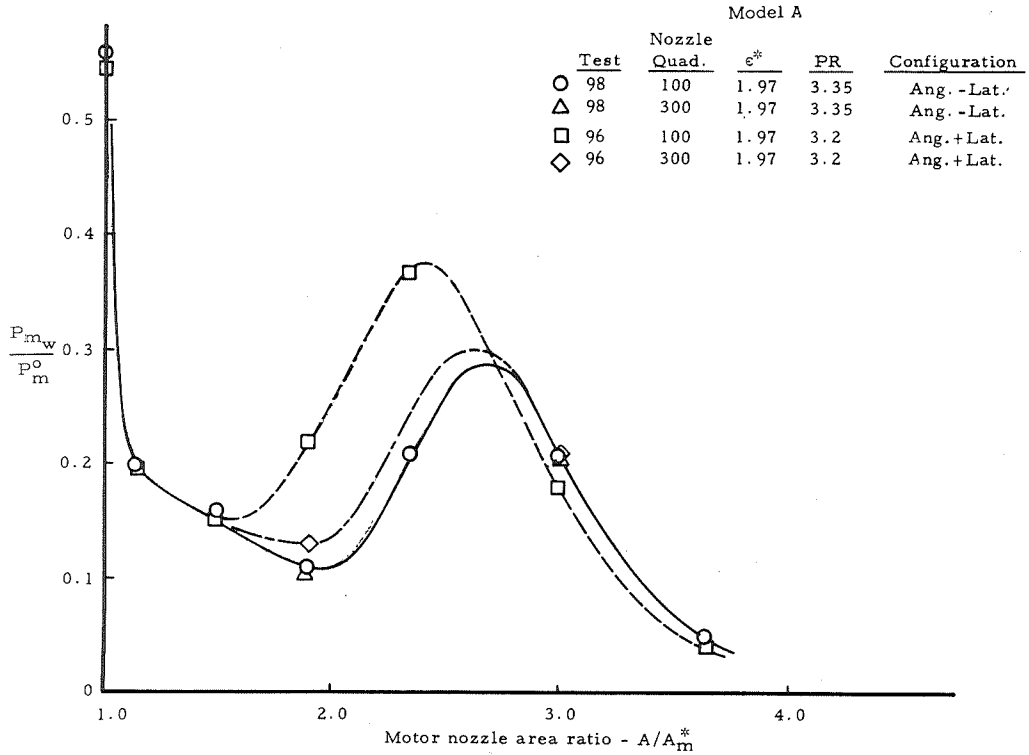

b. High ϵ^* and low PR

Figure 63. Misalignment Nozzle Pressure Distributions

The analytical tools which have been used to correlate data and provide insight into the flow structures involved have all been based upon inviscid, perfect gas models. The greatest uncertainty in the interpretation and direct application of the data of these two programs to other systems is believed to lie in the unknown effect of the two-phase nature of a metallized propellant exhaust upon the gas properties of the streams and especially upon their viscous interaction. It is possible that a large proportion of particulates in the streams could have a profound effect upon the interaction of two opposed streams, each of which experiences severe momentum changes during such interaction. This is believed to be the predominant cause for the displacement of the hot-firing operating map from those of the air tests. It is believed that the condensed phase effects will diminish for larger systems.

In spite of these limitations, the insights into the behavior of aft-end ignition systems gained during these two programs make it possible to define the critical features of a satisfactory design along with a favored approach to that design.

An ideal system for a larger conventional booster is one in which the igniter is in action just long enough to achieve the desired ignition of the main propellant grain and pressure rise of the motor chamber, and then is terminated instantaneously to avoid reblocking and operation in the oscillation region. These latter requirements are difficult to achieve; although with special techniques, termination may be sufficiently rapid so that dwell times in the oscillation region may be short enough to prevent oscillation development. However, this reliance upon complex systems and sophisticated techniques detracts from one of the main virtues of aft-end ignition, namely, its simplicity and reliability. A more favorable approach is to design from the standpoint that standard, reliable, state-of-the-art techniques should be employed, especially in the design of the igniter propellant grain. The system can then be designed to accommodate these standard practices and operation, producing safer, predictable ignition and post-ignition behavior.

3.4.1 Satisfactory Ignition

For the purpose of this report, a system which produces the fastest possible ignition over the entire surface of the propellant grain is considered to be the "satisfactory" system. There are many reasons why this may not be acceptable in a very large booster (e.g., too rapid chamber pressure rise, motor-case expansion, and severely transient loading of the grain and/or upper stage structures). Therefore, it is the responsibility of the designer of a particular motor to establish the ignition requirements of his system and either design to the maximum or reduce the capability of the igniter accordingly.

As was discovered in the previous program, the fastest ignition and chamber filling was achieved when full penetration of the motor cavity by the igniter was accomplished. This provides for the greatest heat transfer over the entire grain surface, and is especially important in the head-end star region, where approximately 60 percent of the grain surface was contained in the forward 20 percent of the motor length.

Maximum penetration is produced by a combination of two factors: First, the jet must have maximum resistance to viscous erosion and dissipation of its axial momentum. This is obtained with a cohesive jet having the highest possible total pressure and jet velocity. Second, because the purpose of the jet is to penetrate through the air cushion in the cavity, it should have a low cross-sectional area and wholly axial flow. This latter property also reduces the tendency for shock-wave dissipation of the jet momentum caused by repetitive changes in cross-sectional area such as occur with a highly underexpanded sonic jet.

A jet having these characteristics is produced by an igniter having a high chamber pressure and expansion to near ambient pressure in a nozzle of moderate divergence angle. Obviously, the "goodness" of the igniter will be limited by practical considerations. The maximum possible state-of-the-art chamber pressure will depend on many factors, especially size of the system and type of propellant used in the igniter. Also, as will be discussed in detail in the next subsection, care must be taken to ensure that the igniter chamber pressure selected for best ignition will not provide undesirable conditions in the post-ignition period, if that igniter pressure is held constant over the entire interval.

Selection of the size and flow rate of the igniter is a matter of determining the largest size igniter jet which will initially penetrate through the motor throat without severely restricting the return flow through the annular area. In the event the return flow is restricted, the jet expands, presenting a large frontal area to the cavity dead air, and acts as a piston to compress that ambient cold air into a zone in the head end of motor. This effectively isolates that portion of the grain from the jet, resulting in slow surface heatup and flame spread.

Much has been said about the maximum igniter flow-rate parameter ($\dot{w}/A^*_m$) (see Reference 1 for a review of past work) above which the igniter jet acts as a piston and does not produce improved ignition. This value has been reported to be approximately 0.3 lbm/sec-in^2 (210.9 kg/sec-m^2). It is important to note that this limit was observed in igniters which were not designed to produce a low cross-section, high-momentum jet without pluming or billowing. No such limit was encountered in the previous program, even though maximum mass flow parameter values of 0.572 lbm/sec-in^2 (402.2 kg/sec-m^2) were tested. Thus, it is postulated that the critical parameter in sizing the igniter to avoid piston-like behavior is the diameter of the igniter jet at the motor throat, even though no significant body of knowledge

has been compiled to support this contention. If the igniter is designed for near-optimum expansion to produce a jet of constant diameter, then the threshold igniter size above which the igniter performs poorly can be described in terms of the size of the jet exit with respect to the motor throat. Although no limiting functional relationships have been established in the current program, a maximum value of the igniter exit diameter to motor throat diameter of 0.55 was tested in the previous program and found to be entirely satisfactory. Hence it is recommended that this value be taken as the maximum to be used for design purposes until other data to the contrary are generated.

There is also a lower limit of the igniter mass-flux parameter below which ignition will not occur or below which the ignition delay will be excessive. This lower limit will depend upon ignition time requirements and cannot be established a priori for all cases.

Placement of the igniter over a moderate range of ϵ^* values from 1.2 to 2.0 does not cause appreciable changes in the igniter jet penetrations, propellant grain heating, or first ignition. However, low ϵ^* values do reduce the time to reach rated chamber pressure because of greater initial motor nozzle throat blockage and corresponding higher pressurization rates. If fast chamber filling is desired, the igniter should be placed at lowest ϵ^* position consistent with post-ignition blockage and oscillation constraints.

Summary

Following are the few key rules which must be followed to design for best penetration and ignition of a large L/D motor:

(1) Highest possible igniter chamber pressure consistent with reliable state-of-the-art practice and with post-ignition requirements.

(2) Ratio between igniter-exit and motor-throat diameters no greater than 0.55.

(3) Near optimum expansion of the igniter flow
$(0.6 < P_{i_e}/P_{ambient} < 2.0)$

(4) The igniter ϵ^* should be as low as possible consistent with safe operation in the post-ignition period.

3.4.2 Post Ignition—Unblocking and Oscillations

Safe operation during the post-ignition period normally requires that reblocking be avoided after the motor has reached design chamber pressure. Neither should severe motor nozzle pressure oscillations be allowed to occur.

Reblocking can be avoided entirely by placing the igniter at an ϵ^* greater than the ϵ^* at which the final unblocking and onset of oscillation lines intersect. This condition is shown in Figure 64. Thus, even if the igniter fails to perform properly during the lift-off or separation of igniter and motor, the motor throat will not reblock in Mode B.

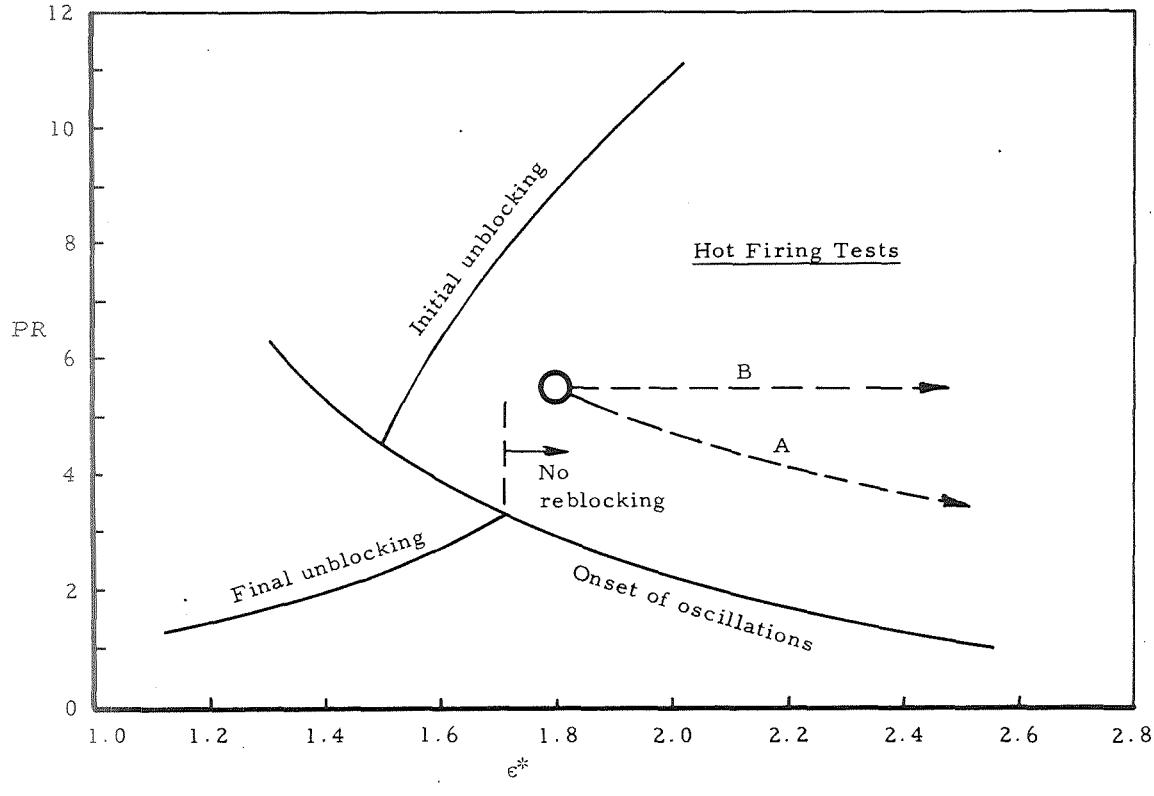

Figure 64. Locus of States for Safe Operation and Withdrawal

The oscillations between Mode A and Mode B flow structure can be avoided by operating at PR values above the onset of oscillation lines. Also, the use of a slotted or stepped igniter nozzle significantly reduces both the amplitude of the oscillations and the span of pressure ratios over which they exist. Both means are recommended for most reliable control. It is doubtful that termination of the igniter action can be sufficiently fast and positive to ensure that no oscillations will occur, although it may prove to be desirable in some instances, in combination with the slotted nozzle.

Proper tailoring of the igniter grain design can produce a wide range of pressure-time curves. Selection of the best igniter action should depend, to a large degree, on the confidence of the designer in designing a reliable, reproducible schedule of igniter chamber pressure and flow.

The most favorable igniter action is one which produces the PR—ϵ^* withdrawal locus labeled A in Figure 64. This provides a comfortable

margin of safety with respect to the onset of oscillations, while also reducing the interfering effects on the main flow of the igniter flow, and the pressure integral on the nozzle wall caused by the shock wave impingment. Reduction of the shock wave pressure on the nozzle is most important at the instant the shock wave intersection with the nozzle wall passes the exit at some point around the periphery of the exit. Because the motor and igniter may no longer be perfectly aligned, and because of slight asymmetry of the bow-shock, a substantial nozzle side force may exist momentarily, until the shock impingment has ceased altogether. Successful use of this technique requires a precise match of the igniter action and motor lift-off, and may be difficult to achieve. The designer will have to trade the reduction of asymmetric nozzle loads with precise tailoring (Curve A) against the the overall increased reliability with the approach resulting in Curve B. The latter ensures that neither reblocking (in either Mode A or Mode B) nor oscillations will occur.

3.4.3 Example Problem

The following example is included to illustrate a way in which the critical aft-end igniter design parameters may be selected. The sample system is described as follows:

(1) Motor design pressure - 500 psi (3.475 MN/m^2)

(2) Motor- and igniter-propellant exhaust-gas properties similar to those of previous hot firings,

$$\gamma = 1.18$$

$$MW = 27.86$$

Total temp. = 5980°R (3320°K)

(3) Igniter chamber pressure is constant after initial rise.

(4) System operating map is identical to that for hot firing from previous program (Figure 65).

(5) Unrestrained launch vehicle; thrust/weight (T/W) at lift-off = 1.4

From Figure 65, values of 1.8 and 5.5 for ϵ^* and PR are selected as being satisfactory for safe post-ignition operation. Then

$$P_i^o = 500.5.5 = 2750 \text{ psia } (18.960 \text{ MN/m}^2)$$

$$D_i = 0.55\ (D_m{}^*)$$

for

$$P_{e_i} = 2.0 \text{ atm } (0.202 \text{ MN/m}^2)$$

$$P_{e_i}/P_{i}o = 0.0117$$

$$A_{e_i}/A_i^* = 11.40$$

then

$$\dot{w}_i/A_m^* = 0.377 \text{ lb}_m/\text{sec-in}^2 \ (265.053 \text{ kg/sec-m}^2)$$

This will provide good penetration into the motor cavity (approximately 9 igniter-nozzle diameters, according to the data of Reference 1). Referring to the locus of states of Figure 65, it can be seen that the motor throat will initially unblock at a PR of 8.9, or motor chamber pressure of 309 psia (2.13 MN/m^2), 62 percent of design chamber pressure. For a design launch T/W of 1.4, assuming that thrust is proportional to chamber pressure, the vehicle begins to lift at a chamber pressure of 357 psia (2.461 MN/m^2) or at a PR of 7.7. Because of the increased nozzle pressure produced by the igniter, thrust will probably be higher, and lift-off slightly sooner. Depending upon the chamber pressure rise and vehicle acceleration, the locus will be generally as shown, with PR decreasing to its steady-state value of 5.5 as ϵ^* increases due to lift-off.

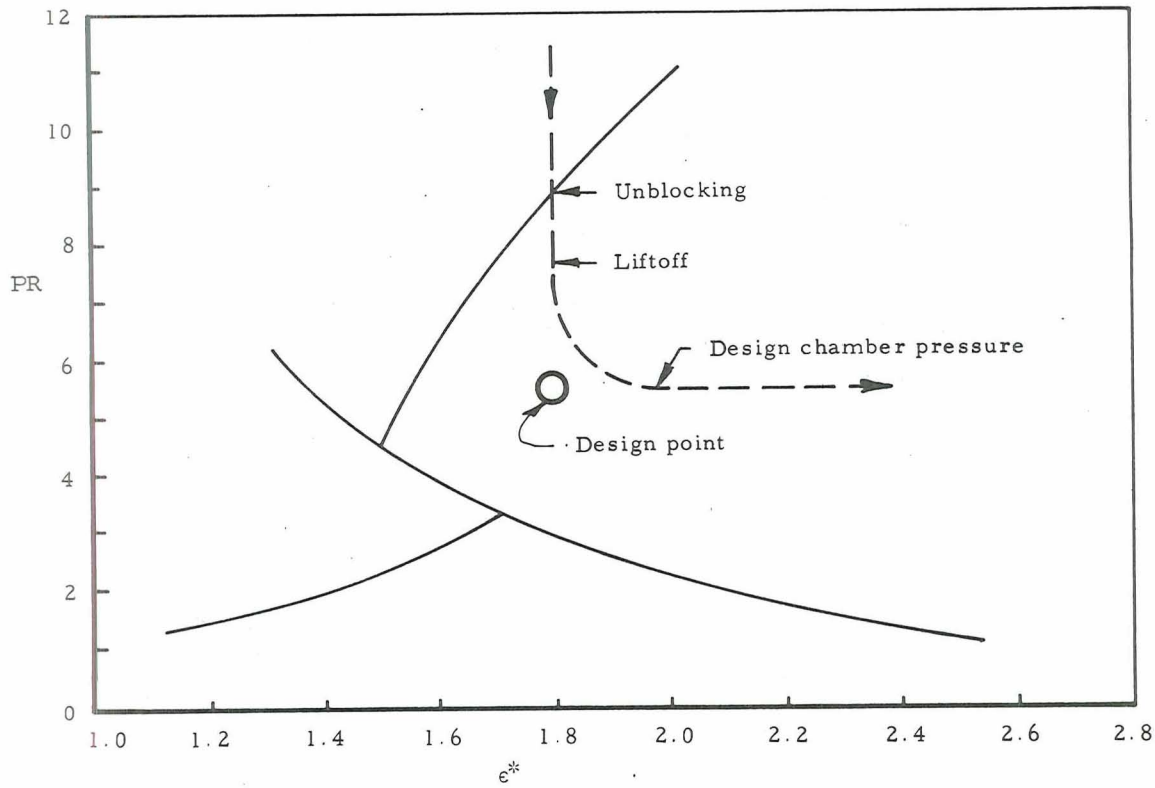

Figure 65. Example Problem for Post-Ignition Operation

For motors having high chamber pressure, e.g. 1000 psia (6.895 MN/m^2), the above technique may fail. Generation of a PR of 5.5 in this circumstance, based upon design motor chamber pressure, is not feasible. In this event, it may be necessary to place the igniter at an ϵ^* greater than 2.0, and terminate igniter action quickly, possibly before lift-off.

All of the above discussion presupposes the existence of a valid operating map. Before undertaking the preliminary design of a system, it is advisable to conduct a minimum of two tests of a subscale configuration with the propellant of the full-scale system. Test at ϵ^* values of 1.6 and 2.0 will probably be sufficient to determine the location of the lines of initial unblocking and onset of oscillations, as well as the severity of the oscillations. It is emphasized that these tests must be performed with high-frequency-response instrumentation.

4.0 CONCLUSIONS

Experimental and analytical studies were conducted to investigate aft-end igniter- and motor-nozzle oscillation and blockage behavior during the post-ignition period. Significant results of the study included:

(1) Characterization of igniter- and motor-nozzle flow interactions.

(2) Definition of techniques which can be used to avoid or suppress dangerous motor-nozzle pressure oscillations.

(3) Determination of igniter-nozzle misalignment effects.

(4) Determination of nozzle interactions at the aftward igniter locations encountered during booster lift-off.

(5) Development of models which can be used to approximate the critical design and position parameters at initial and final motor-nozzle unblocking.

(6) Establishment of general guidelines for successful aft-end igniter design and placement.

The following paragraphs present conclusions pertaining to each of the above results:

4.1 CHARACTERIZATION OF NOZZLE INTERACTIONS

The aft-end cold-flow experiments indicated blockage and oscillatory behavior similar to that in the solid-propellant motor tests. For a given design configuration, the blocking and oscillation events can be mapped by using the two principal design and placement variables, i.e., igniter to motor chamber pressure ratio (PR) and igniter position. The relationship of these mapped events is defined by the constraining motor-nozzle flow and by subsequent operation of the overexpanded igniter in or between two basic modes (Mode A or Mode B). Mode A is characterized by a stable multiple-igniter-shock structure with a high total pressure loss and relatively small penetration distance. Mode B is characterized by an unstable single-shock or subsonic-flow structure with a low total pressure loss and a relatively large penetration distance. The first or initial unblocking (choking) of the motor nozzle throat at high PR's always occurs with the igniter operating in Mode A. Reblocking at low and intermediate ϵ^* values occurs when the igniter transitions to Mode B operation. Final unblocking occurs when the igniter is operating in Mode B. The large-amplitude nozzle-pressure oscillations are caused by transient operation of the igniter flow between Mode A and Mode B structures.

4.2 OSCILLATION CONTROL

Motor-nozzle blockage and oscillations can be avoided by proper selection and control of the PR and by proper igniter placement. Alternatively, the oscillations can be suppressed by use of an igniter nozzle with a step cut into the exit cone. Use of the latter technique should be made with caution, since the effect of the step upon ignition is unknown.

4.3 MISALIGNMENT AND LIFT-OFF

Misalignment of the igniter does not change the blockage and oscillatory mapping characteristic if lateral misalignment is limited to 3 percent of the motor-throat diameter, and the angular component is kept below 1.5° (0.0262 rad).

At high ϵ^* values representative of lift-off, the motor-nozzle oscillations are greatly attenuated. The region (PR vs ϵ^*) of stable unblocked flow at these higher ϵ^* values is greatly increased.

4.4 ANALYTICAL MODELS

The initial unblocking model provides a close prediction of the initial unblocking PR and ϵ^* for all air models with nozzle-expansion ratios of 7.0:1 and less. At higher expansion ratios, neither the air nor live propellant correlations were adequate. Hot-firing data at low expansion ratios were not available to assess the validity of the initial unblocking analysis at these conditions. The final unblocking model presents a conservative prediction of the PR and ϵ^* values at final unblocking for all models and the solid-propellant test data. Efforts to develop an oscillation onset model were not successful, although the significance of the bow-shock total pressure loss was established. Critical areas requiring further work were identified.

4.5 DESIGN GUIDELINES

Critical features of the blockage and oscillation operating map should be experimentally established before final igniter design and placement details are selected. For fast ignition the igniter chamber pressure should be maximized within blockage and oscillation constraints and the igniter nozzle expansion ratio should be selected to give near-ambient pressure at the exit. The igniter should be located at a high enough ϵ^* value so that reblocking in Mode B will not occur.

APPENDIX

INITIAL UNBLOCKING ANALYSIS

A. Objective

The purpose of the analysis and computer program is to predict the igniter-motor chamber pressure ratio (PR) at which the main motor throat becomes choked or unblocked in Mode A flow. From examination of the experimental data, it is concluded that, for ϵ^* values above some lower limit, the motor throat plane is not penetrated or disturbed by the igniter jet at initial unblocking. The boundary of the reversing igniter jet causes a constriction of the main flow against the nozzle wall, resulting in a secondary throat which is choked or sonic. In the normal course of a decreasing PR, the unblocking event occurs when the area of the secondary throat increases sufficiently to allow the main throat to choke or decouple from the downstream interactions. It can be assumed that losses in total pressure between the main throat and secondary throat are negligible. Thus the two throats must be equal in area at the instant of unblocking.

This is the major supposition upon which the initial unblocking analysis is based. The model attempts to reconstruct the structure of the fully flowing igniter jet in its shock adjustment to the total pressure of the main stream, in the lateral expansion or compression of the jet to adjust to the cavity pressure, and in the subsequent subsonic turn of the jet which produces the second constriction of the main flow equal to its critical area.

B. Analytical Development

The control volume of the analysis is shown in Figure 66. The origin of the x-y coordinate system is located at the intersection of the projected nozzle wall and the system centerline, although the coordinates are sometimes transformed for convenience.

The major assumptions upon which the analysis is based are as follows:

(1) Both streams are adiabatic and behave as perfect gases.

(2) The flows are inviscid.

(3) The streams experience no total pressure losses and obey isentropic relations except that the igniter flow undergoes one normal shock which has a total pressure ratio equal to PR, the ratio between igniter and motor chamber (total) pressures.

(4) Downstream of the igniter normal shock, the flows in the motor nozzle, whether they mix to some degree or remain completely separate, are at a uniform total pressure which is equal to motor chamber total pressure.

(5) The nozzle wall pressure between main and secondary throat is uniformly equal to motor critical pressure.

(6) The igniter jet obeys one-dimensional isentropic relations up to the jet exit, from whence it issues as source or radial flow.

(7) Even though the jet Mach number, in fact, may vary along the normal shock because of the effects of the oblique expansion or compression waves from the jet exit, the total pressure behind the shock is everywhere equal to that on the centerline or stagnation streamline.

(8) At the secondary throat, the flow passes through a sonic point, so that the derivative of the flow area with respect to flow direction is zero. Therefore, the flow streamlines at that sonic surface only are assumed to follow a family of hyperbolas which have the property that the flow area between two adjacent hyperboloids of revolution is everywhere equal.

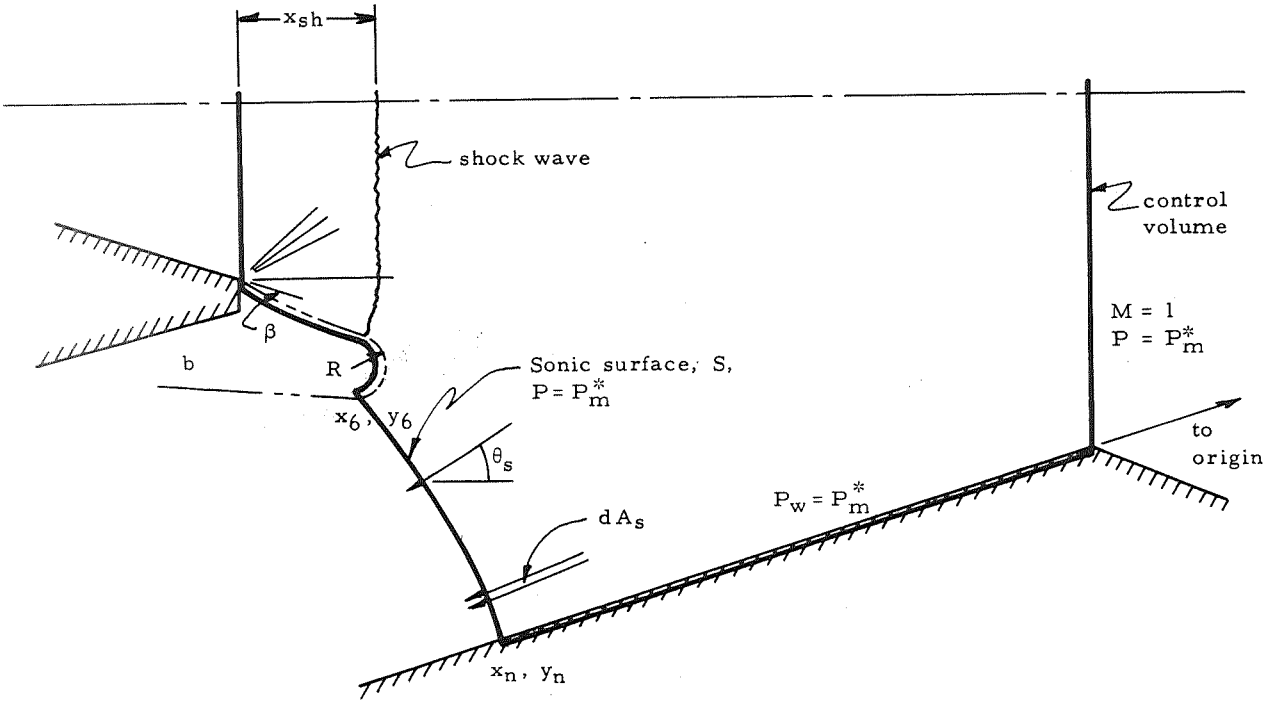

Figure 66. Schematic of Analytical Flow Field

The structure of the igniter jet downstream of its exit was modeled after the observations of Charwat[11] of the interactions between jets and opposed supersonic streams. The normal shock was seen to be planar out to a radius approximately equal to the jet exit radius. From that point it swept around a near circular arc, with center of the arc at the jet exit lip. It was so modeled in this analysis. Charwat's analysis indicated that the subsonic turn of the jet boundary behind the shock was of zero radius of curvature. However, provision was included in the program for specifying a finite radius on the boundary turn.

Calculation Procedure

(1) A table of areas is constructed by numerically summing the normal cross-sectional flow area between the main nozzle cone and a family of hyperboloids of revolution about the x-axis, having the equation

$$y = \tan \theta_n \, (x^2 - a^2) \qquad \text{(A-1)}$$

The summation proceeds from the wall inward, with a increasing from zero by a specified increment. Each incremental area between two hyperboloids is calculated as the surface of a truncated cone, and added to the previous total.

(2) A series of geometric parameters is calculated, based upon the input geometry and input ϵ^*.

(3) A trial value of PR is selected and the normal shock Mach number is calculated by iteration of the relation

$$1/PR = \left[\frac{(\gamma+1)M_{sh}^2}{(\gamma-1)M_{sh}^2+2}\right]^{\gamma/(\gamma-1)} \left[\frac{\gamma+1}{2\gamma M_{sh}^2 - (\gamma-1)}\right]^{1/(\gamma-1)} \qquad \text{(A-2)}$$

(4) The area ratio (A_{sh}/A_{i_e}) of the shock wave is calculated from the one-dimensional isentropic relation, and the shock standoff distance is determined from the source flow relationship:

$$x_{sh} = \left[r_{i_e} \left(\left(A_{sh}/A_{i_e} \right)^{\frac{1}{5}} - \cos \theta_i \right) / \sin \theta_i \right] x_{sf}$$

where x_{sh} is an input parametric multiplier used to evaluate the effect of shock standoff distance.

(5) A trial value of the cavity pressure, P_b, is selected; the edge turn of the jet boundary is calculated from the Prandtl-Meyer relations; the intersection of the shock wave and the boundary and the following boundary radius turn is determined.

(6) The value a is determined for the hyperbola which is tangent to the boundary circular arc, and the value of the area A_s is determined by interpolation of the stored table of A_s vs a. A_s is then compared with the sonic area of the combined flows:

$$A_{sonic} = \pi \left(r_{m_t}^2 + PR \cdot r_{i_t}^2 \right) \tag{A-3}$$

A new value of P_b is selected and steps (5) and (6) are repeated until the combined flow is just choked when A_s equals A_{sonic}.

(7) The stream impulse function across the secondary sonic throat is calculated from

$$F_c = \left[\frac{P_m^* (1 + \gamma)}{P_m^o} \int_6^n \cos \theta_s \, dA_s \right] x_{mf} \tag{A-4}$$

where dA_s is the conical surface area between two adjacent hyperbolas and x_{mf} is a multiplying factor less than 1.0 used to adjust the momentum balance.

(8) A new value of P_b is calculated from the momentum balance of the control volume:

$$\frac{P_b (A_6 - A_{i_e})}{P_m^o} = F_A + F_B - F_C - F_D \tag{A-5}$$

where

$$F_A = \frac{P_m^* A_{m_t} (1 + \gamma)}{P_m^o}$$

$$F_B = \frac{P_m^* (1 + \gamma) \pi (y_n^2 - r_{m_t}^2)}{P_m^o} \tag{A-6}$$

$$F_D = \frac{P_{i_e} A_{i_e} (1 + \gamma M_{i_e}^2)}{P_m^o}$$

(9) The values of P_b, one calculated from the jet expansion or compression and one calculated from the momentum equation, are compared and steps (3) through (9) are repeated until the two are equal. The PR which satisfies this condition is the solution value.

C. Program Input and Output

The program input is simple, and provides for the generation of a large set of parametric data.

Card 1

D_{m_t}, θ_m, D_{i_t}, θ_i, D_{i_b}, $M_{i_{guess}}$, γ

Card 2

Indicator integers M, J, KK, L $\leqq$ 9

Cards 3 and 4

M values of ϵ^*
M values of estimated PR values corresponding to the ϵ^* values.

Card 5

J values of the radius, R, of the subsonic turn of the igniter jet boundary.

Card 6

KK values of x_{sf}, the shock standoff-distance factor.

Card 7

L values of x_{mf}, the secondary-throat impulse-function factor.

The program calculates through four DO loops, in the following order:

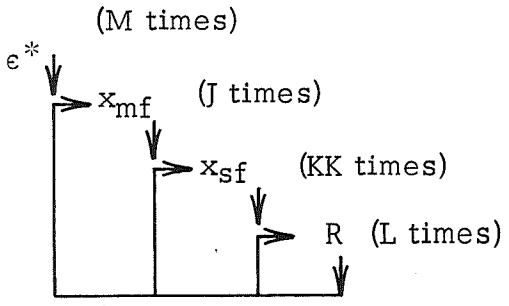

The output data consists of the input set of Card 1, the table of the annular areas between the nozzle wall and the hyperboloids of revolution, and for each separate case are printed 40 geometric and gasdynamical parameters.

D. Validity of the Analysis

The analysis agrees well with the experimental results for air igniter expansion ratios equal to or less than 7, for the following factors:

$$R = 0.1\ D_{i_e}$$

$$x_{sf} = 1.5$$

$$x_{mf} = 0.95$$

At higher expansion ratios for both air and live propellant exhaust the agreement is not satisfactory. The only parameter which appears to improve the agreement is the shock standoff factor, indicating that perhaps the assumption of source flow or the structure of the shock shape are not correct for the higher igniter expansion ratios. In the absence of flow visualization of the interactions there seems to be no way in which these factors may be evaluated.

It is known that the presence of condensed phases in a gas stream can have a profound effect upon the behavior of the stream, especially one which experiences severe streamwise and transverse momentum changes. It is therefore expected that the analysis is less valid for a multiphase stream than for a pure gas, although the overall effect of the condensed phase should diminish as the size of the system increases.

SYMBOLS

a	Hyperbola intercept on x-axis
A	Area
D	Diameter
F	Stream impulse function
$\bar{F}$	Normalized stream impulse function
M	Mach number
MW	Molecular weight
P	Pressure
PR	Igniter chamber pressure/motor chamber pressure
r	Radius
R	Radius of subsonic jet boundary turn
S	Secondary throat surface
t	Time
T	Temperature
$\dot{w}$	Mass flow rate
x	Axial distance
x_{mf}	Multiplying factor on momentum term
x_{sf}	Multiplying factor on shock standoff distance
y	Lateral or radial distance
Δ	Normalized bow shock standoff distance
ϵ	Nozzle expansion ratio
ϵ^*	Igniter placement parameter
γ	Ideal gas ratio of specific heats
θ	Nozzle half-angle
θ_f	Flow direction angle

Superscripts

*	Flow critical (sonic) conditions
o	Stagnation

Subscripts

an	Annulus
1, 2	Conditions before and after shock wave
b	Igniter base cavity
e	Nozzle exit
f	Flow
i	Igniter
m	Motor

Subscripts (concluded)

n	Nozzle
nom	Nominal
0	Start of time sequence
s	Secondary throat surface
sh	Shock wave
sl	Slant area
t	Nozzle throat
w	Wall

REFERENCES

1. Kilgroe, J. D., Fitch, R. E., and Guenther, J. L., "An Evaluation of Aft-End Ignition for Solid Propellant Rocket Motors," NASA CR 72447, Contract NAS 3-10297, CETEC Corporation, September 1968.

2. Falkner, C. E., and Miller, C. L., "Analytical Igniter Design for Solid Propellant Rocket Motors," AFRPL-TR-70-69, Contract AF 04611-67-C-0083, Technology Incorporated, May 1970.

3. Fullman, C. H., and F. B. Nielsen, "(U) Theoretical and Experimental Investigations of Ignition Systems for Very Large Solid Propellant Motors," United Technology Center UTC 2012-FR2, Contract AF04 (611)-7559, 8 May 1963, (CONFIDENTIAL).

4. Aerojet General Corporation "Final Report Aft-End Ignition - Large Solid Rocket Program - Phase II," Contract No. AF04(611)-8012, Program No. 623A (Report No. SSD-TDR-62-103).

5. Aerojet General Corporation, "Final Phase Report 260-in. - Dia. Motor Feasibility Demonstration Program, Vol. I, 260-SL Motor Aft-End Ignition System Development," Contract No. NAS 3-6284.

6. Bretting, Maj. M., and Lt. W. Niessen, "The Study of an Ignition Technique for Large Solid Rocket Motors," 11th Annual AFSC Science and Engineering Symposium, Brooks A. F. B., 20-22 October 1964.

7. Salmi, R. J., "Compressed Air-Model Investigation of Solid Rocket Overpressures due to Interference from Aft-End Ignition Rocket," NASA TND-3537, August 1966.

8. Arens, M., and Spiegler, E., "Shock Induced Boundary Layer Separation in Overexpanded Conical Exhaust Nozzles," AIAA Journal, Vol. I, No. 3, March 1963.

9. Summerfield, M., Foster, C. R., and Swan, W. C., "Flow Separation in Overexpanded Supersonic Exhaust Nozzles," Jet Propulsion 24, 319-321 (1954).

10. Fraser, R. P., Eisenklam, P., and Wilkie, D., "Investigation of Supersonic Flow Separation in Nozzles," J. Mech. Eng. Sci. 1, 267-279 (1959).

11. Charwat, A. F., and Faulmann, D., "Investigation of the Flow and Drag Due to Control Jets Discharging Upstream Into a Supersonic Flow," Proceedings of the XVth International Astronautical Congress, Vol. 3, Warsaw, 1964.

REFERENCES (concluded)

12. Love, E. S., Grigsby, C. E., Lee, L. P., and Woodling, M. J., "Experimental and Theoretical Studies of Axisymmetric Free Jets," NASA TR R-6, 1959.

13. Lawrence, Roy, "Symmetrical and Unsymmetrical Flow Separation in Supersonic Nozzles," Doctoral thesis, SMU, 1967.

DISTRIBUTION LIST

No. of Copies	Recipient
	NASA Lewis Research Center 21000 Brookpark Road Cleveland, Ohio 44135 Attn:
1	Contracting Officer Mail Stop 500-313
8	Solid Rocket Technology Br. Mail Stop 500-205
2	Technical Library Mail Stop 60-3
1	Tech. Report Control Office Mail Stop 5-5
1	J. Kennard Mail Stop 3-17
1	Tech. Utilization Office Mail Stop 3-19
1	Patent Counsel Mail Stop 500-311
	National Aeronautics and Space Administration Washington, D.C. 20546 Attn:
3	RPM/R. Wasel
1	RPS/Robert W. Ziem
2	ATSS-AL/Technical Library
	NASA Ames Research Center Moffett Field, California 94035
1	Attn: Technical Library
	NASA Langley Research Center Langley Station Hampton, Virginia 23365 Attn:
1	Robert L. Swain
1	Technical Library
	NASA Goddard Space Flight Center Greenbelt, Maryland 20771
1	Attn: Technical Library
	NASA Manned Spacecraft Center 2101 Webster Seabrook Road Houston, Texas 77058
1	Attn: Technical Library
	NASA George C. Marshall Space Flight Center Redstone Arsenal Huntsville, Alabama 35812 Attn:
1	Technical Library
1	S&E-ASTN-PJ/D. Burrows
	Jet Propulsion Laboratory Calif. Institute of Technology 4800 Oak Grove Drive Pasadena, California 91103 Attn:
1	Richard Bailey
	Technical Library
	Scientific & Technical Information Facility NASA Representative P. O. Box 33 College Park, Maryland 20740
6	Attn: CRT
	Government Installations
	AF Space Systems Division Air Force Unit Post Office Los Angeles, California 90045
1	Attn: Col. E. Fink
	AF Research & Technology Division Bolling AFB, D.C. 20332
1	Attn: Dr. Leon Green, Jr.

No. of Copies	Recipient
	AF Rocket Propulsion Laboratory Edwards AFB, California 93523
2	Attn: RPM/ Mr. C. Cook
	AF Materials Laboratory Wright-Patterson AFB, Ohio 45433 Attn:
1	MANC/D. Schmidt
1	MAAE
	AF Ballistic Missile Division P. O. Box 262 San Bernadino, California
1	Attn: WDSOT
	Structures Division Wright-Patterson AFB, Ohio 45433
1	Attn: FDT/R. F. Hoener
	Army Missile Command Redstone Scientific Information Center Redstone Arsenal, Alabama 35809
1	Attn: Chief, Document Section
	Ballistic Research Laboratory Aberdeen Proving Ground, Maryland 21005
1	Attn: Technical Library
	Picatinny Arsenal Dover, New Jersey 07801
1	Attn: Technical Library
	Navy Special Projects Office Washington, D.C. 20360
1	Attn: H. Bernstein
	Naval Air Systems Command Washington, D.C. 20360
1	Attn: AIR-330/Dr. O. H. Johnson
	Naval Propellant Plant Indian Head, Maryland 20640
1	Attn: Technical Library
	Naval Ordnance Laboratory White Oak Silver Spring, Maryland 20910
1	Attn: Technical Library
	Naval Ordnance Test Station China Lake, California 93557 Attn:
1	Technical Library
1	C. J. Thelen
	Naval Research Laboratory Washington, D. C. 20390
1	Attn: Technical Library
	Chemical Propulsion Information Agency Applied Physics Laboratory 8621 Georgia Avenue
1	Silver Spring, Maryland 20910
	Defense Documentation Center Cameron Station 5010 Duke Street
1	Alexandria, Virginia 22314
	Defense Materials Information Center Battelle Memorial Institute 505 King Avenue
1	Columbus, Ohio 43201

DISTRIBUTION LIST (concluded)

No. of Copies	Recipient
	Materials Advisory Board National Academy of Science 2101 Constitution Ave., N.W. Washington, D.C. 20418
1	Attn: Capt. A. M. Blamphin
	Institute of Defense Analyses 1666 Connecticut Ave., N.W. Washington, D.C.
1	Attn: Technical Library
	Advanced Research Projects Agency Pentagon, Room 3D154 Washington, D.C. 20301
1	Attn: Technical Information Office
	Industry Contractors
	Aerojet Solid Propulsion Company P. O. Box 13400 Sacramento, California 95813 Attn:
1	Dr. B. Simmons
1	L. Westphal
1	Technical Information Center
	Aerojet-General Corporation P. O. Box 296 Azusa, California 91702
1	Attn: Technical Library
	Lockheed Missiles & Space Company P. O. Box 504 Sunnyvale, California
1	Attn: Technical Library
	Aerospace Corporation 2400 East El Segundo Boulevard El Segundo, California 90245 Attn:
1	Technical Library
1	Solid Motor Dev. Office
	Aerospace Corporation P.O. Box 95085 Los Angeles, California 90045
1	Attn: Technical Library
	Atlantic Research Corporation Shirley Highway at Edsall Road Alexandria, Virginia 22314
1	Attn: Technical Library
	Battelle Memorial Library 505 King Avenue Columbus, Ohio 43201
1	Attn: Edward Unger
	Boeing Company P. O. Box 3999 Seattle, Washington 98124
1	Attn: Technical Library
	Chrysler Corporation Space Division Michoud Operations New Orleans, Louisiana
1	Attn: Technical Library
	Douglas Missiles & Space Systems Huntington Beach, California
1	Attn: T. J. Gordon
	Hercules Company Allegany Ballistics Laboratory P. O. Box 210 Cumberland, Maryland 21502
1	Attn: Technical Library

No. of Copies	Recipient
	Hercules Company Bacchus Works P. O. Box 98 Magna, Utah 84044
1	Attn: Technical Library
	Lockheed Propulsion Company P. O. Box 111 Redland, California 93273
1	Attn: Bud White
	Martin Marietta Corporation Baltimore Division Baltimore, Maryland 21203
1	Attn: Technical Library
	Mathematical Sciences Corporation 278 Renook Way Arcadia, California 91107
1	Attn: M. Fourney
	Philco Corporation Aeronutronics Division Ford Road Newport Beach, California 92660
1	Attn: Technical Library
	Rocketdyne Solid Propulsion Operations P. O. Box 548 McGregor, Texas
1	Attn: Technical Library
	Rocketdyne 6633 Canoga Avenue Canoga Park, California 91304
1	Attn: Technical Library
	Rohm and Haas Redstone Arsenal Research Division Huntsville, Alabama 35807
1	Attn: Technical Library
	Rohr Corporation Space Products Division 8200 Arlington Boulevard
1	Riverside, California
	Thiokol Chemical Corporation Wasatch Division
1	Brigham City, Utah 84302
	Thiokol Chemical Corporation Elkton Division Elkton, Maryland 21921
1	Attn: Technical Library
	United Technology Center P. O. Box 358 Sunnyvale, California 94088
1	Attn: Technical Library
	TRW Systems One Space Park Redondo Beach, California 90278
1	Attn: M. Lipow